



Title	LANGEVIN DYNAMICS STUDY ON TRANSPORT PHENOMENA OF DNA IN MICRO/NANOFLUIDIC CHANNELS
Author(s)	Weixin, Qian
Citation	大阪大学, 2017, 博士論文
Version Type	VoR
URL	<a href="https://doi.org/10.18910/61823">https://doi.org/10.18910/61823</a>
rights	
Note	

*The University of Osaka Institutional Knowledge Archive : OUKA*

<https://ir.library.osaka-u.ac.jp/>

The University of Osaka

**LANGEVIN DYNAMICS STUDY ON  
TRANSPORT PHENOMENA OF DNA IN  
MICRO/NANOFLUIDIC CHANNELS**

**WEIXIN QIAN**

**MARCH 2017**



**LANGEVIN DYNAMICS STUDY ON  
TRANSPORT PHENOMENA OF DNA IN  
MICRO/NANOFLUIDIC CHANNELS**

A dissertation submitted to

THE GRADUATE SCHOOL OF ENGINEERING SCIENCE

OSAKA UNIVERSITY

in partial fulfillment of the requirements for the degree of

DOCTOR OF PHILOSOPHY IN ENGINEERING

**BY**

**WEIXIN QIAN**

**MARCH 2017**



## Abstract

Recently, increased demands for analytical capability in the field of biological sciences have promoted the development of micro/nanofluidic platforms for biomolecular sensing. One of the most highly debated topics concerning micro/nanofluidics is the nanopore sequencing, which is an emerging nonoptical technology for high-throughput single-molecule detection. At the same time, various issues remain to be resolved to make nanopore sequencers practical, including control of DNA transport speed, manipulation of DNA conformation, suppressing stochastic nucleobase motion and so on. The understanding of DNA transport phenomena in nanofluidics is crucially important to address these long-time-remaining challenges. However, the experimental observation and measurement restrictions in the nanopores and nanochannels make the throughout comprehension of DNA transport mechanism difficult. On the other hand, molecular dynamics simulations that provide atomistic resolution analysis of polymer transport are out of capability to reproduce the phenomena in practical temporal and spatial scales. Therefore, this study aims to develop computational methods capable in the larger scale to elucidate the DNA transport mechanism in micro/nanofluidic devices, which complement the experimental studies for further advances in the emerging analytical platforms.

In this study, a Langevin dynamics (LD) simulation technique has been developed and applied to the electrokinetic transport of double-stranded DNA (dsDNA) and single-stranded DNA (ssDNA) in the micro/nanofluidic channels. First, the DNA fragment is represented by a coarse-grained bead-spring model. The key parameters of the coarse-grained model, such as friction coefficient and bead charge, are evaluated from the experimental measurements of diffusion coefficient and electrophoretic mobility of DNA, which are inevitable to quantitatively reproduce the physical properties of DNA. Second, the complex electric field distribution inside the fluidic channels, which dominantly affects the DNA transport process, is evaluated numerically solving the Poisson equation by using the finite element methods. Third, the background electroosmotic flow (EOF) generated due to the surface charges of channel walls is also theoretically considered by solving the Navier-Stokes equations. Coupling these factors with the LD simulation, we carry out simulations for the DNA transport phenomena in a cylindrical nanochannel and a nanopore

in a millisecond and micrometer scales comparable to the real system and as a result, we successfully depict essential points of DNA transport process and characterize the fundamental physics in the coarse-grained molecular level.

Through the computational analysis, we have clarified the mechanism of dsDNA and ssDNA translocation in the nanopores and nanochannels. It is found that the conformation of DNA polymer chains in the nanochannels causes the translocation speed. Varying the cross-sectional area of the nanopores is effective to optimize the translocation process. It is also concluded that the combination of EOF velocity gradients and electric fields due to electrically polarized channel surfaces characterizes the molecular conformations, where the DNA is stretched (compressed) with negative (positive) wall surface potentials in low-concentration solutions.

The simulation methods developed in this study can be further applied to optimize the design of micro/nanofluidic systems concerning the biopolymer transport phenomena. Furthermore, the results of this study have also proposed some subjects concerning the multiscale physics, such as molecular transport phenomena influenced by hydrodynamic effects, which have remained to be solved in the future works.

## Contents

<b>Chapter 1 General Introduction</b> .....	1
<b>1.1 Background</b> .....	1
<b>1.2 Challenges</b> .....	3
<b>1.3 Purpose of this thesis</b> .....	4
<b>Reference</b> .....	7
<b>Chapter 2 Analysis of dsDNA Translocation through Nanopore</b> .....	12
<b>2.1 Introduction</b> .....	12
<b>Nomenclature</b> .....	14
<b>2.2 Computational methods</b> .....	15
<b>2.2.1 Coarse-grained model of <math>\lambda</math>-DNA</b> .....	15
<b>2.2.2 Electric fields in nanochannel and nanogap</b> .....	18
<b>2.2.3 Langevin dynamics simulation</b> .....	19
<b>2.3 Results and discussion</b> .....	19
<b>2.3.1 Validation of the model</b> .....	19
<b>2.3.2 Translocation of DNA in nanochannel and nanogap</b> .....	20
<b>2.4 Conclusion</b> .....	28
<b>Reference</b> .....	30
<b>Chapter 3 Analysis of ssDNA Translocation through Nanopore</b> .....	35
<b>3.1 Introduction</b> .....	35
<b>Nomenclature</b> .....	39
<b>3.2 Computational methods</b> .....	41
<b>3.3 Results and discussion</b> .....	44
<b>3.3.1 Non-uniform electric field inside nanopore</b> .....	44
<b>3.3.2 ssDNA translocation conformation</b> .....	46
<b>3.3.3 Translocation speed</b> .....	49
<b>3.4 Conclusion</b> .....	53
<b>Reference</b> .....	54
<b>Chapter 4 Analysis of DNA Translocation through Nanochannel</b> .....	60
<b>4.1 Introduction</b> .....	60
<b>Nomenclature</b> .....	62
<b>4.2 Computational methods</b> .....	65
<b>4.2.1 Electroosmotic flow in the nanochannel</b> .....	65

<b>4.2.2 Langevin dynamics simulation of a coarse-grained ssDNA model</b> .....	69
<b>4.3 Results and discussion</b> .....	71
<b>4.3.1 Verification of the coarse-grained ssDNA model</b> .....	71
<b>4.3.2 Dependence of DNA mobility on ion concentration</b> .....	74
<b>4.3.3 Molecular conformations of DNA inside nanochannel</b> .....	76
<b>4.4 Theoretical approach to the molecular distribution in a nanochannel</b> .....	84
<b>4.5 Conclusion</b> .....	90
<b>Reference</b> .....	91
<b>Chapter 5 General Conclusions</b> .....	97
<b>List of Publication</b> .....	99
<b>Acknowledgment</b> .....	100

# Chapter 1

## *General Introduction*

### **1.1 Background**

The sequencing of the human genetic code is of significant importance and established a notable milestone in human civilization. The genome has defined human species and supply the path to the better understanding of physiology. However, up to now, only a generic version of the code has been determined. The high-speed reading of deoxyribonucleic acid (DNA) sequences is an important means of elucidating complete genetic sequences, and may enable the development of new medical treatments<sup>1</sup>. The current mature DNA sequencing technologies identify DNA sequence through light emission, which requires polymerase chain reaction (PCR) amplification and fluorescent labeling for generating detectable signals. These existing-generation DNA sequencing platforms take two months and cost approximately 0.1 million dollars for completely determining human genome<sup>2</sup>. The excessive throughput, cost of DNA sequencing and its potential commercial values promotes the development of next-generation DNA sequencing technologies.

Recently, the breakthrough in the nanotechnology, in particular, nanofluidics research field brings about the evolution of emerging technologies in single molecule detection, identification and analysis<sup>3-16</sup>. Nanofluidics is an emerging study and application of the behavior, manipulation, and control of phenomena that involve fluid motions confined in nanometer structures (typically ~100 nm). Fluid motions confined in such scale exhibits physical behaviors not observed in macroscale due to the drastically enhanced

surface-to-volume ratio of the nanostructure. For example, the well-known phenomena, electrical double layer (EDL) and electroosmotic flow (EOF) are unique properties of nanofluidic systems and have a very important impact on the fluid dynamics and motion of charged polymer<sup>17-23</sup>. In many researches, experiments have also shown that the polymer dynamics exists marked difference in nanostructures from their behavior in macro- and micro-systems as well. The studies of these unique transport phenomena at nanoscales, which involve surface chemistry, quantum chemistry, electrostatics, electrokinetics, electrochemistry, heat and mass transfer, molecular biology, and macroscale fluid mechanics simultaneously, supply an opportunity of learning new science and wide ranged advanced analytical platforms.

As an applications of the nanofluidics, nanopore sequencing devices, are the most significant and represent an emerging non-optical process for high-throughput single-molecule detection, in which individual nucleobases are identified based on size by measuring transpore ionic current blockade<sup>3,10,12</sup> or transverse tunneling current<sup>5,9,11</sup> during the transport of single-stranded DNA (ssDNA) through a nanometer-sized pore. The nanopore devices require non-additional intervening amplification or chemical labeling for the single-molecule identification and analysis, which conduces nanopore platforms to the prospect of “next-generation sequencer” that will sequence a mammalian genome less than 1000 dollars in 24 hours. The schematic illustration of basic principle of the nanopore-based sequencing is presented in Figure 1-1. The nanopore consists of a hole with an internal diameter around several nanometers, separating the container into two chambers which are filled with electrolyte solution. A steady-state ionic current could be introduced by applying constant bias voltage on the two side of the membrane. When adding DNA molecules to the solution, the negatively charged DNA will be driven to translocate through the nanopore due to the electrophoresis force. The magnitude of ionic current is very sensitive to the amount of ions insider a nanopore. Once DNA comes into the nanopore, the volumes of nucleotides will exclude ions out of the nanopore, which creates a characteristic change in the magnitude of the current. Different nucleotides (Adenine, Cytosine, Guanine, and Thymine) theoretically cause nucleotide-specific ionic current blockade, providing the information of DNA sequence.

## 1.2 Challenges

Although these throughput and cost of nanopore-based sequencing are exceptionally inspiring, several major technological bottlenecks have to be addressed to implement the nanopore sequencing. A key challenge to nanopore-based sequencing technology is to address the retarding of DNA translocation from microseconds per nucleotide to milliseconds, and reduce the fluctuations during translocation<sup>1</sup>. While the high translocation speed of DNA through a nanopore holds the promise of ultra-fast sequencing<sup>2-16</sup>, the rapid transport velocity of DNA makes recording difficult and prone to background noise, resulting in low temporal resolution of single-base sequencing. Various strategies have been proposed to control the translocation speed of DNA, such as tuning of wall surface charges<sup>24</sup>, ion concentrations<sup>25,26</sup>, temperature gradients<sup>27</sup>, solution viscosity<sup>28</sup>, and pore dimensions<sup>29</sup>. However, these efforts have not yet been shown to improve the controllability issue of nanopore sequencing. Nonetheless, the stochastic motion of DNA caused by thermal fluctuation, which is reflected in the broad distribution of translocation times, generates uncertainty in the nucleotide number passing through a nanopore. The stochastic motion also produces considerable noise for the current signal and prevents the precise manipulation of the DNA during translocation process. Furthermore, the effects of EOF and EDL to the DNA transport in nanofluidics are incomprehension. Moreover, optimization of nanopore structures is an important project as well, but it has rarely been conducted from the theoretical point of view.

The full comprehension of DNA transport phenomena is of crucial importance and absolute indispensable to address these long-time-remaining challenges in nanofluidics as well as in numerous polymer physics<sup>20-23,30</sup>. In order to actively utilize the technological potentials of nanopore devices, polymer translocation through a nanopore has become a main subject in a lot of research topics from theoretical<sup>31-33</sup>, experimental<sup>34-41</sup> and computational<sup>42-50</sup> aspects. These studies concentrated on the translocation dynamics associated with the chain length<sup>31,32,34,36,42-44</sup>, pore dimensions<sup>44</sup>, driving force<sup>34,36,42,42,44</sup>, sequences and secondary structures<sup>36,37,45,46</sup>, polymer-pore interactions<sup>36-38,47</sup>, and polymer configurations<sup>42,48</sup>. In fact, the experimental observation and measurement restrictions at nanoscale in the experiment make the throughout understanding of DNA translocation

mechanism difficult. Direct fluorescent observation of DNA translocation supplies limited information about the whole translocation process and conformation change of DNA in the nanopore. On the other hand, molecular dynamics simulations that provide atomistic resolution analysis are out of range to reproduce the polymer transport phenomena in practical temporal and spatial scales. Even with the most modern computational resource, it is far impossible to calculate the complete translocation process of the whole macromolecular assemblies of hundreds of nanometers in size. The limitation of experimental observation and simulation scale greatly impede the development and advance in nanopore technologies.

### **1.3 Purpose of this thesis**

This study aims to develop the computational method that is capable in the larger scale to elucidate the DNA transport mechanism in macro/nanofluidic devices, which complement the experimental studies for the further advances in the emerging analytical platforms. The complete transport phenomena of DNA through nanopore geometry and nanochannel geometry at experimental spatial and temporal scales are reproduced by the developed computational approach to access to the detailed DNA transport mechanism. The objective is to identify the various significant contribution factors and to assess their relative contributions to DNA transport under nanometer environment.

In this study, coarse-grained bead-spring models for both dsDNA and ssDNA have been developed in this study. Through employing the suitable force field and physical properties measured from experiments, our model is capable to quantitatively reproduce the realistic behavior of polymeric properties such as the radius of gyration, diffusion coefficient, and electrophoretic mobility. The coarse-grained model sacrifices atomistic resolution analysis of the DNA behavior in nanofluidics; on the contrary, it allows probing larger systems on longer time scales.

In Chapter 2 we report the dsDNA transport mechanism in terms of the translocation time for passing through the nanogap, the waiting time of a molecule staying in the nanochannels, and the configuration change associated with the channel dimensions. The simulation confirms the ionic current changes induced by the translocation of dsDNA

through the nanogap. Corresponding to the ionic current response, detailed behavior in the translocation time is visualized and asymmetry in the responses is also clarified with respect to the nanogap. It is concluded that the computational results are crucial to express the essential dynamical perspectives of such bionanofluidic phenomena.

In Chapter 3 we study the ssDNA translocation mechanism through nanopore with various cross-sections, ranging from  $20 \times 20$  to  $50 \times 50$  nm<sup>2</sup>. The results allow a visual analysis of the electrokinetic transport dynamics of ssDNA and allow us to determine the most suitable morphology for nanofluidic flow channels for single molecule detection. Consequently, a relationship among the electrokinetic transport of ssDNA, pore dimensions, and multiply-connected structures of the nanofluidic channel are clarified and a desirable design to control the translocation velocity is concluded.

In Chapter 4, we investigated the relationships between the polymer length, salt concentration, and deformation process in EOF fields. As a result of the present LD simulations, detailed characteristics of ssDNA, such as off-centered alignment in the nanochannel stretching or compressing the polymer chain, were elucidated on a realistic spatiotemporal scale. These results are expected to be applicable to the development of techniques for the manipulation and velocity control of ssDNA during transport.

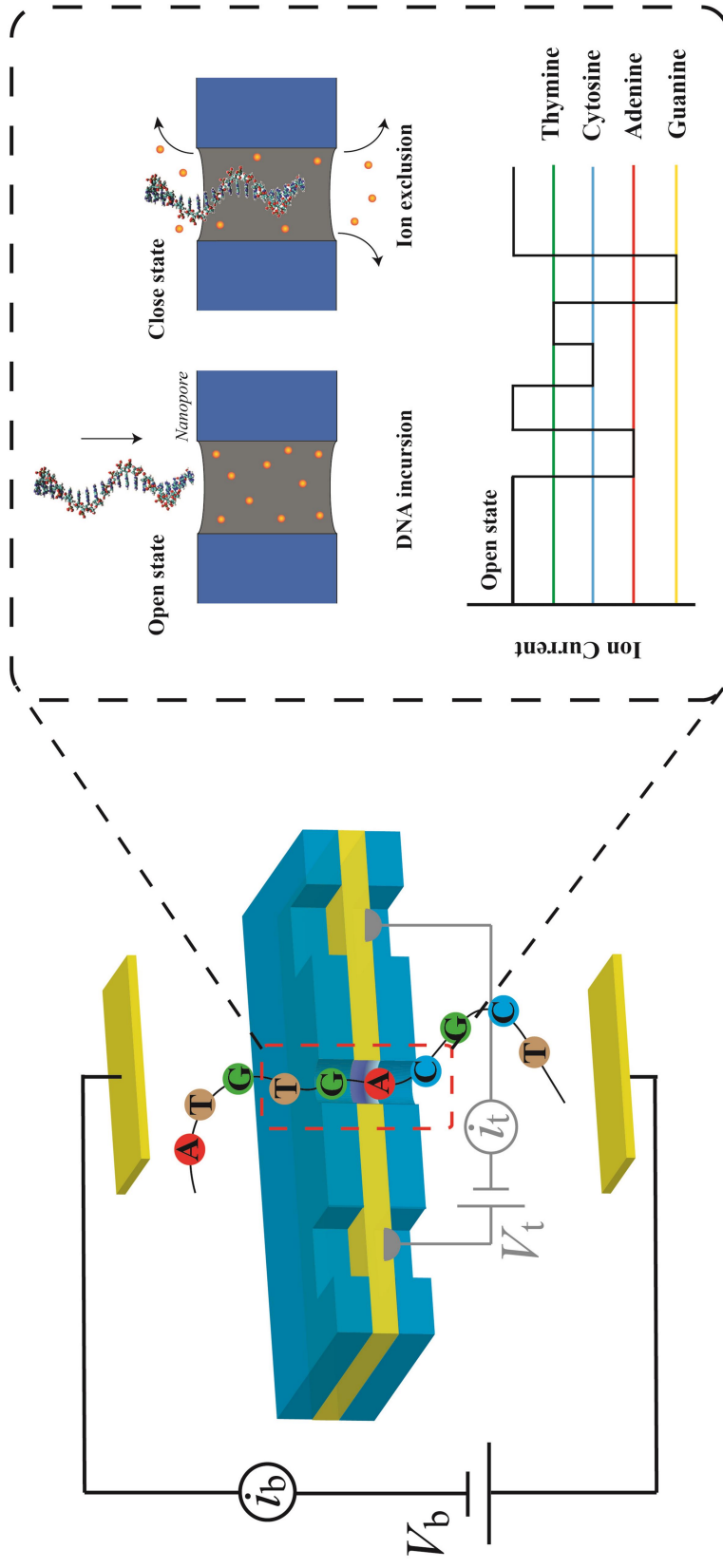


**Figure 1-1.** Schematic of advanced nanopore DNA sequencer. (a) nanopore platform (b) ionic blockade current due to the translocation of ssDNA through nanopore.

## Reference

1. D. Branton, D. W. Deamer, A. Marziali, H. Bayley, S. A. Benner, T. Butler, M. Di Ventra, S. Garaj, A. Hibbs, X. Huang, S. B. Jovanovich, P. S. Krstic, S. Lindsay, X. S. Ling, C. H. Mastrangelo, A. Meller, J. S. Oliver, Y. V. Pershin, J. M. Ramsey, R. Riehn, G. V. Soni, V. Tabard-Cossa, M. Wanunu, M. Wiggin, J. A. Schloss, “The potential and challenges of nanopore sequencing,” *Nat. Biotechnol.* **26**, 1146–1153 (2008).
2. K. Yokota, M. Tsutsui, and M. Taniguchi, “Electrode-embedded nanopores for label-free single-molecule sequencing by electric currents,” *RSC Adv*, **4**, 15886-15899 (2014).
3. J. Kasianowicz, E. Brandin, D. Branton, D. W. Deamer, “Characterization of individual polynucleotide molecules using a membrane channel,” *Proc. Natl. Acad. Sci. U.S.A.* **93**, 13770–13773 (1996).
4. J. B. Heng. C. Ho, T. Kim, R. Timp, A. Aksimentiev, Y. V. Grinkova, S. Sligar, K. Schulten, and G. Timp, “Sizing DNA Using a Nanometer-Diameter Pore,” *Biophys J.* **87**(4), 2905-2911 (2004).
5. J. Lagerqvist, M. Zwolak, M. Di Ventra, “Fast DNA sequencing via transverse electronic transport,” *Nano Lett.* **6**, 779–782 (2006).
6. C. Dekker, “Solid-state nanopores,” *Nat. Nanotechnol.* **2**, 209–215 (2007).
7. J. D. Cross, E. A. Strychalski, and H. G. Craighead, “Size-dependent DNA mobility in nanochannel,” *J. Appl. Phys.* **102**(2), 024701 (2007).
8. M. Zwolak, and M. Di Ventra, “Colloquium: Physical approaches to DNA sequencing and detection,” *Rev. Mod. Phys.* **80**, 141–165 (2008).
9. X. Liang, S. Y. Chou, “Nanogap detector inside nanofluidic channel for fast real-time label-free DNA analysis,” *Nano Lett.* **8**, 1472–1476 (2008).
10. J. Clarke, H. C. Wu, L. Jayasinghe, A. Patel, S. Reid, H. Bayley, “Continuous base identification for single-molecule nanopore DNA sequencing,” *Nat. Nanotechnol.* **4**, 265–270 (2009).
11. M. Tsutsui, M. Taniguchi, K. Yokota, T. Kawai, “Identifying single nucleotides by tunnelling current,” *Nat. Nanotechnol.* **5**, 286–290 (2010).

12. K. R. Lieberman, G. M. Cherf, M. J. Doody, F. Olasagasti, Y. Kolodji, Akeson, M. “Processive replication of single DNA molecules in a nanopore catalyzed by phi29 DNA polymerase,” *J. Am. Chem. Soc.* **132**, 17961–17972 (2010).
13. M. Tsutsui, Y. He, M. Furuhashi, S. Rahong, M. Taniguchi, and T. Kawai, “Transverse electric field dragging of DNA in a nanochannel,” *Sci. Rep.* **2**, 394 (2012).
14. T. Yasui, S. Rahong, K. Motoyama, T. Yanagida, Q. Wu, N. Kaji, M. Kania, K. Doi, K. Nagashima, M. Tokeshi, M. Taniguchi, S. Kawano. and Y. Baba, “DNA Manipulation and Separation in Sublithographic-Scale Nanowire Array,” *ACS Nano.* **7**(4), 3029–3035 (2013).
15. T. Ohshiro, M. Tsutsui, K. Yokota, M. Furuhashi, M. Taniguchi, and T. Kawai, “Detection of post-translational modifications in single peptides using electron tunnelling currents,” *Nat. Nanotechnol.* **9**, 835–840 (2014).
16. S. Rahong, T. Yasui, T. Yanagida, K. Nagashima, M. Kanai, A. Klamchuen, G. Meng, Y. He, F. Zhuge, N. Kaji, T. Kawai, and Y. Baba, “Ultrafast and Wide Range Analysis of DNA Molecules Using Rigid Network Structure of Solid Nanowires,” *Sci. Rep.* **4**, 5252 (2014).
17. B. J. Kirby, and E. F. Hasselbrink Jr, “Zeta potential of microfluidic substrates: 1.Theory, experimental techniques, and effects on separations,” *Electrophoresis.* **25**, 187-202 (2004).
18. B. J. Kirby, and E. F. Hasselbrink Jr, “Zeta potential of microfluidic substrates: 2.Data for polymers,” *Electrophoresis.* **25**, 203-213 (2004).
19. S. Ghosal, “Fluid mechanics of electroosmotic flow and its effect on band broadening in capillary electrophoresis,” *Electrophoresis.* **25**, 214-228 (2004).
20. Z. Yuan, A. L. Garcia, G. P. Lopez, and D. N. Petsev, “Electrokinetic transport and separations in fluidic nanochannels,” *Electrophoresis.* **28**, 595-610 (2007).
21. R. B. Schoch, “Transport phenomena in nanofluidics,” *Rev. Mod. Phys.* **80**, 839-883 (2008).
22. W. Sparreboom, A van den Berg, and J. C. T. Eijkel, “Principles and applications of nanofluidic transport,” *Nat. Nanotechnology.* **4**, 713-720 (2009).
23. W. Sparreboom, A van den Berg, and J. C. T. Eijkel, “Transport in nanofluidic systems:

- a review of theory and applications,” *New Journal of Physics*, **12**, 015004 (2010).
24. Y. He, M. Tsutsui, C. Fan, M. Taniguchi, and T. Kawai, “Controlling DNA Translocation through Gate Modulation of Nanopore Wall Surface Charges,” *ACS Nano* **5**(7), 5509–5518 (2011).
  25. S. Ghosal, “Effect of Salt Concentration on the Electrophoretic Speed of a Polyelectrolyte through a Nanopore,” *Phys. Rev. Lett.* **98**, 238104 (2007).
  26. S. W. Kowalczyk, D. B. Wells, A. Aksimentiev, and C. Dekker, “Slowing down DNA translocation through a nanopore in lithium chloride,” *Nano Lett.* **12**(2), 1038–1044 (2012).
  27. Y. He, M. Tsutsui, R. H. Scheicher, F. Bai, M. Taniguchi, and T. Kawai, “Thermophoretic Manipulation of DNA Translocation through Nanopore,” *ACS Nano* **7**(1), 538–546 (2013).
  28. D. Fologea, J. Uplinger, B. Thomas, D. S. McNabb, and J. Li, “Slowing DNA Translocation in a Solid-State Nanopore,” *Nano Lett.* **5**(9), 1734–1737 (2005).
  29. W. X. Qian, K. Doi, S. Uehara, K. Morita, and S. Kawano, “Theoretical study of the transpore velocity control of single-stranded DNA,” *Int. J. Mol. Sci.* **15**(8), 13817–13832 (2014).
  30. K. D. Dorfman, “DNA electrophoresis in microfabricated devices,” *Rev. Mod. Phys.* **82**, 2903–2947 (2010).
  31. S. M. Simon, C. S. Pdeskin; G. F. Oster, “What drives the translocation of proteins?” *Proc. Natl. Acad. Sci. U.S.A.* **89**, 3770–3774 (1992).
  32. W. Sung, P. J. Park, “Polymer translocation through a pore in a membrane,” *Phys. Rev. Lett.* **77**, 783–786 (1996).
  33. M. Muthukumar, “Polymer translocation through a hole,” *J. Chem. Phys.* **111**, 10371–10374 (1999).
  34. A. Meller; L. Nivon, E. Brandin, J. Golovchenko, D. Branton, “Rapid nanopore discrimination between single polynucleotide molecules,” *Proc. Natl. Acad. Sci. U.S.A.* **97**, 1079–1084 (2000).
  35. A. Meller, L. Nivon; D. Branton, “Voltage-driven DNA translocations through a nanopore,” *Phys. Rev. Lett.* **86**, 3435–3438 (2001).

36. A. Meller, D. Branton, "Single molecule measurements of DNA transport through a nanopore," *Electrophoresis*. **23**, 2583–2591 (2002).
37. J. Li; M. Gershow, D. Stein; E. Brandin, J. A. Golovchenko, "DNA molecules and configurations in a solidstate nanopore microscope," *Nature Materials*. **2**, 611–615 (2003).
38. A. J. Storm, C. Storm, J. Chen; H. Zandbergen, J.-F. Joanny, C. Dekker, "Fast DNA translocation through a solid-state nanopore," *Nano Lett.* **5**, 1193–1197 (2005).
39. O. V. Krasilnikov, C. G. Rodrigues, S. M. Bezrukov, "Single polymer molecules in a protein nanopore in the limit of a strong polymer-pore attraction," *Phys. Rev. Lett.* **97**, 018301-1–018301-4 (2006).
40. G. M. Skinner, M. van den Hout, O. Broekmans, C. Dekker, N. H. Dekker, "Distinguishing single- and double-stranded nucleic acid molecules using solid-state nanopores," *Nano Lett.* **9**(8), 2953–2960 (2009).
41. G. F. Schneider; S. W. Kowalczyk; V. E. Calado; G. Pandraud; H. W. Zandbergen, L. M. L. Vandersypen, C. Dekker, "DNA translocation through graphene nanopores," *Nano Lett.* **10**, 3163–3167 (2010).
42. I. Huopaniemi, K. Luo, T. Ala-Nissila, S.-C. Ying, "Langevin dynamics simulations of polymer translocation through nanopores," *J. Chem. Phys.* **125**, 124901-1–124901-8 (2006).
43. I. Huopaniemi; K. Luo, T. Ala-Nissila, S.-C. Ying, "Polymer translocation through a nanopore under a pulling force," *Phys. Rev. E*. **75**, 061912-1–061912-6 (2007).
44. V. V. Lehtola, R. P. Linna, K. Kaski, "Dynamics of forced biopolymer translocation," *EPL*. **85**, 58006-p1–58006-p6 (2009).
45. C. M. Edmonds, Y. C. Hudiono, A. G. Ahmadi, P. J. Hesketh, S. Nair, "Polymer translocation in solid-state nanopores: Dependence of scaling behavior on pore dimensions and applied voltage," *J. Chem. Phys.* **136**, 065105-1–065105-10 (2012).
46. Luo, K. F.; Ala-Nissila, A.; Ying, S. C.; Bhattacharya, A. "Sequence dependence of DNA translocation through a nanopore," *Phys. Rev. Lett.* **2008**, **100**, 058101-1–058101-4.
47. Luo, K.; Ala-Nissila, A.; Ying, S.-C.; Bhattacharya, A. "Dynamics of DNA

- translocation through an attractive nanopore,” *Phys. Rev. E.* **2008**, **78**, 061911-1–061911-7.
48. A. Ramachandran; Q. Guo, S. M. Iqbal; Y. Liu, “Coarse-grained molecular dynamics simulation of DNA translocation in chemically modified nanopores,” *J. Phys. Chem. B.* **115**, 6138–6148 (2011).
49. C. Forrey, M. Muthukumar, “Langevin dynamics simulations of ds-DNA translocation through synthetic nanopores,” *J. Chem. Phys.* **127**, 015102-1–015102-10 (2007).
50. M. G. Gauthier, G. W. Slater, “Molecular dynamics simulation of a polymer chain translocating through a nanoscopic pore,” *Eur. Phys. J. E.* **25**, 17–23 (2008).

# Chapter 2

## *Analysis of dsDNA Translocation through Nanopore*

### 2.1 Introduction

In recent decades, single-molecule sensing technologies using nanofluidic devices have attracted much attention associated with the fusion of physics, electrochemistry, biology, and nanotechnology<sup>1-12</sup>. Kasianowicz et al.<sup>1</sup> firstly reported that single-stranded ribonucleic acid (RNA) and deoxyribonucleic acid (DNA) could be sensed by using a lipid bilayer membrane. Some review articles are also available to understand the historical background of electrokinetic transport phenomena of polymer chains<sup>6-12</sup>. A large number of researchers engage in such challenging topics by developing their own novel techniques. Biological nanopores<sup>1,3</sup> and solid-state nanopores<sup>2-3</sup> are known to have an important role to detect ionic current signals by the principle of Coulter-counter<sup>9-21</sup>. Meller et al.<sup>10-12</sup>, in their pioneering works, clearly distinguished differences between DNA oligomers resulting from the ionic current blockade. Dekker<sup>2</sup> and his coworkers<sup>14,16,18</sup> have published some important results associated with the identification of DNA and RNA molecules by using solid-state nanopores. Furthermore, tunneling current through single molecules was successfully measured by using nano-gapped electrodes<sup>22-24</sup>. Di Ventra and his coworkers<sup>3,22</sup> theoretically supposed an idea of tunneling current measurement of DNA sequencing, and Tsutsui et al.<sup>23</sup> and Ohshiro et al.<sup>24</sup> experimentally observed it. Theoretical approaches and

simulations were also carried out and provided variable insight into the transport phenomena in confined nanofluidic systems<sup>25–33</sup>. Huopaniemi et al.<sup>28,29</sup> and Luo et al.<sup>31,32</sup> have theoretically investigated the translocation properties of polymer chains which pass through nanopores by using molecular dynamics approaches. Some important review papers were published with respect to the theories and experiments of polymer translocation through nanopores<sup>34,35</sup>. On the other hand, a lot of barriers have remained for the practical use. For example, electrical signals from a single molecule are so weak that the target has to be captured in a molecular-sized confined space; in order to detect such a weak signal, the signal-to-noise ratio has to be improved; the electrophoresis and electroosmosis of electrolytes are required to be properly controlled<sup>21–24</sup>. Some of us also have addressed single-base detection of a long-chained DNA from both experimental<sup>37,38</sup> and theoretical aspects<sup>39–46</sup>. Particularly, using nanochannels and nanopores, responses of ionic current can be measured when DNA molecules translocate such confined spaces. In a previous study<sup>58</sup>, we experimentally investigated electrokinetic transport of  $\lambda$ -DNA, which consists of 48,502 base pairs (48.5 kbp), in one-dimensionally confined slits. It was found that the electrophoretic mobility decreased with increasing the confinement. Furthermore, we developed a theoretical model to predict the duration time of  $\lambda$ -DNA passing through a nanogap mounted in a nanochannel<sup>21,58,46</sup> and could get a reasonable agreement with the experimental result<sup>21</sup>. We are especially interested in detailed dynamical behavior of DNA in nano-sized channels, which is required for efficient sensing of DNA with single molecule resolution<sup>40,43–45</sup>. Herein, we have applied a coarse-grained model<sup>34,35</sup> of  $\lambda$ -DNA to perform Langevin dynamics simulations<sup>39,40</sup> in a nanofluidic system with nonuniform electric fields which are computed by using the finite element method (FEM). There may be a difficulty to develop a model of double-stranded DNA (dsDNA), since the characteristic size of nanochannel is equivalent to the persistence length of dsDNA, which is a characteristic length associated with the bending stiffness<sup>6–12</sup>. This is a challenging topic to elucidate the molecular transport mechanism in terms of the translocation time for passing through the nanogap, the waiting time of a molecule staying in the nanochannels, and the configuration change associated with the channel dimensions. Verifying the validity of diffusion coefficient and electrophoretic mobility of  $\lambda$ -DNA, the simulation can reproduce ionic current changes induced by the translocation of DNA through the nanogap. Corresponding

to the ionic current response, detailed behavior in the translocation time can be visualized and asymmetry in the responses is also clarified with respect to the nanogap. It is concluded that the computational results are crucial to express the essential dynamical perspectives of such bionanofluidic phenomena.

## Nomenclature

$D$	=	diffusion coefficient of dsDNA in free solution ( $\text{m}^2/\text{s}$ )
$\mathbf{F}_i$	=	interactions due to the gradient of potentials (N)
$k_B$	=	Boltzmann constant (J/k)
$k$	=	spring constant (N/m)
$N$	=	number of beads
$N_{\text{bp}}$	=	number of base pairs
$Q$	=	bead charges (C)
$r_{\text{bp}}$	=	distance between a couple of base pairs (m)
$r_{\text{eq}}$	=	equilibrium length between the connected beads (m)
$r_{ij}$	=	distance between the $i$ th and $j$ th beads (m)
$R_g$	=	radius of gyration of dsDNA (m)
$\mathbf{R}_i$	=	random force (N)
$T$	=	temperature (K)
$\Delta t$	=	time step (s)
$t_d$	=	translocation time (s)
$V_b$	=	bond potential (V)
$V_{\text{LJ}}$	=	Lennard-Jones potential (V)

## Greek Symbols

$\delta_{\alpha\beta}$	=	Kronecker's delta
$\delta(t - t')$	=	Dirac's delta function
$\delta$	=	characteristic length considering thermal fluctuations (m)
$\varepsilon$	=	well-depth of Lennard-Jones potential (kJ/mol)
$\zeta$	=	frictions coefficient of bead (kg/s)
$\sigma$	=	effective radius of bead (m)
$\phi$	=	electrostatic potential (V)
$\Omega_{\text{dsDNA}}$	=	volume of dsDNA ( $\text{m}^3$ )
$\Omega_{\text{nanogap}}$	=	volume of nanogap ( $\text{m}^3$ )

## 2.2 Computational methods

### 2.2.1 Coarse-grained model of $\lambda$ -DNA

In order to evaluate the quantities mentioned above from a molecular point of view, coarse-graining is required to express the dynamics of  $\lambda$ -DNA. Herein, we focus on electrokinetic transport phenomena of a long-chained molecule, which are dominated by the electrophoretic mobility and diffusion coefficient. As shown in Figure 2-1, a nanofluidic channel employed in a previous experiment<sup>21</sup> is modeled in the same scale, where a nanogap,  $200 \text{ nm} \times 50 \text{ nm} \times 60 \text{ nm}$  (length  $\times$  width  $\times$  height), is embedded in both *cis* and *trans* nanochannels,  $1000 \text{ nm} \times 500 \text{ nm} \times 60 \text{ nm}$ . There are microchannels,  $2.5 \text{ }\mu\text{m} \times 4.0 \text{ }\mu\text{m} \times 0.5 \text{ }\mu\text{m}$ , in both ends outside the nanochannels.

In our bead-spring model, each neighboring bead is connected with a linear spring. The bond potential  $V_b$  is as follows<sup>40</sup>

$$V_b(\mathbf{r}_i) = \frac{1}{2} \sum_{j \neq i} k (r_{ij} - r_{\text{eq}})^2, \quad (2-1)$$

where  $r_{\text{eq}}$  is the equilibrium length between the connected beads,  $r_{ij}$  is the distance between the  $i$ th and  $j$ th beads, and  $k$  is the spring constant. Here, the  $r_{\text{eq}}$  is given as

$$r_{\text{eq}} = 0.850 r_{\text{bp}} N_{\text{bp}} / N = 34.7 \text{ nm}, \quad (2-2)$$

where we set the distance between a couple of base pairs:  $r_{\text{bp}} = 0.34 \text{ nm}$ , the number of base pairs:  $N_{\text{bp}} = 48,000$ , and the number of beads:  $N = 400$ .  $N$  is fixed to simulate a long period phenomenon with sufficient sampling. Therefore, a single bead corresponds to 120 bp. The factor of 0.850 is selected as a parameter to replicate the experimental value of diffusion coefficient as described later, which was already introduced in some papers to maintain an equilibrium condition of DNA<sup>39</sup>. Although this assumption causes to underestimate the persistence length 50 nm of dsDNA, the estimated value of near 20 nm resulting from simulations in equilibrium conditions is on the same order of the experimental data<sup>6-12</sup>. There has left room for discussion about trade-offs to replicate various properties with bead-spring models<sup>34,35</sup>. As a first step, this moderately flexible model is applied to express the deformation and translocation of dsDNA in the confined narrow space. The spring

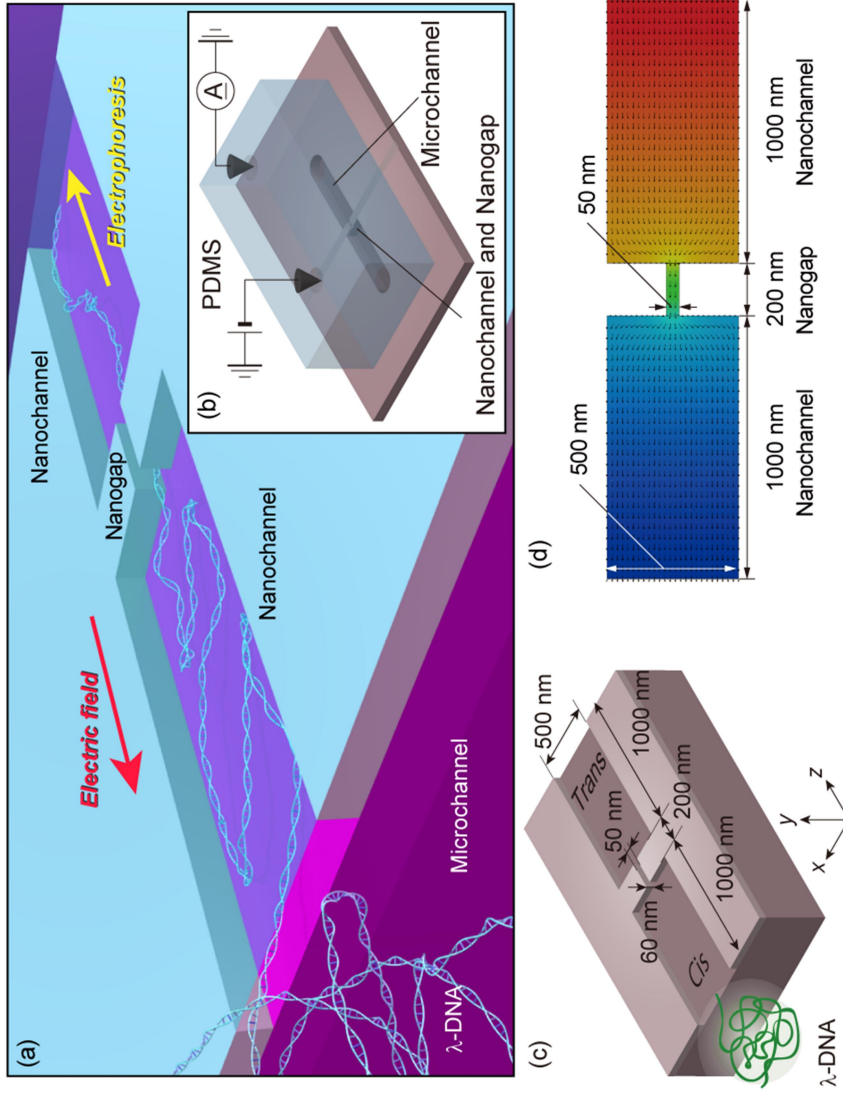


**Figure 2-1.** (a) Schematic diagram of a nanofluidic device,<sup>21</sup> which consists of microchannel, nanochannel, and nanogap. DNA moves against electric fields due to its negative charges in the phosphate group. (b) Whole view of experimental setup. (c) Zoom-in view of nanochannel ( $1000 \text{ nm} \times 500 \text{ nm} \times 60 \text{ nm}$ ) and nanogap ( $200 \text{ nm} \times 50 \text{ nm} \times 60 \text{ nm}$ ). (d) Electrostatic potential and electric field in nanochannel and nanogap, resulting from EFM analysis. Computations are performed in three-dimensional space and the middle section along the  $y$ -axis is presented.

constant is set to  $k = k_B T / \delta^2$ , where  $k_B$  is the Boltzmann constant,  $T = 300$  K is temperature associated with an ambient condition, and  $\delta$  is a characteristic length considering thermal fluctuations such that  $\delta = 0.1\sigma$ , where  $\sigma$  is a parameter for dsDNA described as below<sup>40,47,48</sup>.

Taking into account the volume exclusion effect, another potential  $V_{LJ}$  for the repulsive interaction is defined as follows:<sup>47-50</sup>

$$V_{LJ}(\mathbf{r}_i) = \begin{cases} \sum_{j \neq i} 4\varepsilon \left[ \left( \frac{\sigma}{r_{ij}} \right)^{12} - \left( \frac{\sigma}{r_{ij}} \right)^6 \right] + \varepsilon, & r \leq 2^{1/6} \sigma \\ 0, & r > 2^{1/6} \sigma \end{cases} \quad (2-3)$$

where  $\sigma$  and  $\varepsilon$  denote the effective radius of bead and the well-depth, respectively. Here, we empirically apply  $\sigma = 5$  nm on the assumption that an unfolded form of dsDNA can be detected using a 10 nm-radius pore<sup>21,16,19,28</sup>,  $\varepsilon = k_B T$  for the repulsion between the beads. We assume the elastic surface of the bead, although the detailed function for a coarse-grained model has not yet been accomplished. Using this model, the validity is verified by analyzing the diffusion coefficient and electrophoretic mobility as described later. In addition to the bead-bead interaction, Equation 2-3 is also applied to the wall surface of nanochannel. When the bead approaches the wall, only the normal component to the surface is reflected. Here, the radius of gyration  $R_g$  of  $\lambda$ -DNA is larger than the cross-sectional dimensions of nanochannel and nanogap<sup>51</sup>. It is suspected that  $\lambda$ -DNA runs through such narrow spaces, frequently colliding with the channel walls and changing its configurations. Coupling with a strong electric field in a nanopore, a long chained DNA molecule, which is weakly aggregated in bulk solution, is expected to be uncoiled and elongated when interacting with a stepwise shaped nanochannel. Such a mechanism can be observed in gel electrophoresis and has recently been examined by using artificially fabricated nanofluidic devices<sup>6-12</sup>. In case of solid-state channels, the wall surface is usually negatively charged and screened by positive ions in the electrolyte solution, being referred to as electric double layer. Particular electroosmotic flows may be generated due to high concentrations of electrolyte ions near the surface<sup>52,53</sup>. Although those effects are implied by some reports mentioned above, details have remained to be elucidated and therefore, such ongoing issues beyond our focus here are not involved<sup>54</sup>.

### 2.2.2 Electric fields in nanochannel and nanogap

In the Langevin dynamics simulation, electrostatic fields due to externally applied potentials are taken into account. The nonuniform electric field is analyzed by solving a three-dimensional Laplace equation  $\Delta\phi(\mathbf{r}) = 0$  with a boundary condition of  $\nabla\phi(\mathbf{r}) = 0$  at the side walls and with constant voltages at the end of channels. In this study, we assume some conditions as follows: the electrolyte solution maintains the electroneutrality everywhere; the surface charges are sufficiently screened and the potential gradient perpendicular to the wall surface is negligible; the solution is exposed to the strong electric field along the  $z$ -axis. According to the Debye screening length of 0.1 M KCl solution, the surface charges are usually screened within 1 nm which is quite smaller than the dimension of nanogap<sup>54</sup>. We use an FEM computational code<sup>53</sup> to numerically solve the Laplace equation. Referring to the experimental setup<sup>21</sup>, applied voltages are fixed at the end of microchannel:  $\phi = -0.400$  V at the *cis* channel end and  $\phi = 0.400$  V at the *trans* end. Outside the nanochannels, the dimensions of microchannel,  $2.5 \mu\text{m} \times 4.0 \mu\text{m} \times 0.5 \mu\text{m}$ , are taken into account in the FEM analysis. Furthermore, for the potential values at the inlet and outlet of the nanochannel resulting from the computation of overall system, we carry out an additional computation with higher accuracy focusing on the nanogap embedded in the nanochannel and obtain more precise data available in the Langevin dynamics simulations, as shown in Figure 2-1(d). The electric potentials are  $-0.384$  V and  $0.384$  V at the *cis* and *trans* ends of the nanochannel, respectively. As a result, the electric field strength in the nanogap reaches  $\sim 10^6$  V/m. This order of magnitude is known to be reasonable and required to pull  $\lambda$ -DNA into nanopores<sup>56-59</sup>. Effects of charge distributions, ionic current density, and screening of electrode surfaces, which are hot topics but under discussion, have not been taken into account to avoid causing the complexity. This is a first step to address the molecular simulation replicating  $\lambda$ -DNA, with nonuniform electric fields in a nanofluidic system. In the present system, the cross-section area of nanogap is 150 times smaller than that of microchannel. This is a main reason that the drastic drop of electric voltage can be induced at the nanogap, due to the continuity of electric flux. Thus, the electric field strength of  $10^6$  V/m in the nanogap is reasonably obtained. We focus on the fields of the nanochannel and nanogap properly modeled according to the previous works mentioned above.

### 2.2.3 Langevin dynamics simulation

Using these potentials, the Langevin dynamics simulation is carried out, according to the equation of motion for a coarse-grained bead<sup>39</sup> :

$$\zeta \frac{d\mathbf{r}_i}{dt} = -Q\nabla\phi(\mathbf{r}_i) + \mathbf{F}_i + \mathbf{R}_i, \quad (2-4)$$

where  $\zeta$  is the coefficient of frictions,  $-Q\nabla\phi(\mathbf{r}_i)$  is the electrostatic force on the  $i$ th bead which has a charge  $Q$ ,  $\mathbf{F}_i$  is the interactions due to the gradient of potentials resulting from Equations 2-1 and 2-2, and  $\mathbf{R}_i$  is the random force from the solvent molecules. Based on the fluctuation and dissipation theorem,  $\mathbf{R}_i$  satisfies the relation:

$$\begin{cases} \langle R_\alpha \rangle = 0 \\ \langle R_\alpha(t)R_\beta(t') \rangle = 2\zeta k_B T \delta_{\alpha\beta} \delta(t-t'), \quad \{\alpha, \beta\} = \{x, y, z\} \end{cases} \quad (2-5)$$

where  $\delta_{\alpha\beta}$  and  $\delta(t-t')$  are Kronecker's delta and Dirac's delta function, respectively.

In order to calculate the electrostatic force on a bead, using the result from FEM analysis, the nearest nodes within a 9 nm radius from the center are included to average the electric field. At least two nodes are usually averaged. Although involving four points may be preferable to average the physical property in the three-dimensional space, the electrostatic force due to the strong electric field is dominant on the two-dimensional surface ( $xz$ -plane). According to this procedure, the electrostatic force can be computed. Equation 2-4 is integrated by the Euler method and the time step is suitably set to  $\Delta t = 10$  ps, with which computational results are recognized to be reliable. The center of mass of the DNA chain is initially located at 300 nm apart from the entrance of the nanochannel, where the  $x$ - and  $y$ -coordinates of the mass center are in coincidence with the center of nanochannel. Molecular configurations at the initial conditions are randomly provided, which are confirmed to be stable structures.

## 2.3 Results and discussion

### 2.3.1 Validation of the model

In this study, the friction coefficient  $\zeta$  is determined from the Einstein relation such that  $\zeta D = k_B T$ , where  $D$  is the diffusion coefficient of the DNA. Referring to a previous result<sup>60</sup>,

we obtain  $\zeta = 1.87 \times 10^{-11}$  kg/s when  $D = 5.53 \times 10^{-13}$  m<sup>2</sup>/s. In order to verify the present model and to confirm the value of  $Q$ , we performed the simulation in free solution. The average of 30 samples resulting from 10  $\mu$ s simulations showed clear linearity of the mean square displacement. According to the Einstein relation, the diffusion coefficient was evaluated as  $D = 5.07 \times 10^{-13}$  m<sup>2</sup>/s. Furthermore, in order to determine  $Q$ , the simulation was performed in the same manner, applying a uniform electric field of  $1 \times 10^6$  V/m. The displacement of the mass center was plotted as a function of time, resulting from 90 sampling. Referring to a previous study of mobility<sup>60</sup>, such that  $\mu = 3.11 \times 10^{-8}$  m<sup>2</sup>/Vs, the charge results in  $Q = \zeta\mu = 3.64e$ , where  $\zeta = k_B T / D$ . Using this value, we could obtain the terminal velocity and the electrophoretic mobility resulted in  $\mu = 3.11 \times 10^{-8}$  m<sup>2</sup>/Vs. Thus, our model is confirmed to be available to replicate the electrokinetic transport of  $\lambda$ -DNA in aqueous solutions in external electric fields. On the other hand, the persistence length tends to be underestimated, since the parameters have not been optimized to express the stiffness of dsDNA. As mentioned in previous studies<sup>61-64</sup>, bond-angle potentials and dihedral angle potentials are known to be effective for the double helix of DNA as well as the bond potentials. In this study, focusing on the electrokinetic transport dynamics in the micro/nano-fluidic channel, which occurs in submilliseconds of duration, we have no choice but to overlook the accuracy of stiffness of dsDNA.

### 2.3.2 Translocation of DNA in nanochannel and nanogap

Figure 2-2 shows one of typical time-series data resulting from the simulations for translocation of  $\lambda$ -DNA in the nanochannel. Figure 2-2(a) shows a simulation result and Figure 2-2(b) schematically explains the process of Figure 2-2(a) focusing on near the nanogap. At  $t = 0.25$  ms, the leading head weakly aggregated comes into the nanochannel and moves ahead. The interface of quite different-sized channels causes to stick the DNA and on the other hand, a strong electric field in the narrower channel pulls the charged molecule into it. Successively, the following portion goes through the nanogap with an unfolded form as shown at  $t = 0.30$  ms. At  $t = 0.45$  ms, being one end strongly captured at the *cis* channel, the subchain passes through the nanogap with a multiple folded form. As a consequence, at  $t = 0.80$  ms, some beads captured at the *cis* end has been released and the

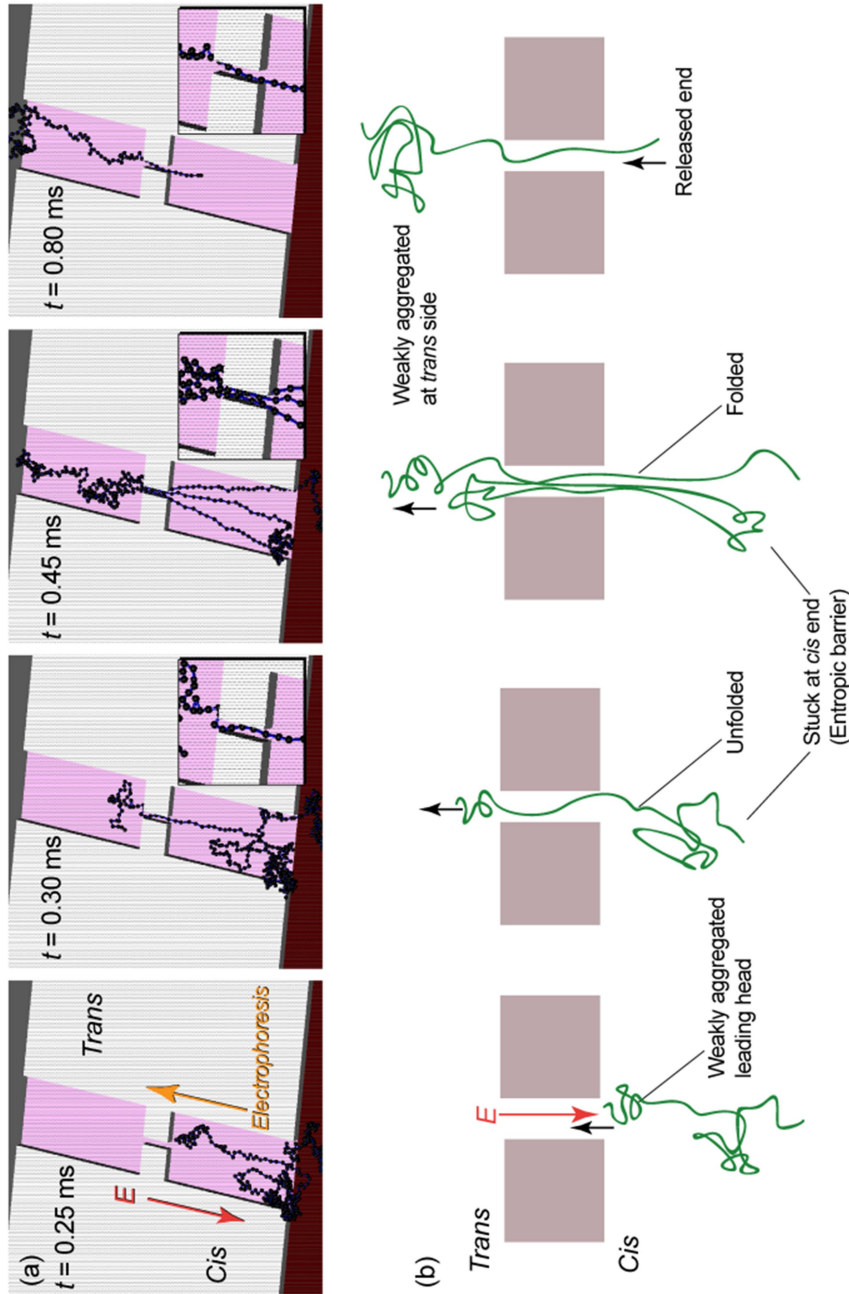


**Figure 2-2.** (a) Snapshots of a typical translocation process of the  $\lambda$ -DNA model passing through nanochannel and nanopore, in which areas near the nanopore are magnified and (b) schematic illustration for a clarification of (a). One end is stuck at the nanochannel entrance and the leading head, which may be weakly aggregated, is pulled into the nanopore; the DNA chain passes through the nanopore with unfolded or folded forms, being remains stuck at the *cis* side; a subchain in the *trans* side weakly aggregates and the released end rapidly shrinks; due to long unfold parts, it takes a long period to penetrate the nanopore.

chain swiftly shrinks, where the following remains run through the nanogap as an unfolded form. For instance, as a typical case, this simulation results in the long translocation time to penetrate the nanogap due to some periods in which the DNA is unfolded. As observed at  $t = 0.30$  ms, unfolded configurations may be desirable from a viewpoint of single molecule detection techniques, since a long-chained molecule should be uncoiled in a channel before approaching sensing probes at a nanogap. Therefore, this kind of nanofluidic channel has a possibility for such applications.

Figure 2-3 shows the force on the mass center of DNA in the nanochannel and nanogap is plotted as a function of position along the  $z$ -axis. The origin of the horizontal axis is at the nanochannel entrance. For the reference, the electrostatic field strength along a field line through the center of each channel cross-section is also presented. As shown in this figure, the force on the DNA increases as the mass center moves ahead and reaches the maximum

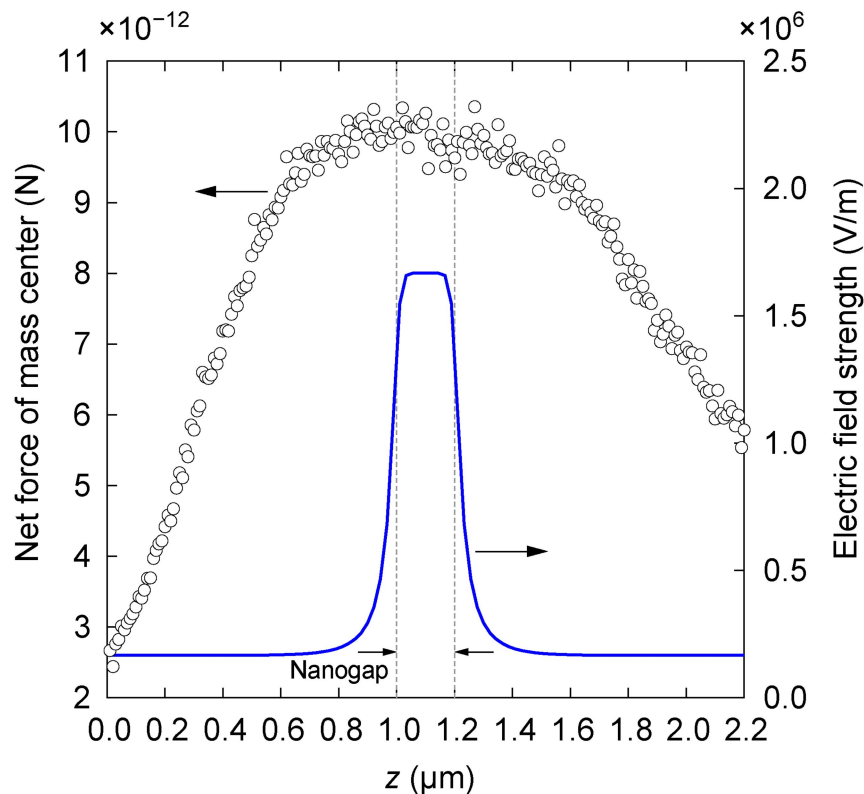


**Figure 2-3.** Profile of net force on the mass center of DNA chain (open circle) and electric field strength (solid line). 50 samples are averaged at each point. The origin of the  $z$ -axis is the entrance of nanochannel; the nanogap is placed between  $z = 1.0$  and  $1.2$   $\mu\text{m}$ .

value in the nanogap which is placed between  $z = 1.0$  and  $1.2 \mu\text{m}$ . After passing through the nanogap, the force decreases moderately compared with the profile in the *cis* side. An interesting point is that there is asymmetry in the force profile between the *cis* and *trans* channels. Such a characteristic is particularly caused by a polymer chain not an ideal single particle. In case of overdamped simulations, the force profile of a “mass point” should be symmetric in both sides of the nanogap, according to the symmetric electric field. On the other hand, the long-chained DNA deforms during translocation through the nanochannel and the degree of deformation seems to be different depending on both the position of the mass center and fields surrounding it.

Figure 2-4 shows the position of the mass center along the  $z$ -axis as a function of time. The translocation velocity is also analyzed by numerical derivative of the position data. Here, we mainly feature two processes, the fastest and slowest translocation processes

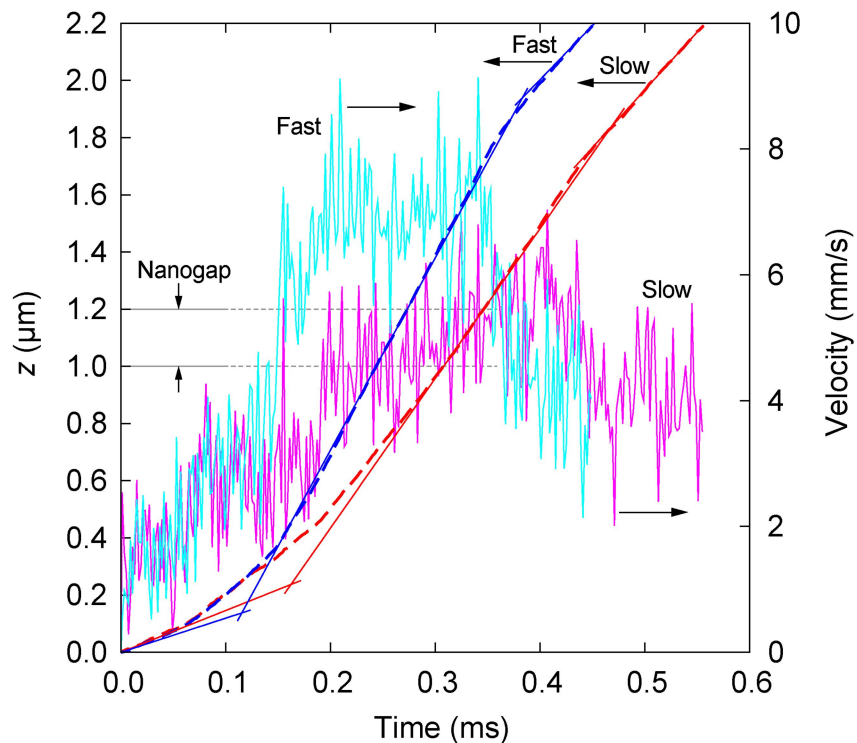


**Figure 2-4.** Position and velocity of the mass center of DNA during passing through the nanochannel and nanogap. Computational results are shown by dashed lines and the velocity is resulted from numerical derivative of position data. The fastest and slowest translocation processes through the nanogap are presented.

during the DNA passing through the 200 nm nanogap. Resulting from 50 times simulations, the translocation time  $t_d$  is evaluated as 0.21 ms for the fastest process and 0.55 ms for the slowest one. Slopes of the curves at the *cis* and *trans* ends and at the nanogap are also shown in addition to the position data. In both cases, it is found that the mass center of DNA chain is clearly affected by the strong field in the nanogap via the elongated subchain, even when it is outside the nanogap. Particularly, in the fastest process, the velocity rapidly increases near the nanogap, since the DNA tends to be folded and is strongly attracted to the nanogap due to the concentration of charges near the mass center. On the other hand, in the slowest process, the DNA is frequently unfolded and therefore, increase in the velocity near the nanogap becomes moderate.

Figure 2-5 shows the histogram of  $t_d$ , in which the experimental result<sup>21</sup> and the theoretical evaluation<sup>46</sup> are also presented for comparison. The  $t_d$  is defined as a period

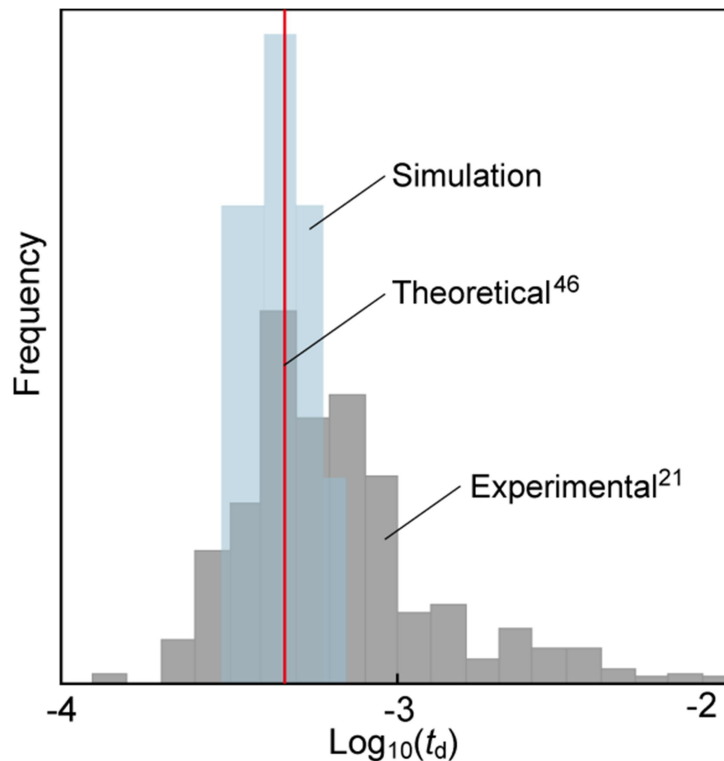


**Figure 2-5.** Histogram of translocation time of  $\lambda$ -DNA for passing through the nanogap. Bright (blue) bars are resulted from 50 sampling of the present simulations; dark (gray) bars are from experimental data<sup>21</sup>, solid line indicates the theoretical estimation by using a previous model<sup>46</sup>.

from the leading head entering the nanogap to the end leaving it. The simulation results are distributed between  $t_d = 0.2$  ms and 0.6 ms. There is a clear peak at near  $t_d = 0.3$  ms. The distribution of  $t_d$  is mainly caused by differences in the folded structures of DNA in the nanogap, as shown in Figure 2-2. In the experiment<sup>21</sup>,  $t_d$  was measured by electrical signals and resulted in 0.5 ms, corresponding to the translocation velocity of 97 bp/ $\mu$ s (33 mm/s). This coarse-grained model validated in comparison with physical properties in equilibrated bulk solution replicates  $t_d$  in the peculiar shape of nanochannel. It is confirmed that the concept of the model is valid. Furthermore, our simulation result is also in close agreement with the experimental data by the other research group<sup>16</sup>.

In a previous study<sup>46</sup>, we also developed a theoretical model to explain  $t_d$  of  $\lambda$ -DNA through the nanogap. Assuming that the whole channel is filled with 0.1 M KCl aqueous solution and then an equivalent circuit is effectively formed, the electric field strength is evaluated as on the order of  $10^5$  V/m and  $10^6$  V/m in the nanochannel and nanogap, respectively. A  $\lambda$ -DNA molecule is assumed to be sufficiently stretched, which has a 20 nm  $\times$  20 nm cross-section and length of 16.5  $\mu$ m (0.34 nm  $\times$  48.5 kbp). According to the theoretical model, the translocation velocity is estimated as 107 bp/ $\mu$ s (37 mm/s)<sup>46</sup>. That is, it takes  $t_d = 0.46$  ms to pass through the 200 nm length nanogap (shown by solid line in Figure 2-5). This evaluation also agrees with the experimental result<sup>21</sup>. On the other hand, there were some assumptions due to the ambiguity of molecular configurations in the narrow channels. The Langevin dynamics simulation clarifies that a subchain, which passes the entrance of nanochannel, tends to diffuse in the channel and form some folded structures as shown in Figure 2-2. This result may support the limitation of the theoretical picture.

In a previous experimental study<sup>37</sup>, the electrophoretic mobility of  $\lambda$ -DNA passing through a slit of submicron height was measured. The height was varied, such as 330 nm, 430 nm, and 650 nm, and the electrophoretic mobility resulted in  $3.25 \times 10^{-8}$  Vs/m<sup>2</sup>,  $4.28 \times 10^{-8}$  Vs/m<sup>2</sup>, and  $8.87 \times 10^{-8}$  Vs/m<sup>2</sup>, respectively. The other dimensions in the device were much larger than the radius of gyration of  $\lambda$ -DNA. That is, the mobility of DNA is clearly modulated by the one-dimensional confinement. We can roughly estimate the velocity in the electric field of  $1 \times 10^6$  ( $1 \times 10^5$ ) V/m and then, the translocation velocity is concluded as 33 (3.3) mm/s, 43 (4.3) mm/s, and 89 (8.9) mm/s for the channel height of 330 nm, 430

nm, and 650 nm, respectively. Although the degree of the confinement may be different from the present system, it is implied that the magnitude of electric field strength reaches  $10^5$  V/m in the nanochannel and  $10^6$  V/m in the nanogap.

Figure 2-6 shows the histogram of waiting time which is measured in both *cis* and *trans* channels. In the *cis* side, the waiting time is defined as a duration in which the mass center of DNA chain moves from the entrance of nanochannel to that of nanogap in the *cis* side and from the exit of nanogap to that of nanochannel in the *trans* side. It is found that it takes longer period in the *cis* channel than that in the *trans*. In the *cis* channel, the molecule is forced to deform in order to enter the narrow channel at the microchannel/nanochannel and nanochannel/nanogap interfaces. In addition, the preceding beads tend to be jammed in the nanogap as the following beads successively come into. On the other hand, in the *trans* channel, the beads leave the nanogap and can form another stable structure in the open

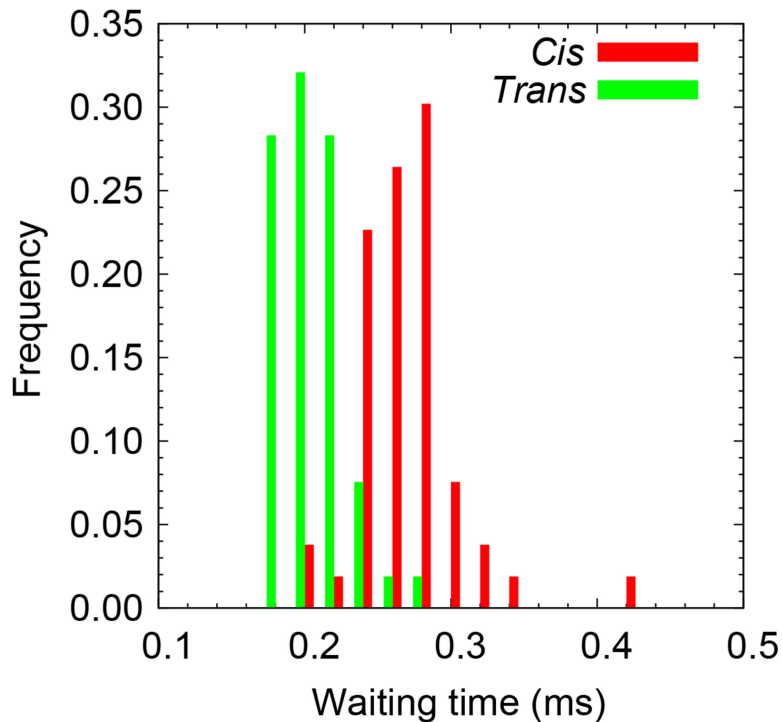


**Figure 2-6.** Histogram of waiting time on the *cis* and *trans* sides of nanochannel: duration time of the mass center of  $\lambda$ -DNA model moving from the nanochannel entrance to the nanogap entrance in the *cis* or from the nanogap exit to the nanochannel exit in the *trans*. Total amount of counts is 50 for each.

space of nanochannel. The beads are enhanced to move forward, being pushed by the following beads. Asymmetry between the *cis* and *trans* channels is indicated with respect to the electrokinetic transport of long-chained molecules.

Figure 2-7 presents the volume exclusion ratio in the nanogap, where the number of beads in the nanogap region is counted and the corresponding volume  $\Omega_{\text{dsDNA}}$  of the DNA is excluded from the volume  $\Omega_{\text{nanogap}}$  of the nanogap. Here, the single bead is empirically set to a 5 nm radius sphere according to  $\sigma$  which is determined from an assumption that the DNA can translocate a 10 nm diameter nanopore by an unfold form. Cases of “Fast”, “Intermediate”, and “Slow” in Figure 2-7 indicate the simulation results from  $t_d = 0.21$ , 0.32, and 0.55 ms, respectively. The volume exclusion seems to be apparent as the translocation time becomes shorter. Drastic decreases and some peaks can be recognized especially in the cases of “Fast” and “Intermediate”. This is due to folded configurations or

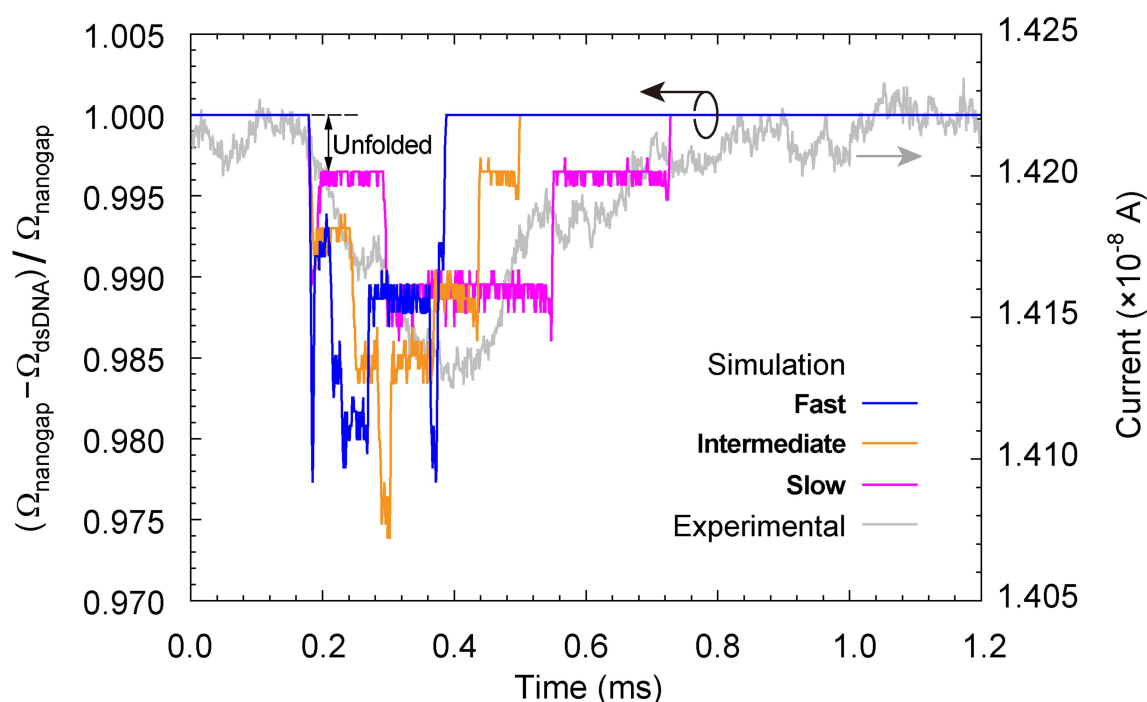


**Figure 2-7.** Transition of residual volume ratio in nanogap:  $(\Omega_{\text{nanogap}} - \Omega_{\text{dsDNA}}) / \Omega_{\text{nanogap}}$ , where  $\Omega_{\text{nanogap}}$  and  $\Omega_{\text{dsDNA}}$  are the volume of nanogap and DNA beads in the nanogap, respectively. Three cases, “Fast”, “Intermediate”, and “Slow”, correspond to  $t_d = 0.21$ , 0.32, and 0.55 ms, respectively and typical ionic current decrease due to the translocation of  $\lambda$ -DNA through the nanogap is presented as experimental<sup>46</sup>.

aggregation of DNA in the nanogap. From the result of case “Slow”, the broad distribution is relevant to the moderate volume exclusion due to unfolding of the entanglement. These phenomena correspond to the ionic current decrease in the experimental measurement as shown in Figure 2-7, in which DNA in the nanogap suppresses the background ionic current. The time scale of the electrical signal can be replicated by the simulations, even though the absolute value of the current decrease may not be compared directly due to the limitation of coarse-grained models. As mentioned above, the computational result can feature the experimental observation and it is concluded that the ionic current response is actually affected by the DNA translocation through the nanogap.

In this study, electrokinetic transport of DNA was discussed focusing on strong electric fields in a nanopore and a stepwise structure of micro/nano-fluidic channels. These two factors are essentially important to control the translocation properties of DNA. Although some effects, such as charge distributions of electrolytes, ionic current density, screening of surfaces, and electroosmosis, are neglected here, we are also recognizing that the behavior of electrolyte ions should be explicitly expressed in the model to clarify the phenomenon in more detail. Our challenging work will be continued to achieve a deeper understanding of electrokinetic transport of DNA in confined nanospaces.

## 2.4 Conclusion

We performed the Langevin dynamics simulation for electrokinetic transport of  $\lambda$ -DNA through a nanogap mounted in a nanochannel by the application of coarse-grained bead-spring model, which required a time scale of one millisecond. It was verified that our model correctly replicated the transport properties of DNA in terms of the diffusion coefficient and electrophoretic mobility. The translocation time through the nanogap was in close agreement with previous experimental<sup>21</sup> and theoretical<sup>46</sup> results. Furthermore, it was indicated that  $\lambda$ -DNA could penetrate the nanochannel and nanogap changing its configurations due to the drastic change of electric fields in the stepwise channel connections. Asymmetry in the transport dynamics between the *cis* and *trans* channels was discussed by means of the force profile and waiting time. The ionic current response in the translocation time was also clarified by our dynamical simulations. Fundamentals of

electrokinetic transport of DNA in excessively confined spaces were concretely understood in comparison with previous studies. We could find that the long-chained molecule was uncoiled and unfolded during the translocation process passing through the narrow gap. That is, applications of the present nanofluidic structure are expected for single base sequencing of DNA, although fine tuning may be required to achieve further high precision.

## Reference

1. J. Kasianowicz, E. Brandin, D. Branton, and D. W. Deamer, "Characterization of individual polynucleotide molecules using a membrane channel," *Proc. Natl. Acad. Sci. U.S.A.* **93**, 13770 (1996).
2. C. Dekker, "Solid-state nanopores," *Nat. Nanotechnol.* **2**, 209 (2007).
3. D. Branton, D. W. Deamer, A. Marziali, H. Bayley, S. A. Benner, T. Butler, M. Di Ventra, S. Garaj, A. Hibbs, X. Huang, S. B. Jovanovich, P. S. Krstic, S. Lindsay, X. S. Ling, C. H. Mastrangelo, A. Meller, J. S. Oliver, Y. V. Pershin, J. M. Ramsey, R. Riehn, G. V. Soni, V. Tabard-Cossa, M. Wanunu, M. Wiggin, and J. A. Schloss, "The potential and challenges of nanopore sequencing," *Nat. Biotechnol.* **26**, 1146 (2008).
4. M. Zwolak and M. Di Ventra, "Colloquium: Physical approaches to DNA sequencing and detection," *Rev. Mod. Phys.* **80**, 141 (2008).
5. J. Clarke, H. C. Wu, L. Jayasinghe, A. Patel, S. Reid, and H. Bayley, "Continuous base identification for single-molecule nanopore DNA sequencing," *Nat. Nanotechnol.* **4**, 265 (2009).
6. J.-L. Viovy, "Electrophoresis of DNA and other polyelectrolytes: Physical mechanisms," *Rev. Mod. Phys.* **72**, 813 (2000).
7. G. W. Slater, C. Holm, M. V. Chubynsky, H. W. de Haan, A. Dubé, K. Grass, O. A. Hickey, C. Kingsbury, D. Sean, T. N. Shendruk, L. Zhan, "Modeling the separation of macromolecules: A review of current computer simulation methods," *Electrophoresis* **30**, 792 (2009).
8. K. D. Dorfman, "DNA electrophoresis in microfabricated devices," *Rev. Mod. Phys.* **82**, 2903 (2010).
9. B. M. Venkatesan and R. Bashir, "Nanopore sensors for nucleic acid analysis," *Nat. Nanotechnol.* **6**, 615 (2011).
10. A. Meller, L. Nivon, E. Brandin, J. Golovchenko, and D. Branton, "Rapid nanopore discrimination between single polynucleotide molecules," *Proc. Natl. Acad. Sci. U.S.A.* **97**, 1079 (2000).
11. A. Meller, L. Nivon, and D. Branton, "Voltage-driven DNA translocations through a nanopore," *Phys. Rev. Lett.* **86**, 3435 (2001).
12. A. Meller, and D. Branton, "Single molecule measurements of DNA transport through a nanopore," *Electrophoresis*. **23**, 2583 (2002).

13. J. Li, M. Gershow, D. Stein, E. Brandin, and J. A. Golovchenko, "DNA molecules and configurations in a solidstate nanopore microscope," *Nature Materials*. **2**, 611 (2003).
14. A. J. Storm, C. Storm, J. Chen, H. Zandbergen, J.-F. Joanny, and C. Dekker, "Fast DNA translocation through a solid-state nanopore," *Nano Lett.* **5**, 1193 (2005).
15. X. Liang and S. Y. Chou, "Nanogap detector inside nanofluidic channel for fast real-time label-free DNA analysis," *Nano Lett.* **8**, 1472 (2008).
16. G. M. Skinner, M. van den Hout, O. Broekmans, C. Dekker, and N. H. Dekker, "Distinguishing single- and double-stranded nucleic acid molecules using solid-state nanopores," *Nano Lett.* **9**, 2953 (2009).
17. K. R. Lieberman, G. M. Cherf, M. J. Doody, F. Olasagasti, Y. Kolodji, and M. Akeson, "Processive replication of single DNA molecules in a nanopore catalyzed by phi29 DNA polymerase," *J. Am. Chem. Soc.* **132**, 17961 (2010).
18. G. F. Schneider, S. W. Kowalczyk, V. E. Calado, G. Pandraud, H. W. Zandbergen, L. M. L. Vandersypen, and C. Dekker, "DNA translocation through graphene nanopores," *Nano Lett.* **10**, 3163 (2010).
19. D. Fologea, J. Uplinger, B. Thomas, D. S. McNabb, and J. Li, "Slowing DNA translocation in a solid-state nanopore," *Nano Lett.* **5**, 1734 (2005).
20. D. Fologea, M. Gershow, B. Ledden, D. S. McNabb, J. A. Golovchenko, and J. Li, "Detecting single stranded DNA with a solid state nanopore," *Nano Lett.* **5**, 1905 (2005).
21. M. Tsutsui, Y. He, M. Furuhashi, S. Rahong, M. Taniguchi, and T. Kawai, "Transverse electric field dragging of DNA in a nanochannel," *Sci. Rep.* **2**, 394 (2012).
22. J. Lagerqvist, M. Zwolak, and M. Di Ventra, "Fast DNA sequencing via transverse electronic transport," *Nano Lett.* **6**, 779 (2006).
23. M. Tsutsui, M. Taniguchi, K. Yokota, and T. Kawai, "Identifying single nucleotides by tunnelling current," *Nat. Nanotechnol.* **5**, 286 (2010).
24. T. Ohshiro, K. Matsubara, M. Tsutsui, M. Furuhashi, M. Taniguchi, and T. Kawai, "Single-molecule electrical random resequencing of DNA and RNA," *Sci. Rep.* **2**, 501 (2012), doi: 10.1038/srep00501.
25. W. Sung and P. J. Park, "Polymer translocation through a pore in a membrane," *Phys. Rev. Lett.* **77**, 783 (1996).
26. M. Muthukumar, "Polymer translocation through a hole," *J. Chem. Phys.* **111**, 10371 (1999).

27. O. V. Krasilnikov, C. G. Rodrigues, and S. M. Bezrukov, "Single polymer molecules in a protein nanopore in the limit of a strong polymer-pore attraction," *Phys. Rev. Lett.* **97**, 018301 (2006).
28. I. Huopaniemi, K. Luo, T. Ala-Nissila, and S.-C. Ying, "Langevin dynamics simulations of polymer translocation through nanopores," *J. Chem. Phys.* **125**, 124901 (2006).
29. I. Huopaniemi, K. Luo, T. Ala-Nissila, and S.-C. Ying, "Polymer translocation through a nanopore under a pulling force," *Phys. Rev. E.* **75**, 061912 (2007).
30. C. Forrey and M. Muthukumar, "Langevin dynamics simulations of ds-DNA translocation through synthetic nanopores," *J. Chem. Phys.* **127**, 015102 (2007).
31. K. F. Luo, A. Ala-Nissila, S.-C. Ying, and A. Bhattacharya, "Sequence dependence of DNA translocation through a nanopore," *Phys. Rev. Lett.* **100**, 058101 (2008).
32. K. Luo, A. Ala-Nissila, S.-C. Ying, and A. Bhattacharya, "Dynamics of DNA translocation through an attractive nanopore," *Phys. Rev. E.* **78**, 061911 (2008).
33. V. V. Lehtola, R. P. Linna, and K. Kaski, "Dynamics of forced biopolymer translocation," *EPL.* **85**, 58006 (2009).
34. W. G. Noid, "Perspective: Coarse-grained models for biomolecular systems," *J. Chem. Phys.* **139**, 090901 (2013).
35. J. P. K. Doye, T. E. Ouldridge, A. A. Louis, F. Romano, P. Šulc, C. Matek, B. E. K. Snodin, L. Rovigatti, J. S. Schreck, R. M. Harrison, and W. P. J. Smith, "Coarse-graining DNA for simulations of DNA nanotechnology," *Phys. Chem. Chem. Phys.* **15**, 20395 (2013).
36. A. Ramachandran, Q. Guo, S. M. Iqbal, and Y. Liu, "Coarse-grained molecular dynamics simulation of DNA translocation in chemically modified nanopores," *J. Phys. Chem. B.* **115**, 6138 (2011).
37. S. Uehara, H. Shintaku, and S. Kawano, "Electrokinetic flow dynamics of weakly aggregated  $\lambda$ DNA confined in nanochannels," *Trans. ASME., J. Fluids Eng.* **133**, 121203 (2011).
38. T. Yasui, S. Rahong, K. Motoyama, T. Yanagida, Q. Wu, N. Kaji, M. Kanai, K. Doi, K. Nagashima, M. Tokeshi, M. Taniguchi, S. Kawano, T. Kawai, and Y. Baba, "DNA manipulation and separation in sublithographic-scale nanowire array," *ACS Nano.* **7**, 3029 (2013).
39. S. Nagahiro, S. Kawano, and H. Kotera, "Separation of long DNA chains using a

- nonuniform electric field: A numerical study,” *Phys. Rev. E*. **75**, 011902 (2007).
40. K. Doi, T. Haga, H. Shintaku, and S. Kawano, “Development of coarse-graining DNA models for single-nucleotide resolution analysis,” *Philos. Trans. R. Soc. A*. **368**, 2615 (2010).
  41. K. Doi, T. Yonebayashi, and S. Kawano, “Perturbation theory analysis for electronic response of DNA base pairs,” *J. Mol. Struct.: THEOCHEM*. **939**, 97 (2010).
  42. K. Doi, T. Uemura, and S. Kawano, “Molecular dynamics study of solvation effect on diffusivity changes of DNA fragments,” *J. Mol. Model.* **17**, 1457 (2011).
  43. K. Doi, M. Ueda, and S. Kawano, “Theoretical model of nanoparticle detection mechanism in microchannel with gating probe electrodes,” *J. Comput. Sci. Tech.* **5**, 78 (2011).
  44. K. Doi, Y. Nishioka, and S. Kawano, “Theoretical study of electric current in DNA base molecules trapped between nanogap electrodes,” *Comput. Theor. Chem.* **999**, 203 (2012).
  45. P. Szarek, S. Suwannawong, K. Doi, and S. Kawano, “Theoretical study on physicochemical aspects of a single molecular junction: application to the bases of ssDNA,” *J. Phys. Chem. C*. **117**, 10809 (2013).
  46. S. Uehara, M. Tsutsui, K. Doi, M. Taniguchi, S. Kawano, and T. Kawai, “Fluid dynamics and electrical detection of  $\lambda$ DNA in electrode-embedded nanochannels,” *J. Biomech. Sci. Eng.* **8**, 244 (2013).
  47. M. G. Gauthier, G. W. Slater, “Molecular dynamics simulation of a polymer chain translocating through a nanoscopic pore,” *Eur. Phys. J. E*. **25**, 17 (2008).
  48. C. M. Edmonds, Y. C. Hudiono, A. G. Ahmadi, P. J. Hesketh, and S. Nair, “Polymer translocation in solid-state nanopores: Dependence of scaling behavior on pore dimensions and applied voltage,” *J. Chem. Phys.* **136**, 065105 (2012).
  49. M. Fyta, S. Melchionna, S. Succi, and E. Kaxiras, E. “Hydrodynamic correlations in the translocation of a biopolymer through a nanopore: Theory and multiscale simulations,” *Phys. Rev. E*. **78**, 036704 (2008).
  50. K. Luo and R. Metzler, “The chain sucker: Translocation dynamics of a polymer chain into a long narrow channel driven by longitudinal flow,” *J. Chem. Phys.* **134**, 135102 (2011).
  51. D. E. Smith, T. T. Perkins, and S. Chu, “Dynamical scaling of DNA diffusion coefficients,” *Macromol.* **29**, 1372 (1996).

52. M. G. Gauthier, G. W. Slater, "Molecular dynamics simulation of a polymer chain translocating through a nanoscopic pore," *Eur. Phys. J. E.* **25**, 17 (2008).
53. A. Izmitli, D. C. Schwartz, M. D. Graham, J. J. de Pablo, "The effect of hydrodynamic interactions on the dynamics of DNA translocation through pores," *J. Chem. Phys.* **128**, 085102 (2008).
54. R. B. Schoch, J. Han, P. Renaud, "Transport phenomena in nanofluidics," *Rev. Mod. Phys.* **80**, 839 (2008).
55. Femtet®, Murata Software Co., Ltd., Tokyo, Japan (2013).
56. X. Zhao, C. M. Payne, and P. T. Cummings, "Controlled Translocation of DNA segments through nanoelectrode gaps from molecular dynamics," *J. Phys. Chem. C.* **112**, 8 (2008).
57. S. van Dorp, U. F. Keyser, N. H. Dekker, C. Dekker, and S. G. Lemay, "Origin of the electrophoretic force on DNA in solid-state nanopores," *Nat. Phys.* **5**, 347 (2009).
58. B. Luan, G. Stolovitzky, and G. Martyna, "Slowing and controlling the translocation of DNA in a solid-state nanopore," *Nanoscale.* **4**, 1068 (2012).
59. M. Zhang, L.-H. Yeh, S. Qian, J.-P. Hsu, and S. W. Joo, "DNA electrokinetic translocation through a nanopore: Local permittivity environment effect," *J. Phys. Chem. C.* **116**, 4793 (2012).
60. E. Stellwagen, Y. Lu, and N. C. Stellwagen, "Unified description of electrophoresis and diffusion for DNA and other polyions," *Biochemistry.* **42**, 11745 (2003).
61. K. Drukker, G. Wu, and G. C. Schatz, "Model simulations of DNA denaturation dynamics," *J. Chem. Phys.* **114**, 579 (2001).
62. J. Wang and H. Gao, "A generalized bead-rod model for Brownian dynamics simulations of wormlike chains under strong confinement," *J. Chem. Phys.* **123**, 084906 (2005).
63. T. A. Knotts IV, N. Rathore, D. C. Schwartz, J. J. de Pablo, "A coarse grain model for DNA," *J. Chem. Phys.* **126**, 084901 (2007).
64. S. P. Mielke, N. Gronbech-Jensen, and C. J. Benham, "Brownian dynamics of double-stranded DNA in periodic systems with discrete salt," *Phys. Rev. E.* **77**, 031924 (2008).

# Chapter 3

## *Analysis of ssDNA Translocation through Nanopore*

### 3.1 Introduction

The high-speed reading of deoxyribonucleic acid (DNA) sequences is an important means of elucidating complete genetic sequences, and may enable the development of new medical treatments<sup>1,2</sup>. Recently, novel DNA and ribonucleic acid (RNA) sequencing technologies have been developed. Among these, nanopore sequencing devices are one of the most significant and represent an emerging non-optical process for high-throughput single-molecule detection<sup>1-4</sup>, in which individual nucleobases are identified based on size by measuring transpore ionic current blockade<sup>5-7</sup> or transverse tunneling current<sup>8-11</sup> during the transport of single-stranded DNA (ssDNA) through a nanometer-sized gap. Understanding biological polymer transport phenomena is a crucial issue in the development of DNA sequencing techniques, as well as in the study of many of the physical properties of polymers<sup>12</sup>, and both the theoretical<sup>13-17</sup> and experimental<sup>18-28</sup> aspects of polymer translocation through nanopores have been widely studied. Computational studies have provided particularly valuable insights into the physics of transport within confined micro/nanochannels and previous works have examined the variation of translocation time with polymer chain length<sup>13-15,19,21,29-31</sup>, pore dimensions<sup>31</sup>, driving force<sup>19,15,21,31</sup>, sequences and secondary structures<sup>21,22,32</sup>, polymer-pore

interactions<sup>21–23,33</sup>, and polymer configurations<sup>15,34</sup>. Table 3-1 lists the various nanopore devices and polymers used in the pioneering research studies investigating these subjects with the aim of achieving an advanced DNA sequencer.

Sung and Park<sup>13</sup> and Muthukumar<sup>14</sup> studied the passage of single polymer molecules through the pores of a membrane during diffusion across a free energy barrier due to chemical potential differences. Both groups modeled the stochastic processes associated with the transport of long polymers based on the Fokker–Planck equation and were able to predict a scaling law describing translocation time,  $\tau$ , as a function of polymer length,  $N$ . Storm et al.<sup>22</sup> and Skinner et al.<sup>24</sup> investigated the translocation of double-stranded DNA (dsDNA) through silicon nitride (SiN) nanopores that were 10 nm in diameter and 30 nm thick. They also identified that a power law best described the relationship between  $\tau$  and the polymer length, such that  $\tau \sim N^{1.27}$ . The use of ultrathin nanopores (0.3 nm thick) fabricated within a graphene monolayer is known to result in a slightly larger  $\tau$  value than that obtained using SiN nanopores<sup>25</sup> and it has been suggested that these small pores as well as interactions with the graphene result in the slower translocation<sup>25</sup>. This phenomenon has also been investigated on the basis of Langevin dynamics simulations<sup>31,34</sup>. In other works, Meller et al.<sup>19</sup> studied the translocation of ssDNA through a biological  $\alpha$ -hemolysin ( $\alpha$ -HL)

**Table 3-1.** Nanopore devices and DNA/RNA used in published experimental studies

Group	Pore type	Diameter (nm)	Length (nm)	Voltage (mV)	Voltage/Length ( $\times 10^6$ V/m)	Polymer length (bp or nt)	Polymer type
Kasianowicz et al. [5]	$\alpha$ -HL	1.3	5.2	120	23	150	ssDNA, ssRNA*
Meller et al. [18–20]	$\alpha$ -HL	1.3	5.2	50–300	9.6–58	5–100	ssDNA
Butler et al. [35]	MspA	1	10	140, 180	14, 18	50	ssDNA
Wendell et al. [36]	Phi29	3.3	7.5	40, 75	5.3, 10	5.5k	dsDNA
Franceschini et al. [37]	ClyA	7.8	13	100	7.7	290bp, 51nt	dsDNA, ssDNA
Li et al. [21]	SiN	3, 10	5–10	60, 120	6–24	3k–10k	dsDNA
Storm et al. [22]	SiN	10	20	100–600	5–30	10k–97k	dsDNA
Skinner et al. [24]	SiN	10	20	100–600	5–30	10k–30k	dsDNA, dsRNA, ssRNA*
Tsutsui et al. [26]	SiN	50	200	1000	5	48.5k	dsDNA
Fologea et al. [27,28]	SiN	10	10, 280	120	0.43, 12	3k	dsDNA, ssDNA
Schneider et al. [25]	Graphene	22	0.3	200	670	48.5k	dsDNA

\* ssRNA denotes poly(A), poly(C), and poly(U).

nanopore and determined that the translocation velocity of short polymers exhibited a significant dependence on the length of the polymer, whereas there was no dependence in the case of long polymers. The engineered *Mycobacterium smegmatis* porin A (MSPA)<sup>35</sup> and phi29<sup>36</sup> protein nanopores were found to allow the translocation of ssDNA and dsDNA with remarkable stability against environmental stresses. It is indicated that an engineered DNA transporter is able to recognize and chaperone the specific DNA molecule across a biological membrane, making a further step for the application of nanofluidic platform<sup>37</sup>. It was also found that, during forced translocation in narrow pores, the scaling exponents depended on the driving force,  $F$ , based on the relationship  $\tau \sim F^{-1}$ <sup>15,30,31</sup>. Although the hydrodynamic effects on polymer chains appear to account for part of the force counteracting external forces<sup>13,29</sup>, these effects seem to make only a minor contribution to the transport of DNA, since it has a large number of charges and small surface areas in comparison to other polymer particles<sup>38-40</sup>. In particular, the electrokinetic transport of DNA passing through very narrow spaces is predominantly affected by collisions with channel walls<sup>41</sup>.

We are interested in a long polymer translocation mechanism in micro/nanochannels and nanopores<sup>42-44</sup> under the effects of nonuniform electric fields, since such mechanisms have not yet been sufficiently elucidated. In the present study, we attempt to gain a better understanding of the translocation mechanism of a DNA-like polymer chain, equivalent to  $48 \times 10^3$  nucleotides (48 knt), penetrating a solid-state nanopore in the presence of nonuniform electric fields, as illustrated in Figure 3-1. The cross-section of the nanopore is expected to play an important role in terms of controlling the translocation process. While nanopores embedded in nanochannels were supposed to be effective to slow down the translocation velocity of ssDNA<sup>42,44</sup>, the mechanism has remained to be clarified. Herein, focusing on the multiply-connected nanofluidic channel, the retardation process and its advantage are discussed from a theoretical point of view. As part of this work, we develop a coarse-grained ssDNA model<sup>16,45,46</sup> and perform Langevin dynamics simulations of ssDNA transport under nonuniform electric fields in a rectangular nanochannel containing a

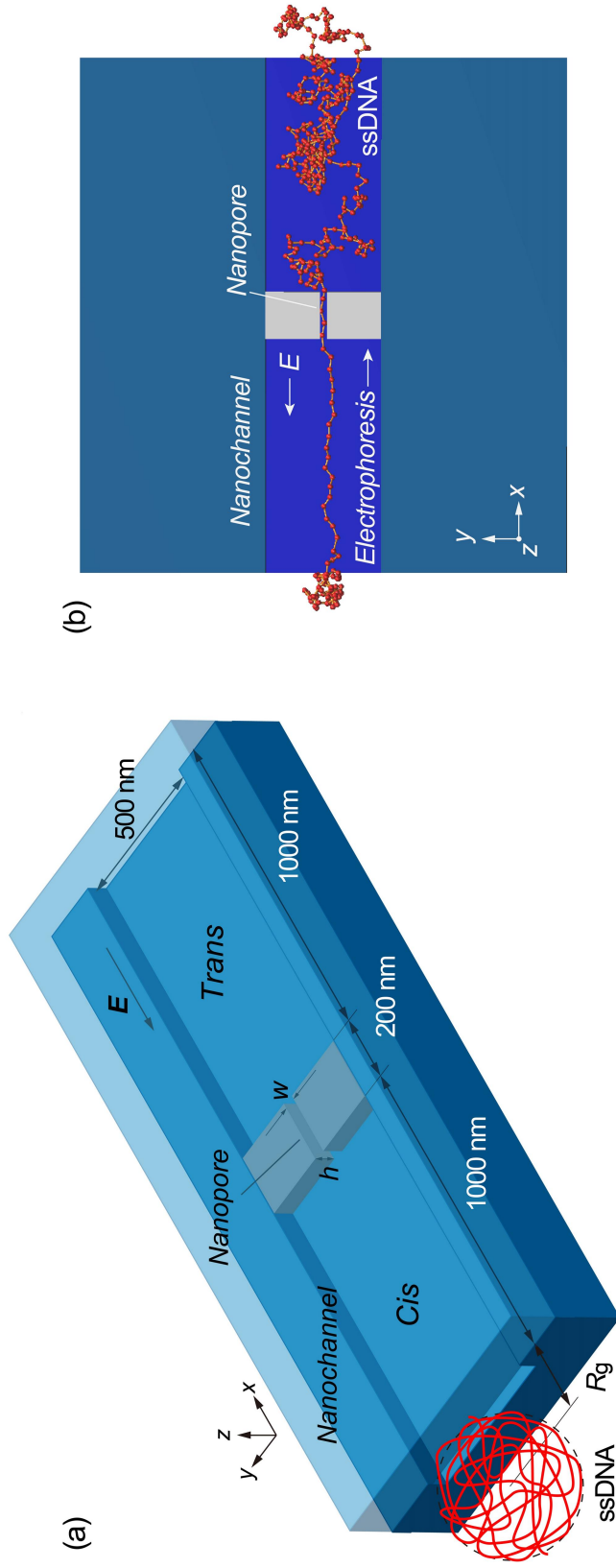


**Figure 3-1.** (a) Schematic illustration of a rectangular nanochannel used in Langevin dynamics simulations, in which a nanopore is embedded in the nanochannel. In the three-dimensional model, the width ( $w$ ) and height ( $h$ ) of a 200 nm long nanopore are varied as simulation parameters in a nanochannel of 2200 nm in length, 500 nm in width, and  $h$  in height. The center of mass of ssDNA is initially located at a distance of the radius of gyration ( $R_g = 300$  nm) away from the nanochannel entrance where the  $x$ - and  $y$ -coordinate of the mass center are in coincidence with the center of nanochannel. (b) An illustration showing the coarse-grained bead-spring model of ssDNA applied during the simulations to assess the electrokinetic transport dynamics and to optimize the structure of the nanofluidic channel for single molecule sensing.

nanopore with various cross-sections<sup>47–51</sup>, where the electric fields are calculated for the cross-sections, ranging from  $20 \times 20$  to  $50 \times 50$  nm<sup>2</sup>. The results allow a visual analysis of the electrokinetic transport dynamics of ssDNA chains and allow us to determine the most suitable morphology for nanofluidic flow channels for single molecule detection. Furthermore, the simulation results are clearly understood by a theoretical model in the framework of the Langevin equation. Consequently, a relationship among the electrokinetic transport of ssDNA, pore dimensions, and multiply-connected structures of the nanofluidic channel are clarified and a desirable design to control the translocation velocity is concluded.

## Nomenclature

$d_{\text{pore}}$	=	diameter of the pore (m)
$d_{\text{eff}}$	=	effective diameter outside the pore (m)
$D$	=	diffusion coefficient of ssDNA in free solution (m <sup>2</sup> /s)
$e$	=	elementary charge (C)
$E_{\text{channel}}$	=	electric field at the center of the nanochannel (V/m)
$E_{\text{pore}}$	=	electric field at the center of the nanopore (V/m)
$\Delta F$	=	external force on the mass center (N)
$\mathbf{F}_i$	=	external electrostatic force (N)
$h$	=	channel height (m)
$k$	=	spring constant (N/m)
$k_B$	=	Boltzmann constant (J/K)
$N$	=	number of beads
$N_{\text{nt}}$	=	number of nucleotides
$N_{\text{pore}}$	=	number of beads in the nanopore
$N_{\text{channel}}$	=	number of beads in the nanochannel
$\mathbf{n}$	=	surface normal vector
$Q_i$	=	bead charges (C)
$r_{ij}$	=	distance between the $i$ th and $j$ th particles (m)
$r_{\text{eq}}$	=	equilibrium distance between each connected pair of bead (m)
$r_{\text{nt}}$	=	equilibrium distance between the nucleotides (m)
$R_g$	=	radius of gyration of ssDNA (m)
$\mathbf{R}_i$	=	random force (N)
$T$	=	temperature (K)

$\Delta t$	=	time step (s)
$\nabla U_i$	=	conservative force (N)
$U_{\text{LJ}}$	=	Lennard–Jones potential (V)
$U_{\text{bond}}$	=	bond potential (V)
$v_0$	=	initial velocity at the entrance (m/s)
$v_G$	=	mass center velocity (m/s)
$w$	=	channel width (m)
$x_G$	=	position of mass center along the $x$ -axis (m)

**Greek Symbols**

$\delta_{ij}$	=	Kronecker's delta
$\delta(t - t')$	=	Dirac delta function
$\zeta$	=	friction coefficient of bead (kg/s)
$\mu$	=	electrophoretic mobility of ssDNA ( $\text{m}^2/\text{Vs}$ )
$\sigma$	=	persistence length of ssDNA (m)
$\phi$	=	electrostatic potential (V)
$\omega$	=	well-depth of Lennard-Jones potential (kJ/mol)

### 3.2 Computational methods

A Langevin dynamics simulation was applied to investigate the behavior of a polymer chain passing through a three-dimensional nanopore embedded in a nanochannel, where the presence of solvent molecules could effectively be treated as a random force acting on the coarse-grained polymer molecule<sup>16,45,46</sup>. In the present model, strong effects of intramolecular interactions on the inertial force were coarse-grained and the kinetics of ssDNA was mainly affected by external electric fields. In such a case, the behavior of a particle can be expressed by an over-damped Langevin equation:<sup>16,45,46</sup>

$$\zeta_i \mathbf{v}_i = -\nabla U_i + \mathbf{F}_i + \mathbf{R}_i \quad (3-1)$$

where  $\zeta_i$  is the friction coefficient of the  $i$ th particle,  $-\nabla U_i$  is the conservative force, including interactions between particles, and  $\mathbf{F}_i$  denotes the external electrostatic force, such that  $\mathbf{F}_i = -Q_i \nabla \phi$ , where  $Q_i$  is the electric charge on the polymer molecule. For the purposes of a three-dimensional simulation, the electric potential  $\phi$ , in a rectangular nanofluidic channel was analyzed by solving for the Laplace equation  $\nabla^2 \phi = 0$  with Neumann boundary conditions  $\mathbf{n} \cdot \nabla \phi = 0$  at the sidewall surfaces, where  $\mathbf{n}$  was the surface normal vector, and with constant electric potentials at both ends of the channel. The FEM<sup>53</sup> was employed to solve for the electric potential.  $\mathbf{F}_i$  was calculated by averaging the gradient of  $\phi$  around each position<sup>46</sup>. In Equation 3-1, the random force  $\mathbf{R}_i$  satisfies the fluctuation-dissipation theorem, such that

$$\begin{cases} \langle \mathbf{R}_i(t) \rangle = 0, \\ \langle \mathbf{R}_i(t) \cdot \mathbf{R}_j(t') \rangle = 6k_B T \zeta_i \delta_{ij} \delta(t-t'), \end{cases} \quad (3-2)$$

where  $k_B$  is the Boltzmann constant,  $T$  is temperature,  $\delta_{ij}$  is Kronecker's delta and  $\delta(t-t')$  is the Dirac delta function where  $t$  and  $t'$  are time. In this study, we focused on ssDNA and developed a bead-spring model for use in the Langevin dynamics simulations. Details of our coarse-grained model are also described in previous studies<sup>16,45,46</sup>. In order to model a ssDNA consisting of 48,000 nucleotides (48 knt), neighboring beads were connected with a harmonic spring<sup>46</sup> :

$$U_{\text{bond}}(\mathbf{r}_i) = \begin{cases} \frac{1}{2} \sum_j k (r_{ij} - r_{\text{eq}})^2 & \text{for neighbors,} \\ 0 & \text{otherwise,} \end{cases} \quad (3-3)$$

where  $k$  was the spring constant and  $r_{ij}$  was the distance between the  $i$ th and  $j$ th particles. The equilibrium distance,  $r_{\text{eq}}$ , between each connected pair of beads was defined as  $r_{\text{eq}} = \alpha r_{\text{nt}} N_{\text{nt}} / N$ , where  $\alpha$  was a variable parameter,  $N_{\text{nt}}$  was the number of nucleotides, and  $N$  was the number of beads. The equilibrium distance between the nucleotides in ssDNA is known to be  $r_{\text{nt}} = 0.43 \text{ nm}$ <sup>59</sup> and so, applying an  $\alpha$  value of 0.847<sup>16</sup>,  $N_{\text{nt}} = 48,000$ , and  $N = 400$ , we obtained  $r_{\text{eq}} = 43.7 \text{ nm}$ . The above value for the parameter  $\alpha$  was selected so as to properly replicate the radius of gyration ( $R_g$ ) of ssDNA<sup>60</sup>, as well as the diffusion coefficient and electrophoretic mobility. The harmonic spring constant was calculated as  $k = k_B T / \chi^2$ , where  $T$  was set to 300 K and a  $\chi$  value of  $0.1\sigma$  was applied for thermal fluctuations based on previous studies<sup>45</sup>, where  $\sigma$  was a Lennard–Jones parameter described below. Interactions between two beads or between a bead and a channel wall were represented by the Lennard–Jones potential,  $U_{\text{LJ}}$ , taking into account the volume exclusion effect:<sup>46</sup>

$$U_{\text{LJ}}(\mathbf{r}_i) = \begin{cases} \sum_{\substack{j=1 \\ j \neq i}}^N 4\omega \left[ \left( \frac{\sigma}{r_{ij}} \right)^{12} - \left( \frac{\sigma}{r_{ij}} \right)^6 \right] + \omega & \text{for } r_{ij} \leq 2^{1/6} \sigma, \\ 0 & \text{for } r_{ij} > 2^{1/6} \sigma, \end{cases} \quad (3-4)$$

where  $\sigma$  was the characteristic length of ssDNA, and  $\omega$  was the energy well-depth. A mirror reflection was assumed, meaning that the repulsive force from the wall effectively worked only along the direction perpendicular to the surface. The length parameter,  $\sigma$ , was determined from the persistence length of ssDNA necessary to reproduce the volume effect, such that  $\sigma = 5 \text{ nm}$ <sup>59</sup>.  $U_{\text{LJ}}$  was applied to non-adjacent beads and  $\omega$  was set to  $k_B T$ <sup>16,46</sup>. For the purposes of volume exclusion, the potential was truncated at  $r = \sqrt[6]{2}\sigma$  to allow for purely repulsive interactions between the beads. The term  $\zeta_i$  in Equations 3-1 and 3-2 was evaluated based on experimental measurements of the ssDNA diffusion coefficient,  $D_i$ , according to  $N\zeta_i D_i = k_B T$ <sup>52</sup>. Applying  $N = 400$ ,  $D_i = 2.21 \times 10^{-12} \text{ m}^2/\text{s}$ , and  $T = 300 \text{ K}$ ,  $\zeta_i$  was determined to be  $4.68 \times 10^{-12} \text{ kg/s}$  for each bead. Considering the existence of counterions around the ssDNA, the effective charge of an individual bead could be calculated according to  $Q_i = \zeta_i \mu_i = \mu_i k_B T / N D_i$ <sup>52</sup>. Thus, based on the experimental value of  $\mu = 2.84 \times 10^{-8} \text{ m}^2/\text{Vs}$ <sup>52</sup>, a  $Q_i$  value resulted in  $-0.83e$  per bead (consisting 120 nt), where  $e$  is the elementary charge. This value was determined in terms of electrophoretic mobility of the

coarse-grained ssDNA including counterions and thus, it might underestimate the monomer charge previously known<sup>58,61</sup>. In order to verify this quantity, we performed Langevin dynamics simulations for the ssDNA model in free solution.

As a result of the Langevin dynamics simulation, Figure 3-2(a) shows the mean square displacement of the center of mass of the ssDNA model as a function of time. This plot represents the average of results from 90 simulations at each data point and is clearly linear. The associated diffusion coefficient,  $D$ , can be obtained according to the Einstein relation and is calculated to be  $2.25 \times 10^{-12} \text{ m}^2/\text{s}$ . Figure 3-2(b) presents a plot of the distance from the origin to the center of mass under an external electric field of  $1 \times 10^6 \text{ V/m}$ , in which each data point is the average of 270 simulations. The electrophoretic mobility calculated from the ratio of the velocity values to the applied electric field strengths is  $\mu = 2.87 \times 10^{-8} \text{ m}^2/\text{Vs}$ . From the viewpoint of diffusivity and electrophoretic mobility, the present parameter set is therefore acceptable when assessing the electrokinetic transport of ssDNA.

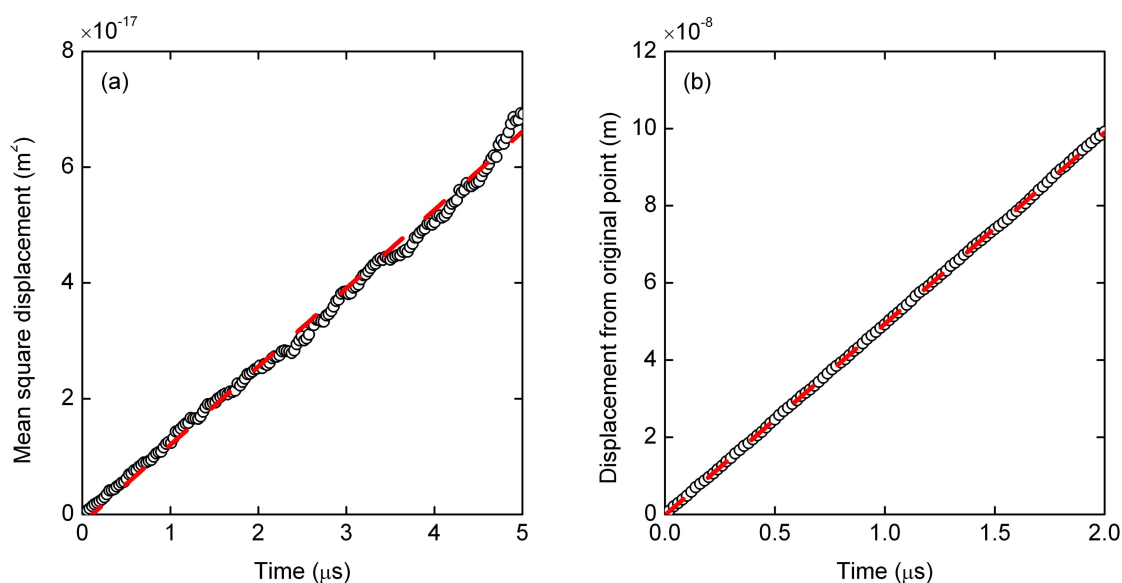


**Figure 3-2.** (a) Mean square displacement of the bead-spring model resulting from 90 simulation runs and (b) displacement of the mass center of the bead-spring chain under an electric field of  $1 \times 10^6 \text{ V/m}$  obtained from 270 simulation runs. Each result is well fitted with straight lines by the least-squares method. The slope of plot (a) corresponds to the diffusion coefficient while that of (b) is the velocity that translates to the electrophoretic mobility.

The overall structure of the fluidic channel, including the reservoirs outside the nanochannel, was taken into account in the preliminary analysis, as shown in Figure 3-3(a). There was a reservoir of  $2.5 \mu\text{m} \times 4.0 \mu\text{m} \times 0.5 \mu\text{m}$  (length  $\times$  width  $\times$  height) on either side of the nanochannel and the electrodes were  $2.5 \mu\text{m}$  from the nanochannel entrance. The electric potentials at the electrodes were set to  $-0.400$  and  $0.400$  V at the *cis* and *trans* sides, respectively, based on the experimental conditions summarized in Table 3-1. Additionally, the Laplace equation was solved in the nanochannel and nanopore with a fine resolution of  $10$  nm.

At equilibrium,  $R_g$  was maintained in the vicinity of  $300$  nm, such that  $R_g^2$  was approximately equal to the product of the persistence length and the contour length<sup>59,62</sup>. Stable configurations such as this were employed as initial conditions for the simulations. The center of mass of the ssDNA was initially placed at a distance equivalent to  $R_g$  from the entrance of the nanochannel, as presented schematically in Figure 3-1(a). In the next stage, the nonuniform electric field resulting from the FEM analysis was applied and the trajectories of the ssDNA were tracked. Equation 3-1 was integrated using the Euler algorithm with time steps of  $\Delta t = 10$  ps<sup>46</sup>.

### 3.3 Results and discussion

#### 3.3.1 Non-uniform electric field inside nanopore

As shown in Figure 3-3, electrostatic potentials across the microchannel, nanochannel, and nanopore are determined from the finite element method (FEM) analysis<sup>53</sup>, in which the potential curves extracted along the central axis are presented for several nanopore cross-sections. It is found that the slope of the electrostatic potential becomes steeper in the narrower channels, as shown in Figures 3-3(a) and 3-3(b). A large drop in the potential at the nanopore suppresses the potential difference outside the nanopore. As can be seen from Figure 3-3(c), the electric field strength increases as the cross-sectional area of the nanopore is reduced. The electric field strengths calculated along the central axis of the nanochannel and nanopore with various cross-sections are also summarized in Table 3-2. In the previous experimental studies summarized in Table 3-1, as well as in numerical analyses, other

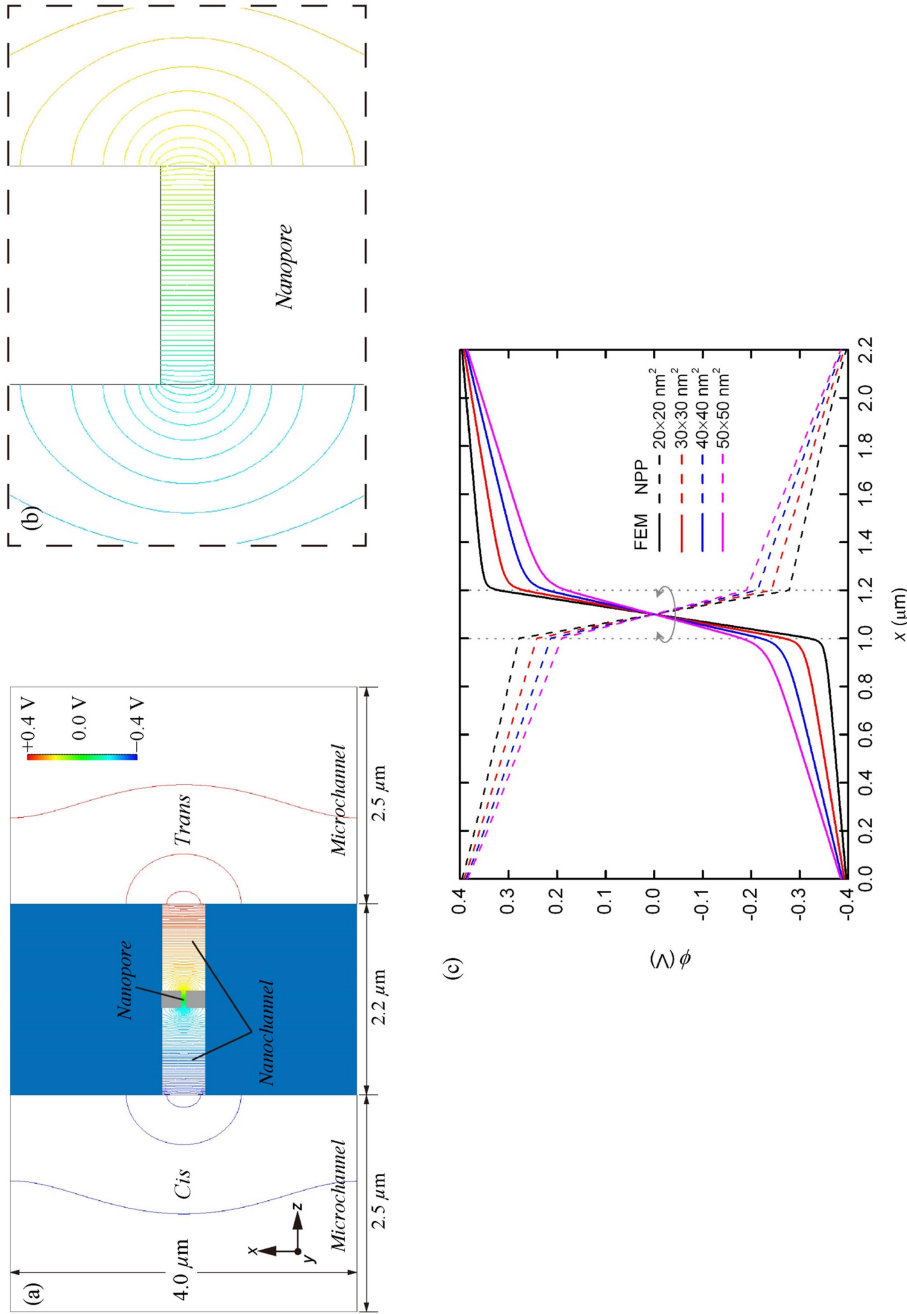


**Figure 3-3.** (a) Electrostatic potential resulting from FEM analysis for the system including microchannel, nanopore, and nanopore whose cross-section is  $50 \times 50 \text{ nm}^2$ . (b) Magnified view of (a) focusing on near the nanopore. (c) Electrostatic potentials,  $\phi$ , for nanopores of cross-section  $20 \times 20$ ,  $30 \times 30$ ,  $40 \times 40$ , and  $50 \times 50 \text{ nm}^2$ , resulting from three-dimensional FEM analyses. The entrance and exit of the nanopores are indicated by the dotted lines.

researchers have also found that strong electric fields are associated with nanopores<sup>54</sup>. Some publications note that this strong electric field tends to be proportional to the value of  $(d_{\text{pore}} / d_{\text{eff}})^2$ , where  $d_{\text{pore}}$  is the diameter of the pore and  $d_{\text{eff}}$  is the effective diameter outside the pore<sup>54,55</sup>. Our computational results also agree with the potential drop resulting from variations in the nanopore cross-section.

### 3.3.2 ssDNA translocation conformation

As shown in Figure 3-4(a), we also ascertained the number of beads along a 200 nm long nanopore during the simulations. In this figure, the entire data set resulting from 20 simulation runs for a  $30 \times 30 \text{ nm}^2$  cross-section nanopore is presented. At  $t = 0 \text{ s}$ , a leading bead entered the pore, at which point the elapsed time was tracked until the end of the chain left the pore. The distribution of bead numbers seems to be discretized at several specific numerical values. As can be seen in the insets to this figure, which show illustrations of the nanopore, the discretized numbers correspond to specific folded structures of the polymer chain. Sufficiently uncoiled ssDNA chains tend to pass through the nanopore in an unfolded form and therefore, the translocation time is relatively long. In contrast, coiled chains adopt folded forms in the pore, resulting in shorter translocation periods. Figure 3-4(b) presents a summary of the data in Figure 3-4(a) in the form of a histogram. The highest peak in this plot corresponds to an unfolded structure, while the second and third highest peaks equate to 1- and 2-fold forms, respectively. More detailed illustrations of the unfolded, 1-fold, and 2-fold forms at the nanopore are also presented in Figures 3-4(c) to 3-4(e), respectively. Figures 3-5(a) and 3-5(b) show the results for  $40 \times 40$  and  $50 \times 50 \text{ nm}^2$  cross-section nanopores, respectively, where four typical samples are presented by color variations. The time series data in the plots apparently fluctuate with increasing cross-sectional areas. The larger the cross-sections become, the more frequently the ssDNA will change its configuration, thus producing multifold forms in the pore. As a result, the distribution of multifold-structures increases as the cross-sectional area increases. The fitted distributions obtained from 20 simulation runs for each condition are summarized in Figure 3-5(c). The concentrations of electric charges resulting from the folded structures increase the translocation speed due to the associated strong electric force. Although we also performed

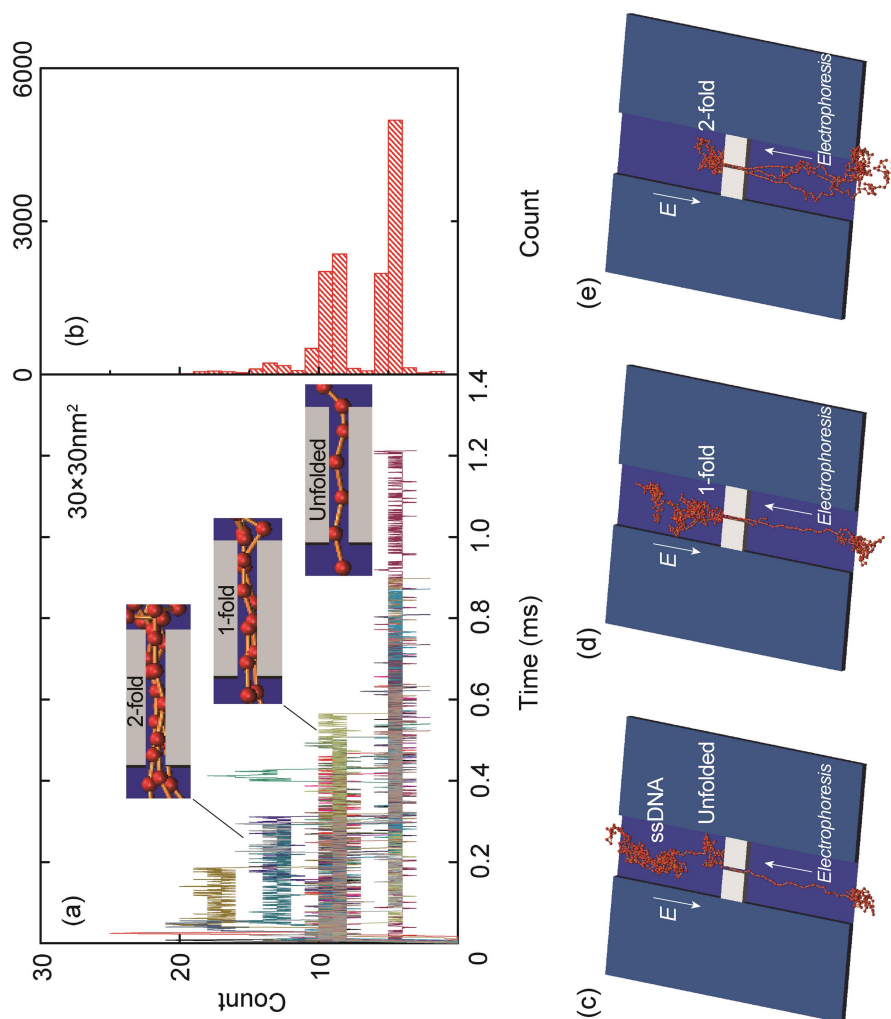


**Figure 3-4.** (a) Time series data, where each run is presented by color variation and (b) histogram of the number of beads in a  $30 \times 30 \text{ nm}^2$  cross-section nanopore, obtained from 20 runs of the Langevin dynamics simulation. A leading head enters the pore at  $t = 0 \text{ s}$  and the time elapsed is recorded until the end bead leaves the pore. Illustrations of the entire ssDNA chain are also presented, showing (c) unfolded, (d) 1-fold, and (e) 2-fold forms.

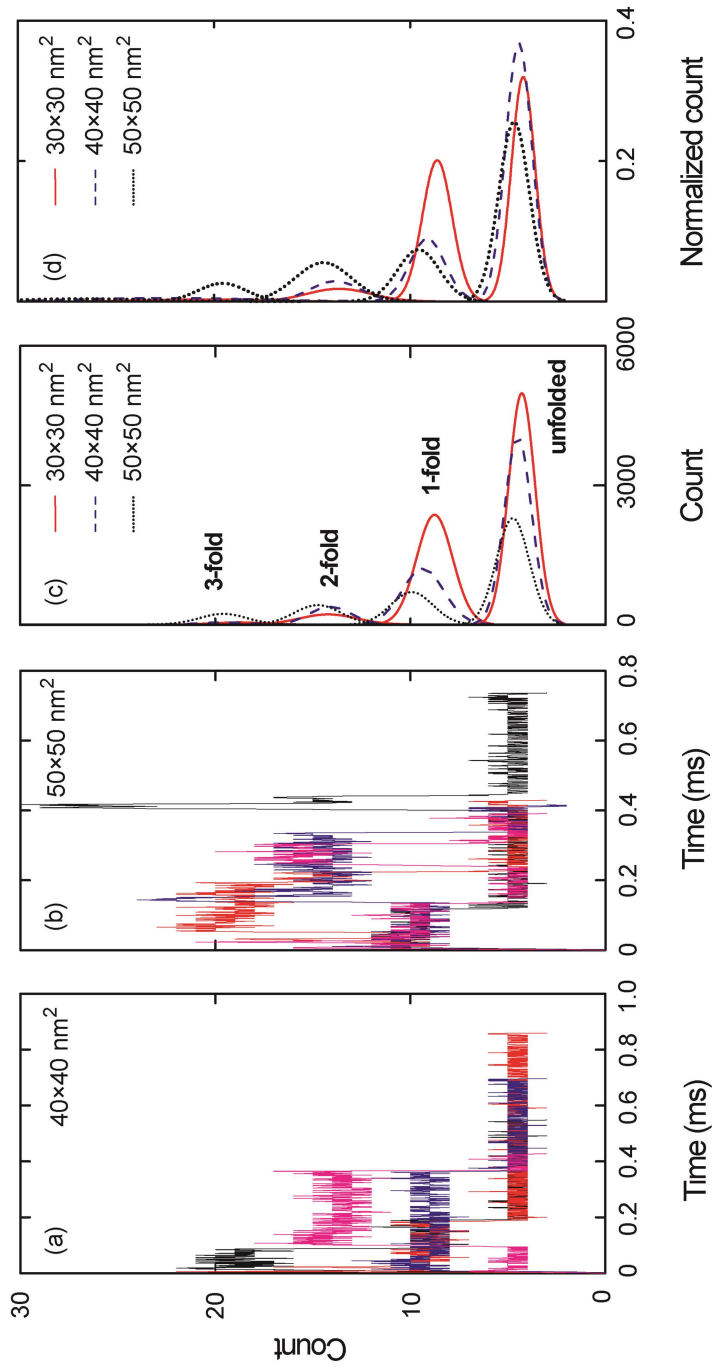


**Figure 3-5.** Time series data indicating the number of beads in nanopores of cross-section (a)  $40 \times 40$  and (b)  $50 \times 50$  nm<sup>2</sup>, in which only four typical data are presented by color variation in each case, (c) fitted distribution resulting from the complete data acquired from 20 simulations for each condition and (d) the normalized distribution of (c).

simulations for a  $20 \times 20 \text{ nm}^2$  cross-section nanopore, the electric field outside a nanopore of this size was evidently too weak to introduce the ssDNA into the pore. This result implies that an excessively small pore will require a long period of time to attract charged molecules to it. A weak electric field outside the pore, as is produced in the case of an overly small pore, is therefore disadvantageous for the polymer chain to overcome the entropic barriers at interconnections in the channel, because the large difference of cross-sections requires strong force to uncoil a coiled structure to introduce it into the nanopore<sup>56,57</sup>. Figure 3-5(d) presents a normalized version of the distribution data in Figure 3-5(c). Comparing the three cross-sections, it is evident that multifold-structures become prominent as the cross-sectional area increases. With respect to single-molecule detection, it is desirable to maintain unfolded configurations for as long as possible to slow down the translocation speed. Thus, the  $30 \times 30 \text{ nm}^2$  cross-section pore is suggested to be the most suited to the sequential transport of ssDNA molecules.

### 3.3.3 Translocation speed

For deep understanding of the electrokinetic transport phenomena in the nanofluidic device, the simulation results are analyzed by the theoretical model based on the Langevin equation as also described in detail in the methodology section. Particularly, a relationship between the translocation velocity and the pore size attracts most of our interests. Figure 3-6 shows velocity profiles of the mass centers of the ssDNA for the three cases presented in Figure 3-5, in which  $x_G$  denotes the position of mass center along the  $x$ -axis measured from the nanochannel entrance (2200 nm in total), and the nanopore is located from  $x_G = 1000$  to 1200 nm. In overdamped Langevin dynamics simulations, the velocity of a particle is directly proportional to the force on it, as theoretically described in the next section. For each cross-section, the velocity linearly increased until the mass center reached an  $x_G$  value of approximately 500 nm, at which point the leading bead moved into the stronger field while the remainder of the chain was still in front of the nanochannel entrance. Therefore, the number of beads in the nanochannel increased in a stepwise fashion over time. According to the Langevin equation, the equation of motion of the mass center along the pore axis may be roughly expressed by

$$v_G = \frac{1}{N\zeta} \sum_{i=1}^N F_{xi} = \frac{1}{N\zeta} \frac{\Delta F}{\Delta x} x_G + v_0 \quad (3-5)$$

where, assuming conservative force and thermal fluctuations, we can apply

$$-\sum_{i=1}^N \frac{\partial U_i}{\partial x} = 0 \quad \text{and} \quad \sum_{i=1}^N R_{xi} = 0. \quad (3-6)$$

The term  $\Delta F/(N\Delta x)$  represents the ratio of the external force on the mass center to the displacement and  $v_0$  is the initial velocity at the entrance.  $\zeta$  is the friction coefficient fitted to represent the property of ssDNA and results in  $4.68 \times 10^{-12}$  kg/s. In Figure 3-6, the slopes of the plotted data in the initial portion of each graph are respectively  $9.09 \times 10^3$ ,  $9.10 \times 10^3$ , and  $9.80 \times 10^3$  s<sup>-1</sup> for the  $30 \times 30$ ,  $40 \times 40$ , and  $50 \times 50$  nm<sup>2</sup> nanopores, giving an average value of  $9.33 \times 10^3$  s<sup>-1</sup>. In this region, the increment in which beads enter the nanochannel is almost constant despite the different channel cross-sections. In addition, when  $\Delta F/\Delta x$  is primarily due to the electric force in the nanochannel, we can write  $\Delta F = QE_{\text{channel}}\Delta N$ , meaning that the change in the force is governed by the increase in the number of beads entering the channel under the almost uniform electric field. Equation 3-5 can then be replaced by

$$v_G = \frac{QE_{\text{channel}}}{N\zeta} \frac{\Delta N}{\Delta x} x_G + v_0 \quad (3-7)$$

using  $E_{\text{channel}}$  approximated by the electric field at the centre of the nanochannel as listed in Table 3-2. For the three cases, the values of  $\Delta N/\Delta x$  are  $1.30 \times 10^9$ ,  $9.64 \times 10^8$ , and  $7.45 \times 10^8$  m<sup>-1</sup> for the  $30 \times 30$ ,  $40 \times 40$ , and  $50 \times 50$  nm<sup>2</sup> nanopores, respectively (Table 3-2). A charged bead in an  $E_{\text{channel}}$  field generates  $QE_{\text{channel}}$  such that the displacement,  $\Delta x$ , of the mass center related to each bead increment is proportional to  $E_{\text{channel}}$  and this explains why  $dv_G/dx_G$  is almost constant for all three cross-sections. In the following region, when the mass center approaches  $x_G = 500$  nm, there are obvious differences in velocity between the three cases. At this point, some beads are already in the nanopore. Subsequently, the velocity shows a moderate increase and appears to reach a terminal velocity when the center of mass passes through the nanopore. At this stage, the beads in the nanopore are driven forward due to the strong electric field and simultaneously experience counteracting

**Table 3-2.** Electric field and ssDNA transpore properties in nanochannel and nanopore

Pore size (nm <sup>2</sup> )	$E_{\text{channel}}$ (V/m)	$E_{\text{pore}}$ (V/m)	$N_{\text{pore}}$	$\Delta N/\Delta x$ (m <sup>-1</sup> )	$v_{\text{channel}}$ (mm/s)	$v_{\text{pore}}$ (mm/s)
30 × 30	$8.2 \times 10^4$	$2.7 \times 10^6$	6.48	$1.30 \times 10^9$	2.3	1.3
40 × 40	$1.2 \times 10^5$	$2.2 \times 10^6$	6.81	$9.64 \times 10^8$	3.3	1.1
50 × 50	$1.5 \times 10^5$	$1.9 \times 10^6$	9.29	$7.45 \times 10^8$	4.3	1.2

force, being pushed back by the leading portion of the chain and pulled by the following portion. Since small nanopore cross-sections produce a strong driving force, the confinement in this region also gives rise to the counteraction including the entropic force and polymer–wall interactions. In this region,  $v_G$  can be represented as

$$v_G = \frac{QN_{\text{pore}}E_{\text{pore}}}{\zeta N} + \frac{QN_{\text{channel}}E_{\text{channel}}}{\zeta N} \quad (3-8)$$

where  $N_{\text{pore}}$  and  $N_{\text{channel}}$  are the number of beads in the nanopore and nanochannel, respectively, and  $E_{\text{pore}}$  is the electric field strength in the pore. Here, the ssDNA chain is usually stretched and rarely collides with the wall as it passes through the interface between the nanochannel and the nanopore, and so the counteracting force is negligibly small compared to the other terms. As shown in Figure 3-5(d) and Table 3-2, the average number  $N_{\text{pore}}$  of beads in the nanopores is determined from the distributions. The remaining beads are in the nanochannel, such that  $N_{\text{channel}} = N - N_{\text{pore}}$ . Using the electric field  $E_{\text{pore}}$  at the center of the nanopore and  $E_{\text{channel}}$ ,  $v_G$  in Equation 3-8 results in 3.54, 4.41, and 5.49 mm/s for the 30 × 30, 40 × 40, and 50 × 50 nm<sup>2</sup> cross-section nanopores, respectively. These theoretically derived values are in good agreement with the simulations shown in Figure 3-6. Particularly, in the 30 × 30 nm<sup>2</sup> pore, the rapid change in curvature of the plot occurs at an  $x_G$  value of approximately 500 nm, indicating that the translocation process immediately reaches a steady state condition as the nanopore works to pump beads into the *trans* channel. In contrast, in the other pores, more moderate transitions of the velocity are observed and apparent transition points cannot be determined. As a result, the terminal velocities approach the theoretical values. Our data indicate that folded configurations of ssDNA chains in large cross-section pores cause moderate increases in the velocity of the mass center, and this results in high terminal velocities. In other words, our results explain

why electrophoretic mobility decreases during transport through a confined space embedded in the fluidic channel<sup>17,26,58</sup>. From the viewpoint of molecular sequencing, increased knowledge of changes in the velocity and suppression of excessive increases in this velocity are desirable when attempting to ascertain details concerning the configuration changes of polymer molecules.

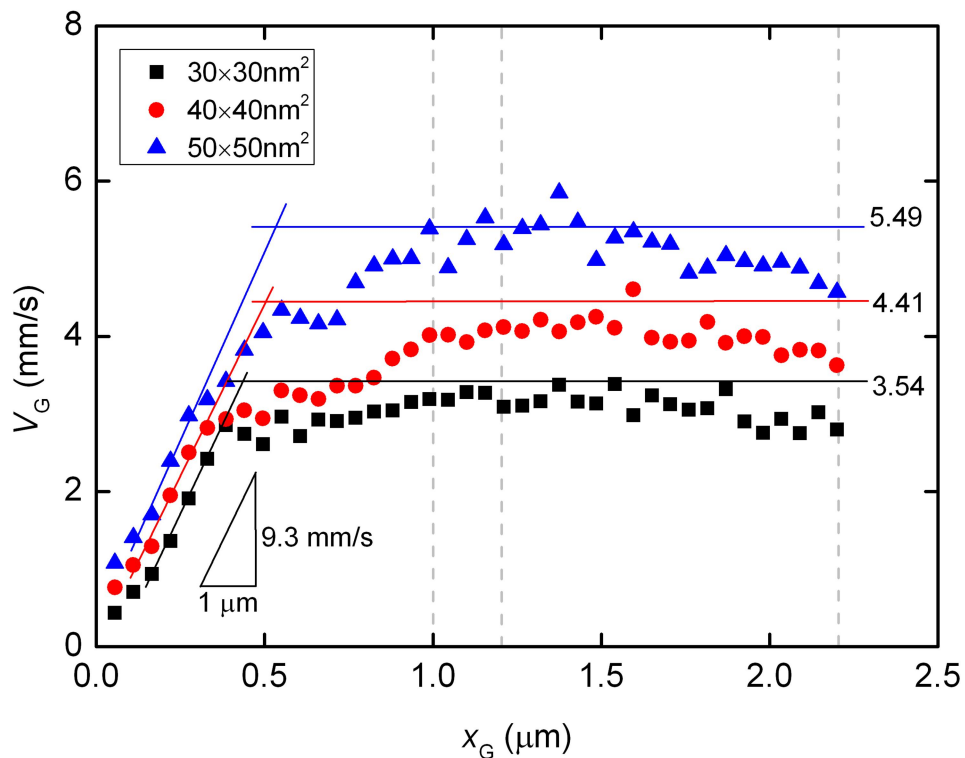


**Figure 3-6.** Velocity profile of the centers of mass of ssDNA chains passing through nanopores of cross-section  $30 \times 30$ ,  $40 \times 40$ , and  $50 \times 50 \text{ nm}^2$ , in which  $x_G$  is the position of mass center measured from the nanochannel entrance along the  $x$ -axis. The results of theoretical calculations using Equations 3-7 and 3-8 are also shown as solid lines. The start and end of the nanopore are situated at  $x_G = 1.0$  and  $1.2 \mu\text{m}$  and the end of the nanochannel is at  $x_G = 2.2 \mu\text{m}$ , all of which are indicated by dashed lines

### 3.4 Conclusion

In this study, we investigated the electrostatic potentials in nanopores embedded in a rectangular nanochannel. We obtained considerable agreement in the electric field strengths on the order of  $10^6$  V/m compared with previously published data<sup>54</sup>. Induction of strong electric fields in the narrowest space due to the connections of different-sized channels was confirmed<sup>55</sup>. Using such electric fields, we performed Langevin dynamics simulations by applying a coarse-grained model of ssDNA. The present model replicated the diffusion coefficient and electrophoretic mobility of long ssDNA, which allowed us to treat electrokinetic transport phenomena in the actual time and spatial scales. It was found that a nanoscale cross-sectional area was important with respect to uncoiling long-chained ssDNA molecules in a strong electric field and, as a result, reducing the translocation speed of the molecules. By adjusting the nanopore size, the quantity of ssDNA chains in the pore region can be constrained at a constant number, effectively producing a terminal velocity. With regard to the aim of obtaining single-molecule detection, this study suggests a preferred structure for nanofluidic channels.

## Reference

1. C. Dekker, "Solid-state nanopores," *Nat. Nanotechnol.* **2**, 209–215 (2007).
2. D. Branton, D. W. Deamer, A. Marziali, H. Bayley, S. A. Benner, T. Butler, M. Di Ventra, S. Garaj, A. Hibbs, X. Huang, S. B. Jovanovich, P. S. Krstic, S. Lindsay, X. S. Ling, C. H. Mastrangelo, A. Meller, J. S. Oliver, Y. V. Pershin, J. M. Ramsey, R. Riehn, G. V. Soni, V. Tabard-Cossa, M. Wanunu, M. Wiggin, J. A. Schloss, "The potential and challenges of nanopore sequencing," *Nat. Biotechnol.* **26**, 1146–1153 (2008).
3. M. Zwolak, M. Di Ventra, "Colloquium: Physical approaches to DNA sequencing and detection," *Rev. Mod. Phys.* **80**, 141–165 (2008).
4. B. M. Venkatesan, R. Bashir, "Nanopore sensors for nucleic acid analysis," *Nat. Nanotechnol.* **6**, 615–624 (2011).
5. J. J. Kasianowicz, E. Brandin, D. Branton, D. W. Deamer, "Characterization of individual polynucleotide molecules using a membrane channel," *Proc. Natl. Acad. Sci. U.S.A.* **93**, 13770–13773 (1996).
6. J. Clarke, H. C. Wu, L. Jayasinghe, A. Patel, S. Reid, H. Bayley, "Continuous base identification for single-molecule nanopore DNA sequencing," *Nat. Nanotechnol.* **4**, 265–270 (2009).
7. K. R. Lieberman, G. M. Cherf, M. J. Doody, F. Olasagasti, Y. Kolodji, M. Akeson, "Processive replication of single DNA molecules in a nanopore catalyzed by phi29 DNA polymerase," *J. Am. Chem. Soc.* **132**, 17961–17972 (2010).
8. J. Lagerqvist, M. Zwolak, M. Di Ventra, "Fast DNA sequencing via transverse electronic transport," *Nano Lett.* **6**, 779–782 (2006).
9. X. Liang, S. Y. Chou, "Nanogap detector inside nanofluidic channel for fast real-time label-free DNA analysis," *Nano Lett.* **8**, 1472–1476 (2008).
10. M. Tsutsui, M. Taniguchi, K. Yokota, T. Kawai, "Identifying single nucleotides by tunnelling current," *Nat. Nanotechnol.* **5**, 286–290 (2010).
11. P. Szarek, S. Suwannawong, K. Doi, S. Kawano, "Theoretical study on physicochemical aspects of a single molecular junction: application to the bases of ssDNA," *J. Phys. Chem. C.* **117**, 109809-1–109809-9 (2013).

12. K. D. Dorfman, "DNA electrophoresis in microfabricated devices," *Rev. Mod. Phys.* **82**, 2903–2947 (2010).
13. W. Sung, P. J. Park, "Polymer translocation through a pore in a membrane," *Phys. Rev. Lett.* **77**, 783–786 (1996).
14. M. Muthukumar, "Polymer translocation through a hole," *J. Chem. Phys.* **111**, 10371–10374 (1999).
15. I. Huopaniemi, K. Luo, T. Ala-Nissila, S. C. Ying, "Langevin dynamics simulations of polymer translocation through nanopores," *J. Chem. Phys.* **125**, 124901-1–124901-8 (2006).
16. S. Nagahiro, S. Kawano, H. Kotera, "Separation of long DNA chains using a nonuniform electric field: A numerical study," *Phys. Rev. E* **75**, 011902-1–011902-5 (2007).
17. S. Uehara, M. Tsutsui, K. Doi, M. Taniguchi, S. Kawano, T. Kawai, "Fluid dynamics and electrical detection of  $\lambda$ DNA in electrode-embedded nanochannels," *J. Biomech. Sci. Eng.* **8**, 244–256 (2013).
18. A. Meller, L. Nivon, E. Brandin, J. Golovchenko, D. Branton, "Rapid nanopore discrimination between single polynucleotide molecules," *Proc. Natl. Acad. Sci. U.S.A.* **97**, 1079–1084 (2000).
19. A. Meller, L. Nivon, D. Branton, "Voltage-driven DNA translocations through a nanopore," *Phys. Rev. Lett.* **86**, 3435–3438 (2001).
20. A. Meller, D. Branton, "Single molecule measurements of DNA transport through a nanopore," *Electrophoresis* **23**, 2583–2591 (2002).
21. J. Li, M. Gershow, D. Stein, E. Brandin, J. A. Golovchenko, "DNA molecules and configurations in a solid-state nanopore microscope," *Nature Materials* **2**, 611–615 (2003).
22. A. J. Storm, C. Storm, J. Chen, H. Zandbergen, J. F. Joanny, C. Dekker, "Fast DNA translocation through a solid-state nanopore," *Nano Lett.* **5**, 1193–1197 (2005).
23. O. V. Krasilnikov, C. G. Rodrigues, S. M. Bezrukov, "Single polymer molecules in a protein nanopore in the limit of a strong polymer-pore attraction," *Phys. Rev. Lett.* **97**, 018301-1–018301-4 (2006).

24. G. M. Skinner, M. van den Hout, O. Broekmans, C. Dekker, N. H. Dekker, “Distinguishing single- and double-stranded nucleic acid molecules using solid-state nanopores,” *Nano Lett.* **9**, 2953–2960 (2009).
25. G. F. Schneider, S. W. Kowalczyk, V. E. Calado, G. Pandraud, H. W. Zandbergen, L. M. K. Vandersypen, C. Dekker, “DNA translocation through graphene nanopores,” *Nano Lett.* **10**, 3163–3167 (2010).
26. M. Tsutsui, Y. He, M. Furuhashi, S. Rahong, M. Taniguchi, T. Kawai, “Transverse electric field dragging of DNA in a nanochannel,” *Sci. Rep.* **2**, 394, doi:10.1038/srep00394 (2012).
27. D. Fologea, J. Uplinger, B. Thomas, D. S. McNabb, J. Li, “Slowing DNA translocation in a solid-state nanopore,” *Nano Lett.* **5**, 1734–1737 (2005).
28. D. Fologea, M. Gershow, B. Ledden, D. S. McNabb, J. A. Golovchenko, J. Li, “Detecting single stranded DNA with a solid state nanopore,” *Nano Lett.* **5**, 1905–1909 (2005).
29. V. V. Lehtola, R. P. Linna, K. Kaski, “Dynamics of forced biopolymer translocation,” *EPL*. **85**, 58006-p1–58006-p6 (2009).
30. H. Yong, Y. Wang, S. Yuan, B. Xu, K. Luo, “Driven polymer translocation through a cylindrical nanochannel: interplay between the channel length and the chain length,” *Soft Matter*. **8**, 2769–2774 (2012).
31. C. M. Edmonds, Y. C. Hudiono, A. G. Ahmadi, P. J. Hesketh, S. Nair, “Polymer translocation in solid-state nanopores: Dependence of scaling behavior on pore dimensions and applied voltage,” *J. Chem. Phys.* **136**, 065105-1–065105-10 (2012).
32. K. Luo, T. Ala-Nissila, S. C. Ying, A. Bhattacharya, “Sequence dependence of DNA translocation through a nanopore,” *Phys. Rev. Lett.* **100**, 058101-1–058101-4 (2008).
33. A. Ramachandran, Q. Guo, S. M. Iqbal, Y. Liu, “Coarse-grained molecular dynamics simulation of DNA translocation in chemically modified nanopores,” *J. Phys. Chem. B*. **115**, 6138–6148 (2011).
34. C. Forrey, M. Muthukumar, “Langevin dynamics simulations of ds-DNA translocation through synthetic nanopores,” *J. Chem. Phys.* **127**, 015102-1–015102-10 (2007).
35. T. Z. Butle, M. Pavlenok, I. M. Derrington, M. Niederweis, J. H. Gundlach,

- “Single-molecule DNA detection with an engineered MspA protein nanopore,” *PNAS*. **105**, 20647-20652 (2008).
36. D. Wendell, P. Jing, J. Geng, V. Subramaniam, T. J. Lee, C. Montemagnom, P. Guo, “Translocation of double stranded DNA through membrane adapted phi29 motor protein nanopore,” *Nat Nanotechnol.* **4**, 765-772 (2009).
  37. L. Franceschini, M. Soskine, A. Biesemans, G. Maglia, “A nanopore machine promotes the vectorial transport of DNA cross membranes,” *Nat communication.* **4**, 2415 (2013).
  38. M. G. Gauthier, G. W. Slater, “Molecular dynamics simulation of a polymer chain translocating through a nanoscopic pore,” *Eur. Phys. J. E.* **25**, 17–23 (2008).
  39. A. Izmitli, D. C. Schwartz, M. D. Graham, J. J. de Pablo, “The effect of hydrodynamic interactions on the dynamics of DNA translocation through pores,” *J. Chem. Phys.* **128**, 085102-1–085102-7 (2008).
  40. M. Fyta, S. Melchionna, S. Succi, E. Kaxiras, “Hydrodynamic correlations in the translocation of a biopolymer through a nanopore: Theory and multiscale simulations,” *Phys. Rev. E.* **78**, 036704-1–036704-7 (2008).
  41. K. Luo, R. Metzler, “The chain sucker: Translocation dynamics of a polymer chain into a long narrow channel driven by longitudinal flow,” *J. Chem. Phys.* **134**, 135102-1-135102-8 (2011).
  42. C. Kawaguchi, T. Noda, M. Tsutsui, M. Taniguchi, S. Kawano, T. Kawai, “Electrical detection of single pollen allergen particles using electrode-embedded microchannels,” *J. Phys.: Condens. Matter.* **24**, 164202-1–164202-6 (2012).
  43. T. Yasui, S. Rahong, K. Motoyama, T. Yanagida, Q. Wu, N. Kaji, M. Kanai, K. Doi, K. Nagashima, M. Tokeshi, M. Taniguchi, S. Kawano, T. Kawai, Y. Baba, “DNA manipulation and separation in sublithographic-scale nanowire array,” *ACS Nano.* **7**, 3029–3035 (2013).
  44. Y. He, M. Tsutsui, C. Fan, M. Taniguchi, T. Kawai, “Controlling DNA translocation through gate modulation of nanopore wall surface charges,” *ACS Nano.* **5**, 5509–5518 (2011).
  45. K. Doi, T. Haga, H. Shintaku, S. Kawano, “Development of coarse-graining DNA models for single-nucleotide resolution analysis,” *Philos. Trans. R. Soc. A.* **368**, 2615–

- 2628 (2010).
46. K. Doi, W. Qian, S. Uehara, M. Tsutsui, M. Taniguchi, T. Kawai, S. Kawano, “Langevin Dynamics Study on Electrokinetic Transport of Long-Chained DNA through Nanogap Embedded in Nanochannel,” *Int. J. Emerg. Multi. Fluid. Sci.* 2017 in press.
  47. I. Hanasaki, H. Takahashi, G. Sazaki, K. Nakajima, S. Kawano, “Single-Molecule Measurements and Dynamical Simulations of Protein Molecules near Silicon Substrates,” *J. Phys. D: Appl. Phys.* **41**, 095301-1–095301-9 (2008).
  48. I. Hanasaki, H. Shintaku, S. Matsunami, S. Kawano, “Structural and Tensile Properties of Self-Assembled DNA Network on Mica Surface,” *Comput. Model. Eng. Sci.* **46**, 191–207 (2009).
  49. K. Doi, T. Uemura, S. Kawano, “Molecular dynamics study of solvation effect on diffusivity changes of DNA fragments,” *J. Mol. Model.* **17**, 1457–1465 (2011).
  50. K. Doi, Y. Toyokita, S. Akamatsu, S. Kawano, “Reaction–diffusion wave model for self-assembled network formation of poly(dA)·poly(dT) DNA on mica and HOPG surfaces,” *Compt. Method. Biomech. Biomed. Eng.* iFirst article, 1–17 (2012).
  51. K. Doi, H. Takeuchi, R. Nii, S. Akamatsu, T. Kakizaki, S. Kawano, “Self-assembly of 50 bp poly(dA)·poly(dT) DNA on highly oriented pyrolytic graphite via atomic force microscopy observation and molecular dynamics simulation,” *J. Chem. Phys.* **139**, 085102-1–085102-9 (2013).
  52. E. Stellwagen, Y. Lu, N. C. Stellwagen, “Unified description of electrophoresis and diffusion for DNA and other polyions,” *Biochemistry.* **42**, 11745–11750 (2003).
  53. Femtet®, Murata Software Co., Ltd., Tokyo, Japan, 2013.
  54. Y. He, M. Tsutsui, C. Fan, M. Taniguchi, T. Kawai, “Gate manipulation of DNA capture into nanopores,” *ACS Nano.* **5**, 8391–8397 (2011).
  55. E. H. Trepargnier, A. Radenovic, D. Sivak, P. Geissler, J. Liphardt, “Controlling DNA capture and propagation through artificial nanopores,” *Nano Lett.* **7**, 2824–2830 (2007).
  56. J. T. Mannion, C. H. Reccius, J. D. Cross, H. G. Craighead, “Conformational analysis of single DNA molecules undergoing entropically induced motion in nanochannels,”

- Biophys. J.* **90**, 4538–4545 (2006).
57. G. B. Salieb-Beugelaar, K. D. Dorfman, A. van den Berg, J. C. T. Eijkel, “Electrophoretic separation of DNA in gels and nanostructures,” *Lab Chip*. **9**, 2508–2523 (2009).
58. S. Uehara, H. Shintaku, S. Kawano, “Electrokinetic flow dynamics of weakly aggregated  $\lambda$ DNA confined in nanochannels,” *Trans. ASME., J. Fluids Eng.* **133**, 121203-1–121203-8 (2011).
59. B. Tinland, A. Pluen, J. Sturm, G. Weill, “Persistence length of single-stranded DNA,” *Macromol.* **30**, 5763-5765 (1997).
60. J. Kuszewski, A. M. Gronenborn, G. M. Clore, “Improving the packing and accuracy of NMR structures with a pseudopotential for the radius of gyration,” *J. Am. Chem. Soc.* **121**, 2337–2338 (1999).
61. G. S. Manning, “Limiting laws and counterion condensation in polyelectrolyte solutions. 7. electrophoretic mobility and conductance,” *J. Phys. Chem.* **85**, 1506–1515 (1981).
62. K. Rechendorff, G. Witz, J. Adamcik, G. Dietler, “Persistence length and scaling properties of single-stranded DNA adsorbed on modified graphite,” *J. Chem. Phys.* **131**, 095103-1–095103-6 (2009).

# Chapter 4

## *Analysis of ssDNA Translocation through Nanochannel*

### **4.1 Introduction**

An increased demand for analytical capability in the biological sciences has prompted the development of micro/nanofluidic devices that enable the manipulation and analysis of biological molecules with higher speed and accuracy than conventional technologies. These new devices have significant potential in the fields of molecular biology and biophysics. Among the various technologies being researched, the stability and size-controllability of solid-state nanochannels show promise with regard to the fabrication of ideal, robust platforms for biomolecular separation, detection, and analysis<sup>1-8</sup>.

One of the most well studied topics concerning nanofluidic devices is the controllability of transport velocity and conformational change of biopolymers. Various strategies have been proposed to control the translocation velocity of electrically charged polymers, such as tuning of wall surface charges<sup>9</sup>, ion concentrations<sup>9,11</sup>, temperature gradients<sup>12</sup>, solution viscosity<sup>13</sup>, and pore dimensions<sup>14</sup>. However, these efforts have not yet been shown to improve the controllability. Thus the development of biopolymer analysis platforms will require a detailed understanding of biopolymer transport dynamics on the nanoscale so as to overcome these remaining challenges.

Recent experimental works have partially addressed the polymer-length dependent

mobility that is evident in nanochannels, as a means of allowing the velocity control of biopolymers. Although a constant mobility independent of polymer length was demonstrated in a capillary with a 60 nm diameter<sup>4,15-17</sup>, this control was lost when employing nanoslits with a height of 20 nm<sup>4,18</sup>. Cross et al.<sup>4</sup> reported that the effect of polymer length,  $N$ , on the mobility of DNA can be described by a scaling law as  $N^{-1/2}$  in a 19 nm deep nanoslit. Cao et al.<sup>19</sup> found a significant length dependence of the electrophoretic mobility of DNA in a nanocapillary and nanowire array. Rahong et al.<sup>8</sup> proposed two different separation mechanisms associated with the dsDNA length and the density of the nanowire array. These experiments<sup>4,8,19</sup> were carried out using long-chain double-stranded DNA (dsDNA >  $10^3$  base pairs) molecules and small slit heights to evaluate the separation. The results demonstrated that electrophoretic mobility was primarily affected by both the polymer length and the channel size.

The separation and velocity control of short-chain ssDNA is currently an important issue in DNA sequencing, and our own group has developed coarse-grained models of DNA to assist in investigating transport properties<sup>14,20-22</sup>. In this prior work, the time spans and folded structures of dsDNA passing through nanogaps<sup>14</sup> or nanowire arrays<sup>6</sup> were determined, using practical spatial and temporal dimensions. More recently, a technique for manipulating microparticles mimicking charged polymer chains was successfully demonstrated by applying ac electric fields across a micropore, such that the motions of microparticles could be aligned in the radial direction depending on the field frequency<sup>23</sup>. However, the placement and conformation of polymer chains can be controlled even more precisely in nanochannels exposed to electroosmotic flow (EOF) fields. Furthermore, when the channel radius approaches the thickness of the electric double layer (EDL), the effect of the electrically polarized channel surfaces has been shown to play an important role in polymer transport<sup>24,25</sup>. Clarification of the DNA deformation process in nanochannels in response to wall surface charges and ion concentrations is also of great importance to the further development of nanofluidic devices such as nanopore-based sequencers<sup>26</sup>.

Polymer transport regimes<sup>27,28</sup> are frequently employed to illustrate the static conformations of confined macromolecules. These include  $R_g \ll a$  (bulk regime),  $R_g \approx a$  (de Gennes regime<sup>27</sup>), and  $l_p \approx a$  (Odijk regime<sup>28</sup>), where  $R_g$  is the radius of gyration of the polymer,  $a$  is the channel radius, and  $l_p$  is the persistence length. These regimes represent

distinct confinement effects on the polymer conformations and transport dynamics in nanochannels.

Computational studies of polymer transport phenomena in nanochannels have also been found to provide significant insight regarding the dynamics of biopolymers<sup>14,29-41</sup>. In previous works, Luo and coworkers<sup>34,35</sup> numerically investigated the movement of polymers through nanochannels and nanopores, while Slater et al.<sup>36,37</sup> performed pioneering work in the field of the electrokinetic transport of DNA by developing coarse-grained models. Jendrejack et al.<sup>39-41</sup> theoretically and computationally clarified the shear-induced migration and confinement effects on long-chain DNA dynamics in microfluidic devices. Based on these previous studies, the present project assessed the transport of short-chain ssDNA through nanochannels using computational simulations. In particular, this study focused on the dependence of polymer mobility, deformation characteristics, and spatial distribution on the salt concentration in a narrow channel with dimensions comparable to the EDL thickness.

Specifically, the transport properties of ssDNA in a nanochannel were simulated using Langevin dynamics (LD) in conjunction with a bead-spring model to determine the relationships between the polymer length, salt concentration, and deformation process in EOF fields. As a result of the present LD simulations, detailed characteristics of ssDNA, such as off-centered alignment in the nanochannel stretching or compressing the polymer chain, were elucidated on a realistic spatiotemporal scale. These results are expected to be applicable to the development of techniques for the manipulation and velocity control of ssDNA during transport.

## Nomenclature

$a$	=	radius of the nanochannel (m)
$b$	=	thickness of the constant viscosity layer (m)
$C$	=	ion concentration in solution (M)
$D$	=	diffusion coefficient of ssDNA in free solution (m <sup>2</sup> /s)
$E_r$	=	radial electric field (V/m)
$E_z$	=	axially applied electric field (V/m)
$f(r)$	=	distribution functions of ssDNA in nanochannels
$G$	=	Meijer G function

$I_0$	=	the zeroth-order modified Bessel function of the first kind
$k_B$	=	Boltzmann constant (J/k)
$\langle L^2 \rangle$	=	mean-square end-to-end distances of ssDNA in nanochannel ( $m^2$ )
$\langle L_0^2 \rangle$	=	$\langle L^2 \rangle$ of ssDNA in nanochannel without applin radical electric field ( $m^2$ )
$n_i$	=	bulk concentration of the $i$ th electrolyte species (M)
$N$	=	bead number
$q$	=	bead charges (C)
$R_g$	=	radius of gyration of ssDNA (m)
$\mathbf{R}_i$	=	random force (N)
$r$	=	nanochannel radical position
$r_c$	=	center of mass of the chain
$\langle r_c \rangle$	=	ensemble average of the mass-center radial position of ssDNA
$r_{ij}$	=	distance between the two molecules (m)
$T$	=	temperature (K)
$r_{eq}$	=	equilibrium distance between the connected molecules (m)
$v_c$	=	the velocity of the center of mass of ssDNA along the $z$ -axis (m/s)
$\mathbf{v}_i$	=	velocity of the $i$ th particle (m/s)
$u_z(r)$	=	EOF velocity profile (m/s)
$\nabla U_i$	=	conservative force (N)
$U_{LJ}$	=	Lennard Jones potential (V)
$U_{bond}$	=	bond potential (V)
$z_i$	=	valence of the $i$ th electrolyte species

### Greek Symbols

$\delta_{ij}$	=	Kronecker's delta
$\delta(t-t')$	=	Dirac delta function
$\varepsilon_{LJ}$	=	Lennard-Jones energy well-depth (kJ/mol)
$\varepsilon$	=	the relative dielectric constant of solution
$\varepsilon_0$	=	dielectric constant of vacuum (F/m)
$\eta_0$	=	bulk viscosity (Pa·s)
$\eta(r)$	=	viscosity near the nanochannel surface (Pa·s)
$\zeta$	=	zeta potential (V)
$\kappa$	=	inverse of Debye length ( $m^{-1}$ )
$\lambda_D$	=	Debye length (m)
$\mu$	=	electrophoretic mobility of ssDNA in nanochannel ( $m^2/Vs$ )
$\mu_{EOF}$	=	electrophoretic mobility of EOF ( $m^2/Vs$ )
$\mu_{free}$	=	electrophoretic mobility of ssDNA in free solution ( $m^2/Vs$ )

$\zeta$	=	friction coefficient of bead (kg/s)
$\sigma$	=	bead diameter (m)
$\phi$	=	electrostatic potential (V)

## 4.2 Computational methods

### 4.2.1 Electroosmotic flow in the nanochannel

Figure 4-1 is a schematic illustration of ssDNA that electrophoretically passes through a cylindrical nanochannel, where liquid flows induced by interactions between an electrically charged channel surface and polar solvent also affect the polymer translocation. Focusing on such a velocity field, we discuss electrokinetic transport phenomena of ssDNA in nanochannel. Taking into account the effect of velocity gradients due to highly concentrated ions near wall surfaces, the nanochannel is divided into two parts with respect to the radius  $r$ , such as the constant viscosity layer (CVL) in  $0 \leq r < b$ , where the viscosity  $\eta(r)$  is equal to the bulk value  $\eta_0$ , and the nonconstant viscosity layer (NVL) in  $b \leq r \leq a$ , where  $a$  is the radius of cylindrical channel and  $b$  is the boundary at the CVL and NVL. The viscosity expressed by  $\eta(r) = \eta_0 r^2 / b^2$  quadratically increases very near the channel surface as suggested by Wang et al.<sup>42</sup>. Under an axially applied electric field  $E_z$  along the nanochannel, charged molecules and liquids are forced to migrate along the  $z$ -axis. Additionally, the  $\zeta$  potential of a channel surface causes to form an EDL and a nonuniform electric field  $E_r$  along the  $r$ -axis, such that  $E_r = -d\phi/dr$ . Based on previous theoretical studies<sup>14,44</sup>, an electric field is independently separated into two components, such as  $E_z$  and  $E_r$ . Here, we assume  $E_z$  is axially constant in the infinitely long narrow channel. Additionally, pressure gradient along the  $z$ -axis is assumed to be negligibly small according to the conventional models of EOF<sup>45</sup>. The EOF velocity  $u_z(r)$  varied along the radial direction can be written in the cylindrical coordinate system as follows:

$$\frac{1}{r} \frac{d}{dr} \left( r \eta(r) \frac{du_z}{dr} \right) = \varepsilon_0 \varepsilon E_z \frac{1}{r} \frac{d}{dr} \left( r \frac{d\phi}{dr} \right) \quad (4-1)$$

where  $\varepsilon_0$  is the dielectric constant of vacuum and  $\varepsilon$  the relative dielectric constant of solution. The electric force on the right-hand side is derived from the Poisson equation. The electric potential  $\phi(r)$  in the nanochannel is written as follows:

$$\phi = \zeta \frac{I_0(\kappa r)}{I_0(\kappa a)}, \quad (4-2)$$

where  $I_0$  is the zeroth-order modified Bessel function of the first kind, and  $\kappa$  is the

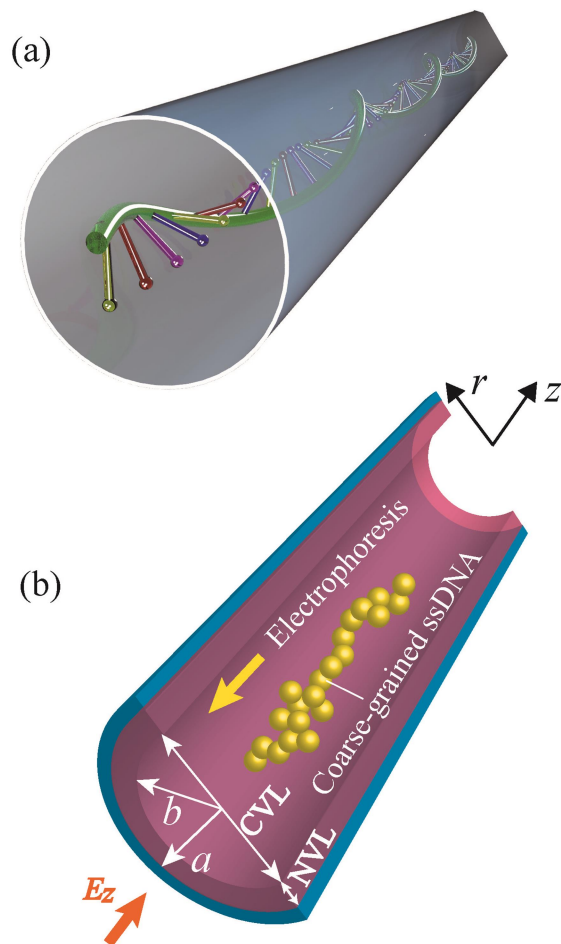


**Figure 4-1.** Schematic illustrations of (a) ssDNA passing through a cylindrical nanochannel and (b) a coarse-grained bead-spring model of the polymer chain. The longitudinal electric field,  $E_z$ , results in electrophoresis of the negatively charged DNA and an EOF due to the wall surface charges. The surface of the nanochannel is either negatively or positively charged associated with the  $\zeta$  potential. A non-constant viscosity layer is known to exist very near the surface and EDLs affect the EOF flow pattern.

reciprocal of Debye length  $\lambda_D$ :

$$\kappa = \frac{1}{\lambda_D} = \sqrt{\frac{e^2 \sum_i n_i z_i^2}{\varepsilon_0 \varepsilon k_B T}}, \quad (4-3)$$

where  $k_B$  is the Boltzmann constant,  $n_i$  the bulk concentration of the  $i$ th electrolyte species, and  $z_i$  the valence. The relation between  $\lambda_D$  and  $n_i$  for monovalent ions is summarized in Table 4-1. Since the electric potential in nanochannel depends only on  $r$ ,  $\nabla^2 \phi$  can be reduced to an ordinary differential equation and results in

$$\frac{du_z}{dr} = \frac{\varepsilon_0 \varepsilon E_z}{\eta(r)} \frac{d\phi}{dr}, \quad (4-4)$$

The concrete solution of Equation 4-4 can be expressed according to the boundary conditions. In the CVL, the solution of Equation 4-4 is expressed replacing  $\eta(r)$  by the constant viscosity  $\eta_0$ . The solution is represented in the form as follows:

$$u_z = \frac{\varepsilon_0 \varepsilon E_z \zeta}{\eta_0} \left[ \frac{I_0(\kappa r)}{I_0(\kappa a)} + C_1 \right] \quad \text{in } 0 \leq r < b, \quad (4-5)$$

where  $C_1$  is an integral constant determined later. On the other hand, in the NVL, the viscosity near the surface is represented by  $\eta(r) = \eta_0 r^2 / b^2$  and therefore, Equation 4-5 is expressed as follows

$$u_z = \frac{\varepsilon_0 \varepsilon E_z \zeta b^2}{\eta_0 I_0(\kappa a)} \int \frac{\kappa I_1(\kappa r)}{r^2} dr \quad \text{in } b \leq r \leq a. \quad (4-6)$$

To solve Equation 4-6, Meijer  $G$  function is introduced<sup>43</sup>. The integral of the first order modified Bessel function divided by  $r^2$  is calculated as

$$\int \frac{\kappa I_1(\kappa r)}{r^2} dr = -\frac{\kappa^2}{4} G_{1,3}^{2,0} \left( \begin{matrix} 1 \\ 0, 0, -1 \end{matrix} \middle| -\frac{\kappa^2 r^2}{4} \right) + C_2, \quad (4-7)$$

and thus, the solution can be simplified, such that

$$u_z = -\alpha G(\kappa r) + C_2, \quad (4-8)$$

where  $G(\kappa r) = G_{1,3}^{2,0} \left( \begin{matrix} 1 \\ 0, 0, -1 \end{matrix} \middle| -\frac{\kappa^2 r^2}{4} \right)$  calculated by using Matlab<sup>®</sup> libraries and  $\alpha$  is an EOF velocity parameter  $\alpha = \varepsilon_0 \varepsilon E_z \zeta \kappa^2 b^2 / (4\eta_0 I_0(\kappa a))$ . Based on the nonslip boundary condition

$u_z|_{r=a} = 0$ ,  $C_2$  is determined and the solution results in

$$u_z = \alpha [G(\kappa a) - G(\kappa r)]. \quad (4-9)$$

The velocity profile is continuous at  $r = b$ , such that

$$u_z(r \rightarrow b_{+0}) = u_z(r \rightarrow b_{-0}), \quad (4-10)$$

that leads to  $C_1$  as follows:

$$C_1 = I_0(\kappa b) + \frac{4}{\kappa^2 b^2} [G(\kappa a) - G(\kappa b)]. \quad (4-11)$$

Sorting out the equations above, the solution of EOF velocity profile in the whole nanochannel results in

$$u_z(r) = \begin{cases} \alpha \left[ \frac{4}{\kappa^2 b^2} (I_0(\kappa r) - I_0(\kappa b)) + G(\kappa a) - G(\kappa b) \right], & r \in [0, b) \\ \alpha [G(\kappa a) - G(\kappa r)], & r \in [b, a] \end{cases} \quad (4-12)$$

In these simulations, the channel surface was either positively or negatively polarized, and the applied  $\zeta$  potential was controlled between  $-25$  and  $25$  mV. The bulk viscosity of water,  $\eta$ , was set to  $0.893 \times 10^{-3}$  Pa·s and a uniform electric field of  $E_z = 1.0 \times 10^5$  V/m was applied along the  $z$ -direction. The EOF was found to become stronger with increases in the  $\zeta$  potential because the highly concentrated electrolyte ions in the EDL dragged the solvent molecules.

The electrokinetic transport phenomena introduced above involve both electrophoresis and electroosmosis. Theoretical approaches to electroosmosis typically require several assumptions to simplify the original problem and so reduce the physical and mathematical complexities. A lack of knowledge regarding the viscosity gradients near the channel surfaces often leads to overestimation of the EOF flow rate<sup>47</sup>. These factors should be taken into consideration in future work so as to obtain a better understanding of viscous flows very near the channel surfaces. In this work, we also examined a numerical approach to determine the EOF velocity profile in the presence of viscosity gradients near the channel walls as shown in Supporting Material. As a result, it was found that these viscosity gradients did not seriously affect the translocation properties of the ssDNA model. Thus, hereafter, we apply a constant viscosity for the solution in a cylindrical nanochannel.

### 4.2.2 Langevin dynamics simulation of a coarse-grained ssDNA model

In our model, intramolecular interactions are represented by a linear spring, and the electrokinetics of polymer molecules are mainly affected by external electric fields in liquids. In such a case, the behavior of particles can be expressed by an over-damped Langevin equation<sup>14,20</sup>:

$$\zeta(\mathbf{v}_i - \mathbf{u}) = -\nabla U_i + \mathbf{R}_i + q(\mathbf{E} - \nabla\phi), \quad (4-13)$$

where  $\mathbf{v}_i$  is the velocity of the  $i$ th particle,  $\mathbf{E} = E_z \mathbf{e}_z$  where  $E_z$  is the electric field strength and  $\mathbf{e}_z$  is the unit vector in the  $z$ -direction,  $\zeta$  is the friction coefficient of particle,  $\mathbf{u}$  is the EOF velocity field that is treated as a field fixed in the space for the polymer translocation such that  $\mathbf{u}(r) = u_z(r) \mathbf{e}_z$ ,  $-\nabla U_i$  is the conservative force including interactions between particles,  $q$  is the electrical charge of single particle, and  $\mathbf{R}_i$  denotes the random force that satisfies the fluctuation-dissipation theorem:

$$\begin{cases} \langle R_{v_i}(t) \rangle = 0 \\ \langle R_{v_i}(t) \cdot R_{v_j}(t') \rangle = 2k_B T \zeta \delta_{ij} \delta(t-t'), \quad v = \{x, y, z\} \end{cases} \quad (4-14)$$

where  $k_B$  is the Boltzmann constant,  $T$  is temperature,  $\delta_{ij}$  is Kronecker's delta, and  $\delta(t-t')$  is the Dirac delta function where  $t$  and  $t'$  are time. The polymer chain consists of  $N$  individual particles bonded to neighbors with a linear spring<sup>14,20</sup>. Interactions between the nearest neighbors and between the coarse-grained molecule and channel surface are represented by the Lennard-Jones potential taking the volume exclusion effect into account<sup>14-20</sup>:

$$U_{\text{LJ}}(\mathbf{r}_i) = \begin{cases} \sum_{\substack{j=1 \\ j \neq i}}^N 4\epsilon_{\text{LJ}} \left[ \left( \frac{\sigma}{r_{ij}} \right)^{12} - \left( \frac{\sigma}{r_{ij}} \right)^6 \right] + \epsilon_{\text{LJ}} & \text{for } r_{ij} \leq 2^{\frac{1}{6}} \sigma \\ 0 & \text{for } r_{ij} > 2^{\frac{1}{6}} \sigma \end{cases} \quad (4-15)$$

where  $r_{ij}$  is the distance between the two molecules,  $\sigma$  is the diameter, and  $\epsilon_{\text{LJ}}$  is the energy well-depth set to  $k_B T$ . The coarse-grained molecule corresponds to 12 nucleotides (nt), which is determined by dividing the persistence length of 5.0 nm for ssDNA by 0.43 nm associated with the interval between nucleotides, holding the internal structure and properties of ssDNA.  $U_{\text{LJ}}$  was applied to non-adjacent molecules. For the purposes of volume exclusion, the potential was truncated at  $r = \sqrt[6]{2} \sigma$  to allow for purely repulsive

interactions between the molecules. The repulsive force from the channel surface works only on the surface normal direction. Bonding between two consecutive molecules along the chain is given by<sup>14,20</sup>

$$U_{bond}(\mathbf{r}_i) = \begin{cases} \frac{1}{2} \sum_j k(r_{ij} - r_{eq})^2 & \text{for neighbors} \\ 0 & \text{otherwise} \end{cases} \quad (4-16)$$

where  $r_{eq}$  is the equilibrium distance between the connected molecules and given by 5.0 nm. The spring constant is written by  $k = k_B T / \delta$ , and  $\delta$  is caused by thermal fluctuations around the average and  $\delta = 0.1\sigma$  is applied<sup>14,20</sup>. The other parameter set employed in the present simulations was already published<sup>14</sup>. The friction coefficient  $\zeta$  and effective bead charge  $q$  in Equation 4-1 are evaluated referring to experimental data of diffusion coefficient  $D$  and electrophoretic mobility  $\mu$  of ssDNA<sup>15</sup>. In this study, we set  $T = 300$  K and  $\varepsilon = 80.1$  for aqueous solutions. Resulting from the relationship of  $\zeta = k_B T / ND$  and  $q = \zeta \mu = \mu k_B T / ND$ <sup>15</sup>, both  $\zeta$  and  $q$  are described as a function of  $N$ .

At the beginning of LD simulations, a polymer structure equilibrated in free solution is placed at the cylindrical nanochannel inlet apart from the distance of  $R_g$  and forced to pass into the channel by applying a uniform electric field of  $E_z = 1.0 \times 10^5$  V/m. Linear increase in the electrophoretic velocity to applied electric fields is also confirmed for the case of  $E_z = 1.0 \times 10^6$  V/m. That is, the mobility is constant for each  $N$ . Based on this fact, we discuss the electrophoretic characteristics of ssDNA for the actual magnitude of the electric field. Entering the polymer into the nanochannel, its structure deforms and reaches a steady state during translocation in the cylindrical channel. This preliminary computation is carried out for each trial to determine the initial condition in the nanochannel. Based on previous studies<sup>14,20</sup>, the time step of LD simulation is set to 1.0 ps, and the total computational time is 2.0 ms for each. The time step of 1.0 ps is constrained by both stability and accuracy, which was already verified in a previous study<sup>14</sup>. The analysis of the polymer transport is evaluated by at least 20 individual trials in all cases with different surface charges and ion concentrations.

## 4.3 Results and discussion

### 4.3.1 Verification of the coarse-grained ssDNA model

In the simulation, the electric field in the nanochannel is assumed to be not altered by the presence of ssDNA. The charge density of ssDNA is calculated by:

$$\rho = Nq / \left( \frac{4}{3} \pi N \left( \frac{\sigma}{2} \right)^3 \right) = 6q / \pi \sigma^3 \quad (4-17)$$

where  $N$  is the number of beads,  $q$  is the electrical charge of a bead, and  $\sigma$  is the bead diameter. The electrical charge density is defined by dividing the total charge of a polymer by the volume. The  $\rho$  of the ssDNA chain and for comparison, that of the monovalent electrolyte solution with the concentration of  $C$  are listed in Table 4-2 in the unit of elementary charge per cubic nanometer. It is found that for  $C = 1, 2 \times 10^{-2}, 4 \times 10^{-3}, 9 \times 10^{-4}$ , and  $4 \times 10^{-4}$  M, the charge density of ssDNA bead is at least one order of magnitude larger or smaller than that of the electrolyte solution, except in the case of  $C = 2 \times 10^{-2}$  M. Thus, it is preferably assumed that the electrical charge of ssDNA is sufficiently screened and the presence of the DNA does not disturb the electric field in the nanochannel.

The polymer transport properties, i.e.,  $D$ ,  $\mu$ , and  $R_g$ , were evaluated by performing the LD simulation in free solution as shown in Figure 4-2.  $D$  was determined from the Einstein relation calculating mean square displacements of the ssDNA and  $\mu$  was directly analyzed from the simulations applying uniform electric fields to obtain the terminal velocity as a function of the electric field.  $R_g$  was determined as  $R_g^2 = \sum_{i=1}^N (\mathbf{r}_i - \mathbf{r}_c)^2 / (N+1)$ , where  $\mathbf{r}_c$  is the center of mass of the chain. Our simulation results were in close agreement with the theoretical evaluations of  $D$  and  $\mu$ . This means that the coarse-graining method is suitable to represent the behavior of ssDNA in terms of diffusion and electrophoresis. Setting  $q$  and  $\zeta$  for a single bead to reproduce the  $D$  and  $\mu$ ,  $R_g$  of the ssDNA consequently agreed with the theoretical model as shown in Figure 4-2(c). As listed in Table 4-3, appropriately determined  $q$  and  $\zeta$  for a coarse-grained molecule resulted in the constant mobility of  $3.0 \times 10^{-8} \text{ m}^2/\text{Vs}$  equivalent among each polymer length. Thus, this model is valid to mimic various lengths of ssDNA, corresponding to from 60 to 600 nt.

**TABLE 4-1.** Relationship between EDL thickness  $\lambda_D$ , and ion concentration,  $C$ .

$C$ (M)	$\lambda_D$ (nm)
$10^0$	0.3
$2 \times 10^{-2}$	2
$4 \times 10^{-3}$	5
$9 \times 10^{-4}$	10
$4 \times 10^{-4}$	15

**Table 4-2.** Charge densities  $\rho$  of the electrolyte solution with  $C$  and ssDNA with the length  $N$ .

$C$ (M)	$\rho$ ( $e/\text{nm}^3$ )	$N$	$\rho$ ( $e/\text{nm}^3$ )
1	$6 \times 10^{-1}$	5	$3 \times 10^{-2}$
$2 \times 10^{-2}$	$1 \times 10^{-2}$	10	$3 \times 10^{-2}$
$4 \times 10^{-3}$	$2 \times 10^{-3}$	20	$2 \times 10^{-2}$
$9 \times 10^{-4}$	$5 \times 10^{-4}$	30	$1 \times 10^{-2}$
$4 \times 10^{-4}$	$2 \times 10^{-4}$	50	$1 \times 10^{-2}$

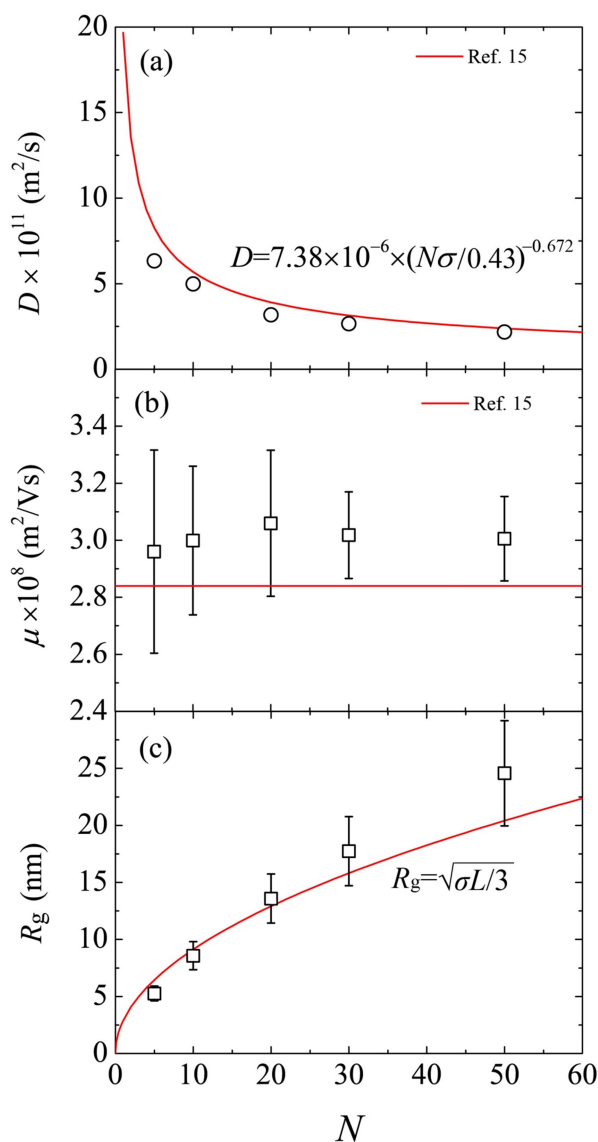


**FIGURE 4-2.** (a) Diffusion coefficient,  $D$ , (b) electrophoretic mobility,  $\mu$ , and (c) radius of gyration,  $R_g$ , as a function of the polymer length of coarse-grained ssDNA,  $N$ . Error bars mean standard deviations at each data point. In (a), each data point was evaluated from the mean square displacement and the Einstein relation, averaged by 50 individual simulations in free solution. In (b), the displacement of the center of mass of the ssDNA chain was evaluated in the electric field of  $E_z = 1.0 \times 10^5 \text{ V/m}$  as a result of 60 trials, where the mobility of the coarse-grained ssDNA,  $\mu = q/\zeta$ , was evaluated as  $3.0 \times 10^{-8} \text{ m}^2\text{/Vs}$  that was constant for each  $N$  as shown in Table 4-3 in the main text. In (c), each data point results from 2000 data samples.  $\sigma$  and  $L$  are the persistence length and contour length of polymer, respectively, where we applied  $\sigma = 5 \text{ nm}$  and  $L = N\sigma$  for ssDNA.

### 4.3.2 Dependence of DNA mobility on ion concentration

Figure 4-3(a) shows the electrophoretic mobility of coarse-grained ssDNA,  $\mu$  ( $= v_c/E_z$ , where  $v_c$  is the velocity of the center of mass along the  $z$ -axis), as a function of ion concentration for both positive and negative  $\zeta$  potentials. The EOF mobility,  $\mu_{\text{EOF}}$  ( $= u_z/E_z$ ), was also evaluated at  $r = 0$ . This graph demonstrates the significant effect of the ion concentration on the transport of the long polymer chains. Increases in  $C$  evidently caused a pronounced shift in the mobility. In the case of  $N = 50$ , the mobility was reduced from  $2.7 \times 10^{-8}$  to  $1.1 \times 10^{-8}$   $\text{m}^2/\text{Vs}$  for  $\zeta = -25$  mV and increased from  $3.3 \times 10^{-8}$  to  $5.0 \times 10^{-8}$   $\text{m}^2/\text{Vs}$  for  $\zeta = 25$  mV. Due to the negative  $\zeta$  potential, the direction of the EOF was opposite to the ssDNA transport direction and the electrophoretic mobility decreased with increasing  $C$  for both  $N = 5$  and 50, as shown in Figure 4-3(a). In contrast, for the positive  $\zeta$  potential, the mobility increased with  $C$  due to the EOF being in the same direction as the ssDNA transport. This result suggests the possibility of controlling the translocation velocity of the polymer chains by effectively inducing EOFs as a function of  $C$ . However, as shown in Figure 4-3(b), the electrophoretic mobility was not affected by  $N$ , even though it was modulated in the nanochannel compared to that in a free solution. The electrophoretic mobility can be approximated by the superposition of  $\mu_{\text{EOF}}$  and the mobility in a free solution,  $\mu_{\text{free}}$ , such that  $\mu \approx \mu_{\text{EOF}} + \mu_{\text{free}}$ . Similar observations concerning the length-independent mobility of DNA even in nanochannels as the result of saturated confinement effects have been reported for long-chain dsDNA<sup>4,8</sup>. Either increasing the nanoslit height<sup>4</sup> or decreasing the DNA length<sup>8</sup> leads to a loss in separation resolution. This constant mobility of long-chain dsDNA is believed to break down in nanoslits narrower than 20 nm<sup>4,18</sup>, in which the DNA molecules interact strongly with the wall surfaces and inelastically dissipate their energy due to friction on the nanoscale<sup>16</sup>. This issue has attracted much attention and is still being debated. Our simulation results demonstrate that the electrophoretic mobility of short-chain ssDNA is length independent in a straight nanochannel with a 30 nm diameter. In practical applications, the velocity control of short-chain ssDNA in nanopores or separation in nanochannels involves a greater degree of confinement, such as occurs in gel media<sup>27</sup> and artificial nanochannels with nanoscale obstacles<sup>8,19</sup>.

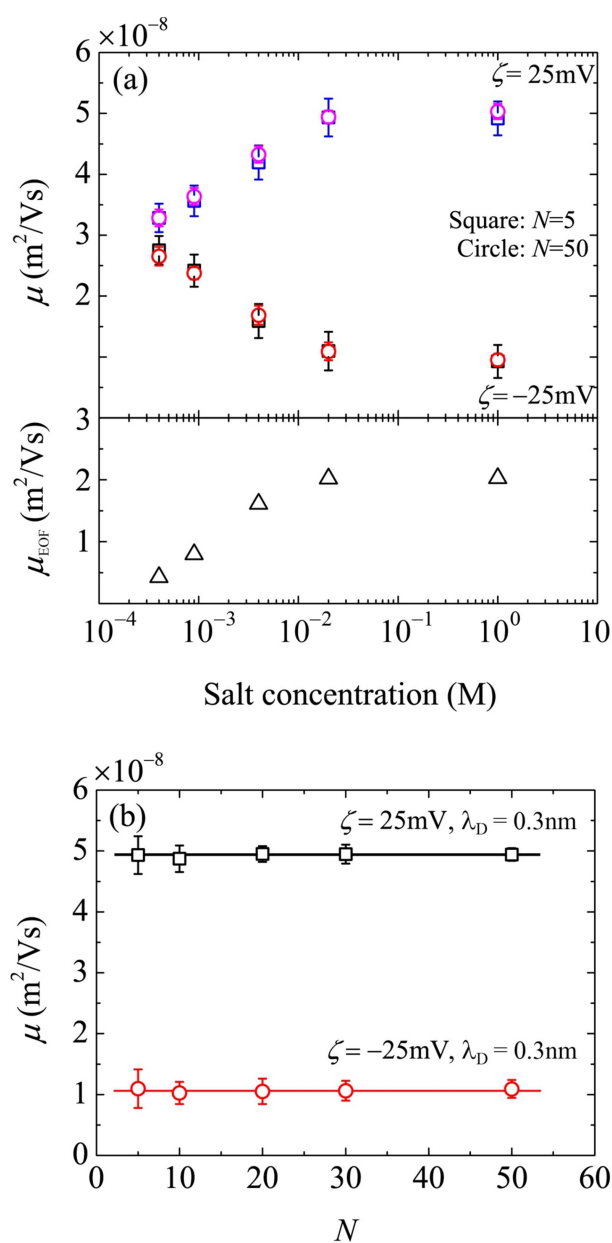
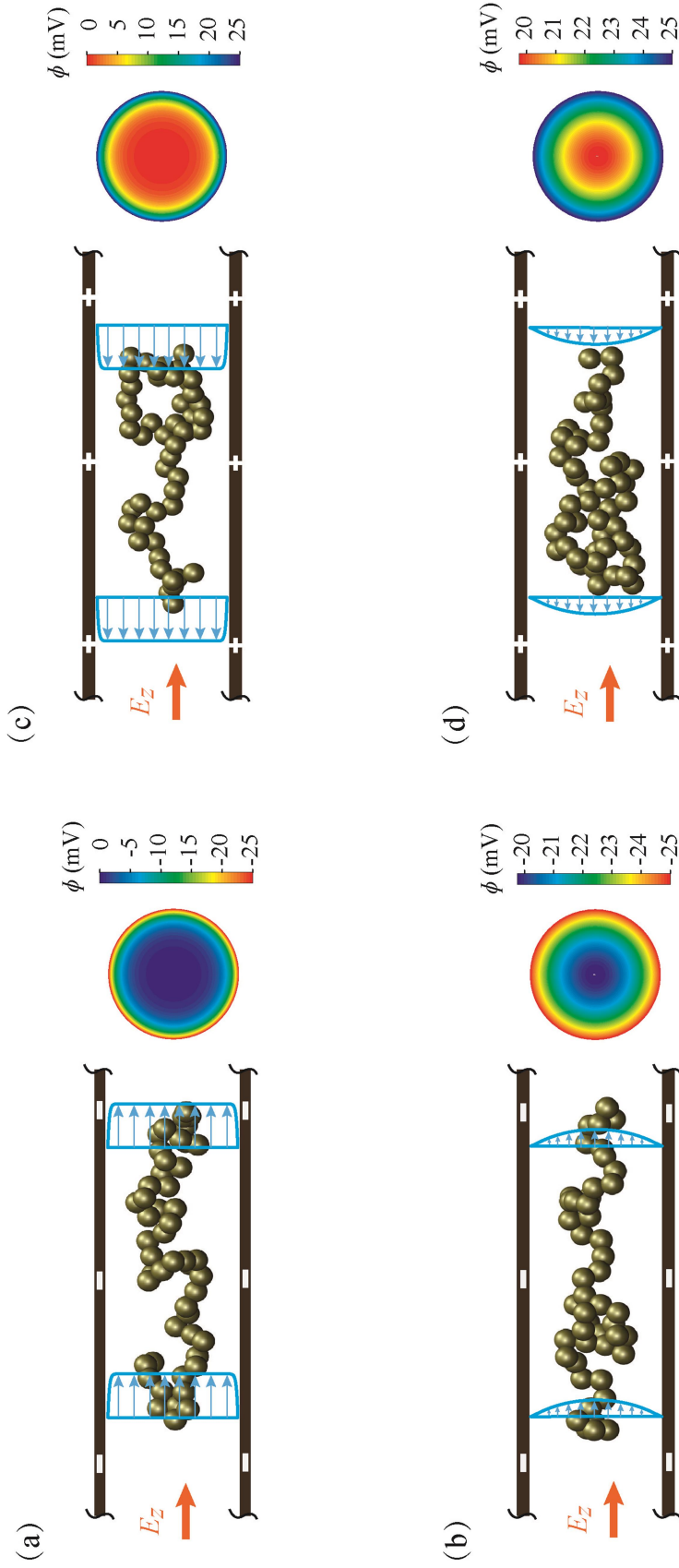


**Figure 4-3.** Electrophoretic mobility,  $\mu$ , of ssDNA in the presence of an EOF with negative and positive  $\zeta$  potentials as functions of (a) ion concentration, and (b) polymer length,  $N$ . In (a),  $\mu$  is presented for the cases of  $N = 5$  (squares) and 50 (circles), and the EOF mobility,  $\mu_{\text{EOF}}$ , values are also shown (triangles).

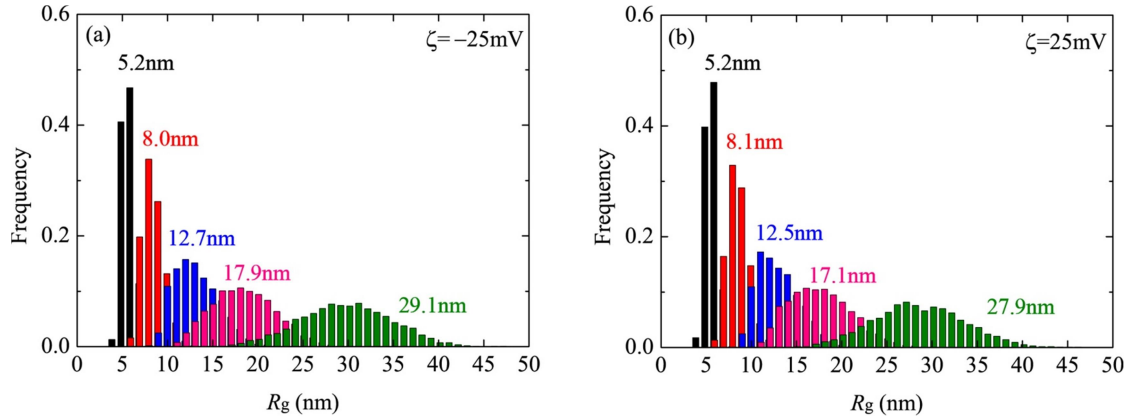
### 4.3.3 Molecular conformations of DNA inside nanochannel

Figure 4-4 presents the typical conformations of ssDNA in a nanochannel as obtained from the LD simulations, in which ion distributions in the nanochannel are affected by the radial electric field  $E_r$ . In the case of a negative (positive)  $\zeta$  potential,  $E_r$  repels (attracts) negatively charged molecules. The right panel in Figure 4-4 presents color maps for the electrostatic potential across the nanochannel cross-section. At  $\lambda_D = 0.3$  nm ( $C = 1$  M), as shown in Figure 4-4(a), the steep gradient in the  $\phi$  values resulted in a strong  $E_r$ , ranging from 0 at the center to  $8.2 \times 10^7$  V/m at the channel surface. A broader distribution is evident at  $\lambda_D = 15$  nm ( $C = 4 \times 10^{-4}$  M), varying from  $E_r = 0$  V/m at the center to  $7.4 \times 10^5$  V/m at the channel surface. These data indicate that altering  $C$  caused  $\lambda_D$  to vary and this, in turn, produced a flow profile transition from plug flow to Poiseuille-like flow, as shown in Figures 4-4(a) and 4-4(b), respectively. At positive  $\zeta$  potentials, the direction of the EOF was opposite to the direction obtained with a negative potential, as shown in Figures 4-4(c) and 4-4(d). The molecular conformations resulting from the LD simulations demonstrate a typical deformation trend inside the nanochannel, affected by both the EOF and  $E_r$ . The velocity gradient of the EOF induced shear force between two coarse-grained molecules in different stream lines tends to stretch the bonds between neighboring molecules. These trends are discussed in more detail below.

Figure 4-5 presents the temporal and ensemble averages of  $R_g$  for  $N$  values from 5 to 50. The definition of  $R_g$  is also provided in Supporting Material.  $R_g$  and the deviation of the distribution both increased with increasing  $N$  at both negative and positive  $\zeta$  potentials. Based on the  $R_g$  of ssDNA in a free solution, this value will exceed the channel radius when  $N$  is above 20. This explains why the deviation of  $R_g$  increased so dramatically above  $N = 20$ . In addition, an unexpected non-monotonic change in  $R_g$  is observed here. At  $N = 5$ , the short chain length limited the deformation of the ssDNA and so there was almost no variation in  $R_g$ . For  $N = 10$ , the average  $R_g$  value decreased from 8.1 to 8.0 nm upon switching the  $\zeta$  potential from positive to negative. In contrast, the average  $R_g$  increased by 1.6, 4.7, and 4.3% for  $N = 20, 30,$  and  $50$ , respectively, upon applying a negative  $\zeta$  potential instead of a positive potential. This result indicates that switching the  $\zeta$  potential affects the polymer conformation in the nanochannel.



**Figure 4-4.** Images showing the results of LD simulations for both (a and b)  $-25$  mV and (c and d)  $25$  mV  $\zeta$  potentials (left panel) and the electrostatic potential,  $\phi$ , in the channel cross-section (right panel). Various combinations of  $\zeta$  and EOF cause specific deformation patterns in the polymer chain, including a plug-like EOF with  $\lambda_D = 0.3$  nm (a and c) and a Poiseuille-like EOF with  $\lambda_D = 15$  nm (b and d).



**FIGURE 4-5.** Distributions of  $R_g$  in the nanochannel for a variety of  $N$  resulting from (a)  $\zeta = -25$  mV and (b)  $\zeta = 25$  mV. Mean values of  $R_g$  in the case of  $N = 50$  are 29.1 and 27.9 nm for  $\zeta = -25$  and 25 mV, respectively. Legend: black,  $N = 5$ ; red,  $N = 10$ ; blue,  $N = 20$ ; pink,  $N = 30$ ; green,  $N = 50$ .

To characterize the deformation of the ssDNA in the nanochannel, we evaluated the mean-square end-to-end distances,  $\langle L^2 \rangle$ , of polymer chains exposed to the  $E_r$  and EOF, and compared these values to those predicted for equilibrium in the nanochannel,  $\langle L_0^2 \rangle$ . The ratio of these values,  $\langle L^2 \rangle / \langle L_0^2 \rangle$ , indicates the degree of polymer deformation, whether by stretching ( $> 1$ ) or compression ( $< 1$ ). Figures 4-6(a) and 4-6(b) present the histograms of these ratios for  $N = 50$  and 5, respectively, as functions of the  $\zeta$  potential and  $\lambda_D$ . As can be seen, the ratio varied non-monotonically as a function of  $C$ . The compression and stretching of the ssDNA were greatest at  $C = 4 \times 10^{-3}$  M ( $\lambda_D = 5$  nm). At  $\zeta = 25$  mV, the plot shows a deviation between 0.89 and 0.99, implying a maximum 11% compressive deformation of the long-chain ssDNA ( $N = 50$ ). In contrast, a maximum stretch of 10% was obtained from a negative  $\zeta$  potential. These trends were reversed in the case of  $N = 5$ , as shown in Figure 4-6(b). the distribution concentrates near 1.00, and the deformation is less than 2%.

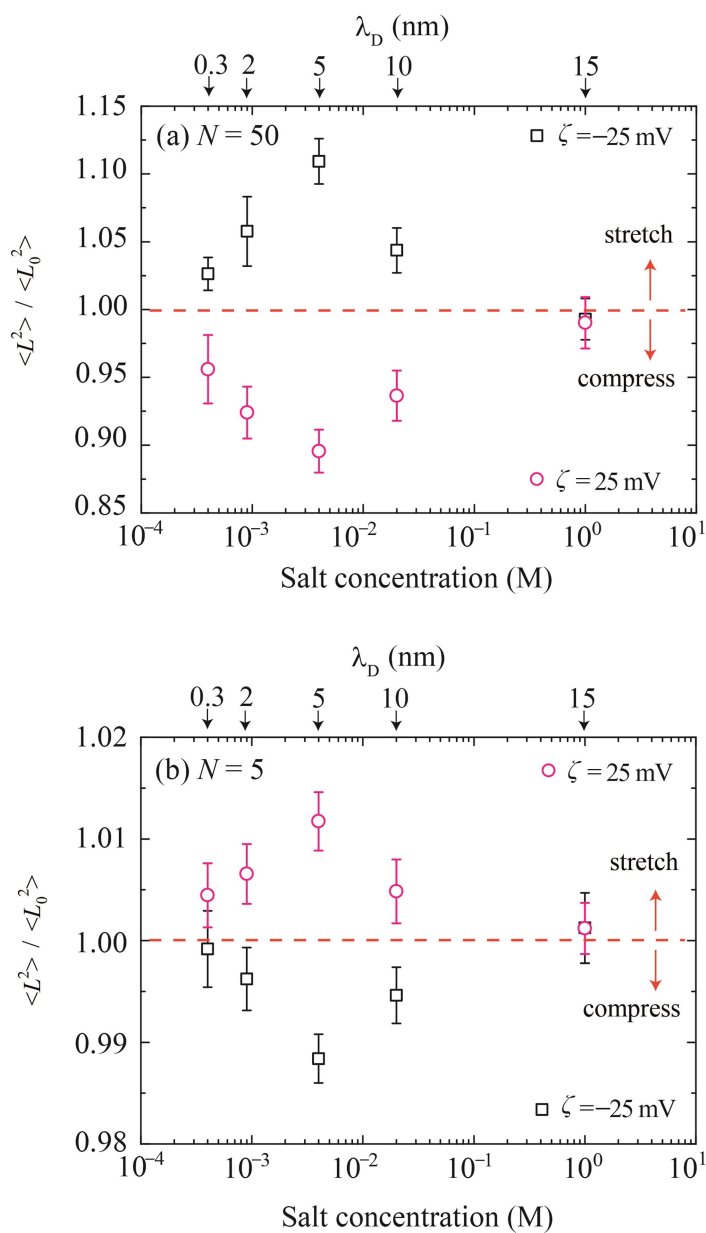


**Figure 4-6.** Mean-square end-to-end distances,  $\langle L^2 \rangle$ , of ssDNA exposed to  $E_r$  in a nanochannel at various values of  $\zeta$  potential and  $\lambda_D$ . Here  $\langle L^2 \rangle$  is normalized by the mean-square end-to-end distance,  $\langle L_0^2 \rangle$ , in an equilibrated solution in the channel. Data are shown for the polymer lengths (a)  $N = 50$  and (b) 5.

### 4.3.3 Radial position of DNA inside nanochannel

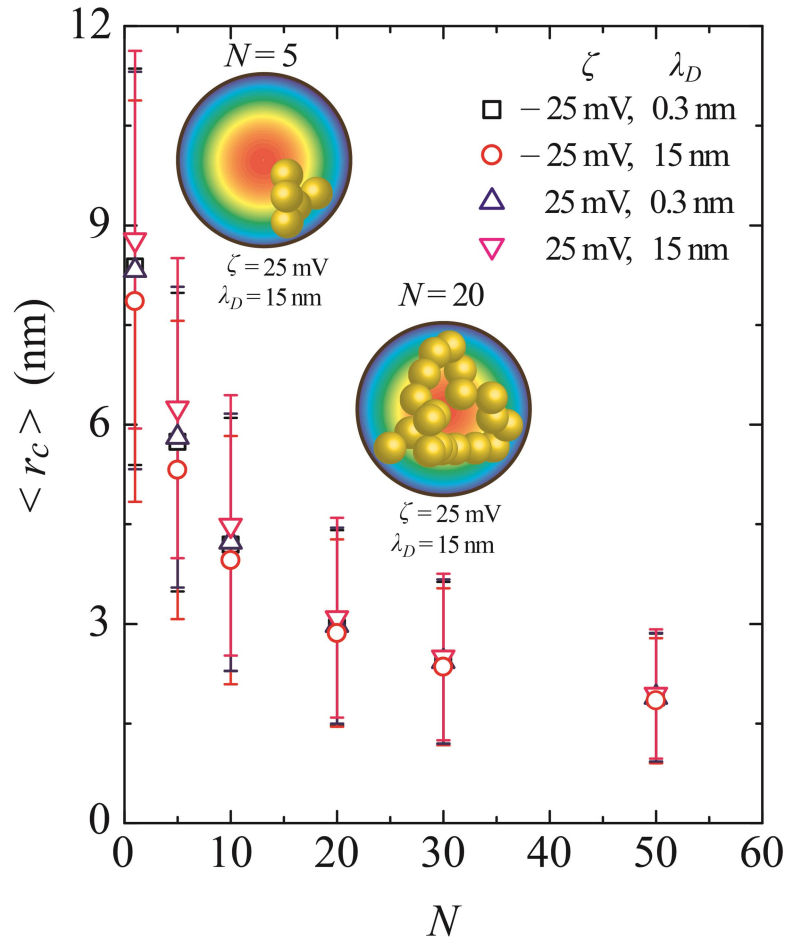
The ensemble average of the mass-center radial position  $\langle r_c \rangle$  of the ssDNA was subsequently evaluated as a function of  $N$ . Figure 4-7 demonstrates that the center of mass tended to concentrate near the center of the nanochannel with increasing  $N$ , regardless of the sign of the  $\zeta$  potential or the  $\lambda_D$ . Above  $N = 20$ , in the range of  $R_g > a$ , the long polymers were tightly packed in the nanochannel and thus, the center of mass was located in the center of the channel as a result of the distribution of the connected beads. However, in the case of short polymers (such as  $N = 1, 5$ , and  $10$ ),  $\langle r_c \rangle$  appeared to become more sensitive to the  $\zeta$  potentials of  $-25$  and  $+25$  mV at  $\lambda_D = 15$  nm ( $C = 4 \times 10^{-4}$  M), as shown in Figure 4-7. The different polymer structures at  $N = 5$  and  $20$  are also provided in this figure. At  $N < 20$ , the numerical data show large deviations because the effect of thermal fluctuations dominated the motion, in addition to electric forces resulting from the wall potential. Although the short-chain ssDNA appeared to be more readily controlled by applying electric fields, the Brownian motion of these molecules disturbed the alignment of the molecules. As a consequence of the specific polymer conformations,  $\langle r_c \rangle$  tended to monotonically approach the channel center with increasing  $N$  as the molecules were exposed to the EOF fields. As  $N$  increased, the long polymer chains behaved as though they are coiled within the inner wall of the cylinder. This explains why the center of mass of long-chain ssDNA always appeared near the channel center and there was no difference between positive and negative  $\zeta$  potentials.

Figure 4-8 presents the distribution functions,  $f(r)$ , of the radial positions of coarse-grained beads in the channel for a variety of  $\lambda_D$ , where  $f(r)$  is discretized and

normalized, such that  $2\pi \sum_{i=1}^n r_i f(r_i) \Delta r = 1$ . Here, we set  $\Delta r = a/n$ , where  $n = 15$  for  $a = 15$  nm,

such that  $\Delta r = 1$  nm. During the LD simulation run, the radial position of each individual bead was calculated at  $10 \mu\text{s}$  intervals during the last  $1.0$  ms of simulation time. The results showed the detailed behavior of each bead as well as that of the center of mass, as presented in Figure 4-7. For the negative  $\zeta$  potential, as shown in Figures 4-8(a) and 4-8(b), the coarse-grained beads appear to have been repelled by the surface potentials and thus migrate toward the channel center. At  $N = 5$ , as in Figure. 4-8(a),  $E_r$  clearly pushed the

distribution in the radial direction and, at  $\lambda_D = 5$  nm ( $C = 4 \times 10^{-4}$  M), the peak position at approximately  $r = 2.5$  nm was the nearest to the center. Because of the spring force between the connected beads, the peak positions were not coincident with the center, which is obviously different from the random walk of a single particle. For  $\lambda_D = 15$  nm,  $E_r$  was also broadly expanded along the channel cross-section and so the charged beads were exposed to the electric field. In contrast, the electric force was weakened in the case of a thick EDL and the peak position was further from the center than in the case of  $\lambda_D = 5$  nm ( $C = 4 \times 10^{-3}$  M). At  $N = 50$ , as shown in Figure 4-8(b), there was not such a clear difference in the distributions as a function of  $\lambda_D$ . It is evident that, especially in the case of short polymer chains, the negative  $\zeta$  potential and EDL thickness can potentially affect the positioning of the ssDNA in the channel. At a positive surface potential, as shown in Figures 4-8(c) and 4-8(d), although the electrically charged molecules were attracted to the wall surface, they were also repelled due to the elastic wall potential. As a result, peak positions appeared apart from the attractive wall surface. It is especially evident in Figure 4-8(c) that the histograms exhibit different peaks depending on  $\lambda_D$ . At  $\lambda_D = 5$  nm ( $C = 4 \times 10^{-3}$  M), the ssDNA was more strongly attracted to the surface. Some hot spots through which there was greater bead movement were obvious as the result of the coexistence of radial electric fields, the EOF, and the elastic wall potential. Conversely, the distributions were not so clearly distinguished based on variations in  $\lambda_D$ . The short-chain ssDNA appears to have been particularly affected by these factors and these variables may therefore play a significant role in defining the radial positions of molecules in conjunction with negatively polarized channel surfaces. Figure 4-8 shows an off-center distribution of the connected beads in the channel in the presence of  $E_r$  and the EOF. Butler et al.<sup>55</sup> has reported that the maximum distribution of polymer molecules modelled by a dumbbell structure similarly appears at an off-center position in response to an applied external force and imposed flow field, based on the kinetic theory. The present study confirmed these previous results in terms of the coarse-grained LD model simulating ssDNA on practical spatial and temporal scales.



**Figure 4-7.** Ensemble averages of the center-of-mass radial position  $\langle r_c \rangle$  as a function of the polymer length,  $N$ , at  $\zeta = -25$  mV,  $\lambda_D = 0.3$  nm (black squares);  $\zeta = -25$  mV,  $\lambda_D = 15$  nm (red circles);  $\zeta = 25$  mV,  $\lambda_D = 0.3$  nm (blue triangles); and  $\zeta = 25$  mV,  $\lambda_D = 15$  nm (pink inverted triangles). The error bars that represent the standard deviations reflect the Brownian motion of ssDNA inside the nanochannel.

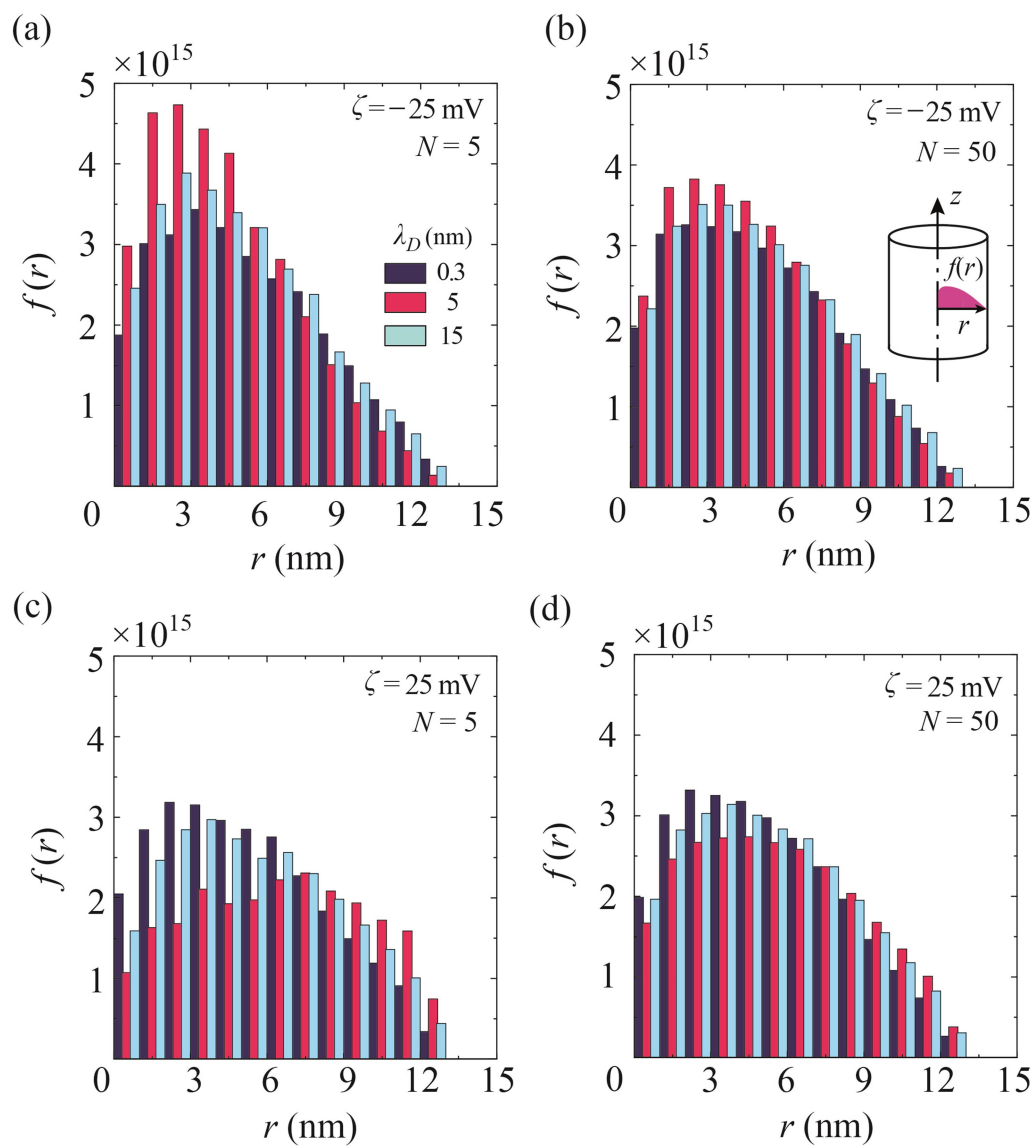


**Figure 4-8.** Discretized distribution functions,  $f(r)$ , of the radial positions of individual coarse-grained beads in a channel at  $\lambda_D = 0.3, 5,$  and  $15$  nm, for (a and b) a negative  $\zeta$  potential of  $-25$  mV and polymer lengths of (a)  $N = 5$  and (b)  $50$ , and for (c and d) a positive  $\zeta$  potential of  $25$  mV and (c)  $N = 5$  and (d)  $50$ . The radial position of each molecule was sampled at  $10 \mu\text{s}$  intervals over the last  $1.0$  ms of simulation time.

#### 4.4 Theoretical approach to the molecular distribution in a nanochannel

For comparison purposes, we also carried out a numerical analysis by solving Nernst-Planck and Poisson equations, as described below. In these analyses, electrically charged single particles with diffusion coefficients and electrophoretic mobilities equal to those of coarse-grained ssDNA responded to  $E_r$  and EOF more obviously, and the radial distributions reflected the attractive and repulsive interactions in the nanochannel. In the present case, ionic currents and the EOF due to the transport of electrolyte ions were assumed to be at a steady state. Thus, the electrostatic potential,  $\phi$ , and the velocity field,  $\mathbf{u}$ , of the EOF are solved analytically. Additionally, it was assumed that the electric fields could be represented as separate transversal and longitudinal components:

$$\mathbf{E} = E_r \mathbf{e}_r + E_z \mathbf{e}_z = -\frac{d\phi}{dr} \mathbf{e}_r + E_z \mathbf{e}_z. \quad (4-18)$$

In such a field, the behavior of negatively charged beads can be evaluated. When the number density,  $n$ , of beads, the charge,  $q$ , the friction coefficient,  $\xi$ , and the diffusion coefficient,  $D$ , are fixed, the flux,  $\mathbf{f} = (f_r, f_z)$ , can be expressed as follows:

$$f_r(r) = -\frac{q}{\xi} \frac{d\phi}{dr} n - D \frac{dn}{dr} = 0, \quad (4-19)$$

and

$$f_z(r) = \frac{qE_z}{\xi} n + u_z n. \quad (4-20)$$

Assuming a uniform electric field,  $E_z$ , the ion distribution gradient along the  $z$ -axis is negligibly small. Solving Equation 4-19 with the fluctuation-dissipation theorem, such that  $\xi D = k_B T$ , we obtain

$$n(r) = n_0 \exp\left[-\frac{q\phi}{k_B T}\right], \quad (4-21)$$

where  $n_0$  is a constant. At this point,  $f_z$  is normalized to the channel cross-section to allow a qualitative discussion of the results. According to Equations 4-20 and 4-21, we obtain

$$f_z(r) = \frac{\left[\frac{qE_z}{\xi} + u_z\right] \exp\left[-\frac{q\phi}{k_B T}\right]}{2\pi \int_0^a \left[\frac{qE_z}{\xi} + u_z\right] \exp\left[-\frac{q\phi}{k_B T}\right] r dr}. \quad (4-22)$$

To simplify the discussion, we apply the velocity field  $u_z$  resulting from the constant viscosity  $\eta_0$  and nonslip boundary condition in the cylindrical nanochannel:

$$u_z(r) = \frac{E_z \varepsilon_0 \varepsilon}{\eta_0} \left[ \frac{I_0(\kappa r)}{I_0(\kappa a)} - 1 \right]. \quad (4-23)$$

The electric potential  $\phi$  were determined from Equations 4-2, and the other properties were set to those of the water, as noted above.

Figure 4-9 presents the electric field strengths in terms of the channel radial position calculated from Equation 4-2, such that  $E_r = -d\phi/dr$ . Varying the salt concentration affected  $E_r$  in two respects: the magnitude and the effective area. The highest salt concentration,  $C = 1$  M and  $\lambda_D = 0.3$  nm, resulted in an extremely short-range but strong  $E_r$  on the order of  $10^7$  V/m, within a span of 2 nm from the wall surface. It is evident that there was a critical point near  $\lambda_D = 5$  nm ( $C = 4 \times 10^{-3}$  M) at which the  $E_r$  plot transitioned from an exponential curve to a linear relationship. Further decreases in  $C$  reduced the magnitude of the  $E_r$  that broadly affected the channel. This critical condition clearly modified the distribution of electrically charged particles, as described below.

Figure 4-10 shows the distribution function,  $f_z$ , using  $q$  and  $\zeta$  as the parameters that determine the properties of the ssDNA, as summarized in Table 4-3. Figure 4-10(a) presents the results for  $\zeta = -25$  mV,  $q = -1.88e$ , and  $\xi = 10.02 \times 10^{-12}$  kg/s in the case of  $N = 5$ . As  $\lambda_D$  was increased, the charged particles tended to locate near the center and exhibited a minimum peak position when  $\lambda_D = 5$  nm ( $C = 4 \times 10^{-3}$  M). Equation 4-19 demonstrates that the repulsive force from the channel surface was significantly stronger than the diffusive force at  $\lambda_D < 5$  nm ( $C > 4 \times 10^{-3}$  M). Further increases in  $\lambda_D$  ( $> 5$  nm) moved the distribution away from the center. In addition, Equations 4-22 and 4-23 demonstrate that the EOF velocity field that varied with  $r$  enhanced the off-center behavior. In the case of  $q = -0.649e$  and  $\xi = 3.47 \times 10^{-12}$  kg/s for  $N = 50$ , as shown in Figure 4-10(b), the difference between the peaks in each distribution was reduced at  $\zeta = -25$  mV, compared with the values in Figure 4-10(a). Conversely, at  $\zeta = 25$  mV, the negatively charged particles were attracted to the positively charged surface, as in Figure 4-10(c), such that the charged particles shielded the wall surface in conjunction with an extremely thin EDL of  $\lambda_D = 0.3$  nm. The greatest variation in radial distribution occurred at  $\lambda_D = 5$  nm ( $C = 4 \times 10^{-3}$  M). At

$\lambda_D > 5 \text{ nm}$  ( $C < 4 \times 10^{-3} \text{ M}$ ), the particles were weakly attracted to the center. At  $\zeta = 25 \text{ mV}$  for  $N = 50$ , as shown in Figure 4-10(d), the particles dissociated from the surface, although the attractive force from the channel surface remained in effect.

These theoretical results indicate that the deformation evident in Figure 4-6 and the distribution shown in Figure 4-8 actually result from the electric force due to the presence of  $E_r$ , because the ssDNA experiences either repulsive or attractive electric force in the radial direction. More importantly, the deformation and distribution of the polymer both exhibit non-monotonic behavior because of the combined effects of the magnitude and effective range of  $E_r$ . Consequently, the distribution shown in Figure 4-8 demonstrates that polymers tend to be transported through the off-center regions of a nanochannel having a 30 nm diameter. This explains the experimental observation of a reptation-like motion of DNA in a 30 nm nanoslit, which is clearly different from the behavior seen in less confined nanoslits (wider than 40 nm)<sup>24</sup>. Our study confirms that surface charges (in addition to confinement effects) influence the transport mechanism of biopolymers when the channel dimension is reduced to less than 30 nm (that is, a value comparable to  $\lambda_D$ ).

The results described above for long-chain ssDNA ( $N \geq 20$ ) are summarized schematically in Figure 4-11. In the case of negatively polarized wall surfaces, the EOF and the electrophoretic transport of the ssDNA are in opposite directions, as in Figures 4-11(a) and 4-11(b). In this scenario, a thin EDL at high concentrations results in a plug-like EOF that is almost constant regardless of  $r$ , as presented in Figure 4-11(a). As the molarity decreases, the flow field clearly generates a velocity gradient that causes a relative velocity difference between molecules in different stream lines. Additionally, due to the radial electric force, the effective volume of the nanochannel decreases and the polymer chain is stretched, as in Figure 4-11(b). In contrast, positively polarized wall surfaces provide electrokinetic transport of the ssDNA in the same direction as the EOF, as in Figures 4-11(c) and 4-11(d). The radial electric force, which becomes stronger at medium ion concentrations, induces intramolecular interactions and compressive deformations along the axial direction, as in Figure 4-11(d).

**TABLE 4-3** Electrical charge and friction coefficient for corresponding polymer length.

$N$	$q$ ( $-e$ )	$\zeta$ ( $10^{-12}$ kg/s)	$q/\zeta$ ( $10^{-8}$ m <sup>2</sup> /Vs)
1	4.01	21.42	3.00
5	1.88	10.02	3.00
10	1.36	7.28	2.99
20	0.97	5.18	3.00
30	0.82	4.40	3.00
50	0.65	3.47	3.00

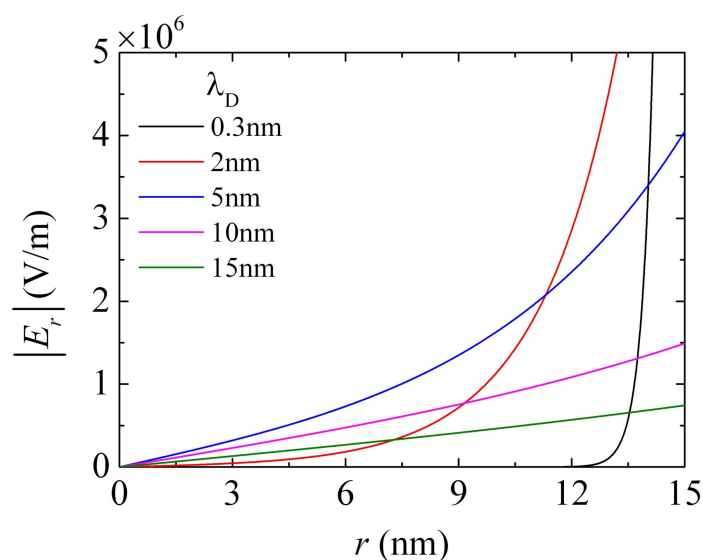


**Figure 4-9.** Radial electric field strengths,  $E_r$ , as a function of the radial position,  $r$ , in a nanochannel at different salt concentrations. Legend: black:  $\lambda_D = 0.3$  nm; red:  $\lambda_D = 2$  nm; blue line:  $\lambda_D = 5$  nm; pink line:  $\lambda_D = 10$  nm; green line:  $\lambda_D = 15$  nm. The radial electric field was calculated using Equation 4-2.

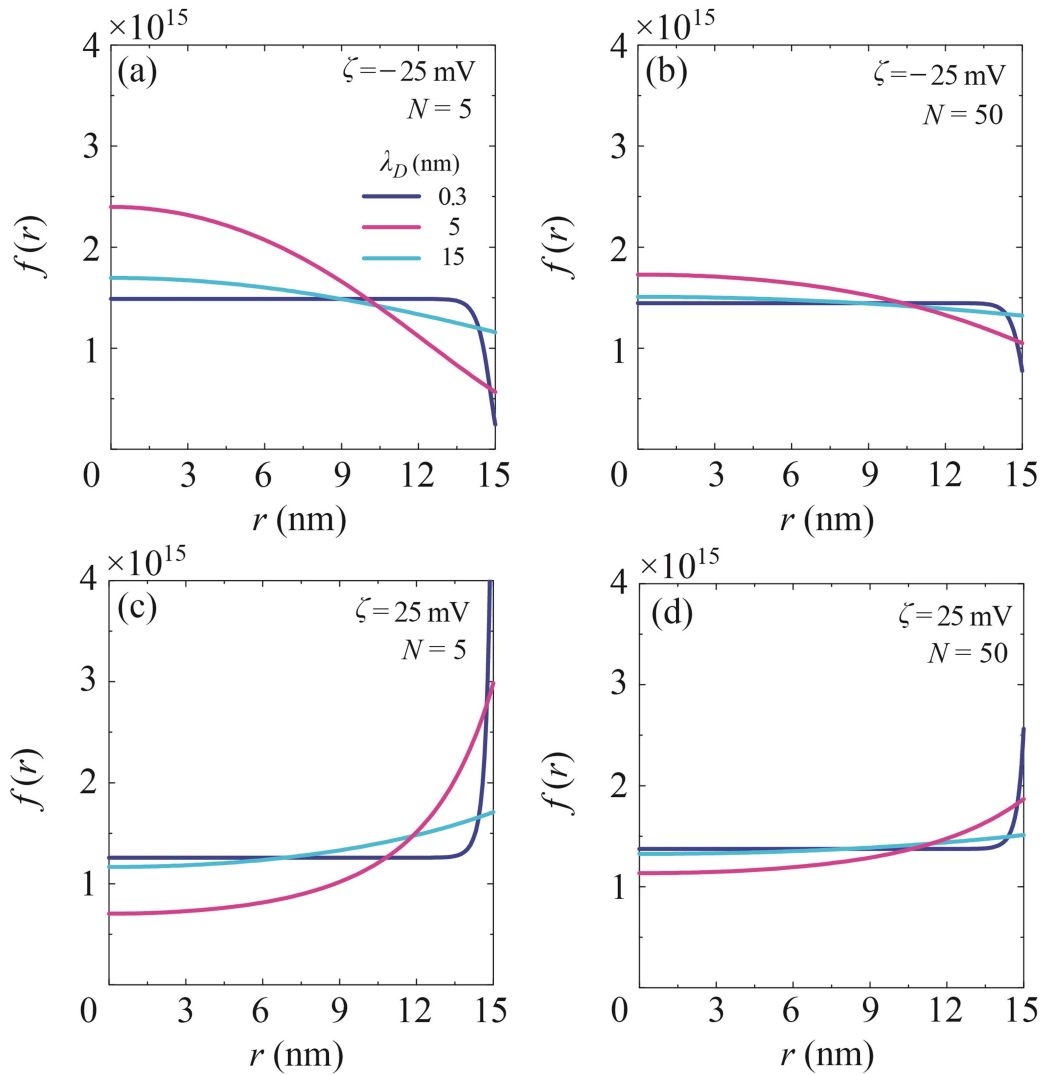


**Figure 4-10.** Radial distribution functions,  $f(r)$ , of electrically charged particles in a nanochannel at  $\lambda_D = 0.3, 5,$  and  $15$  nm, obtained by solving the Nernst-Planck and Poisson equations (Equations 4-19 and 4-20), for (a and b) a negative  $\zeta$  potential of  $-25$  mV and (a)  $N = 5$  and (b)  $50$ , and for (c and d) a positive  $\zeta$  potential of  $25$  mV and (c)  $N = 5$  and (d)  $50$ .

Here  $f(r)$  is normalized by  $\int_0^a 2\pi f(r)rdr = 1$ .

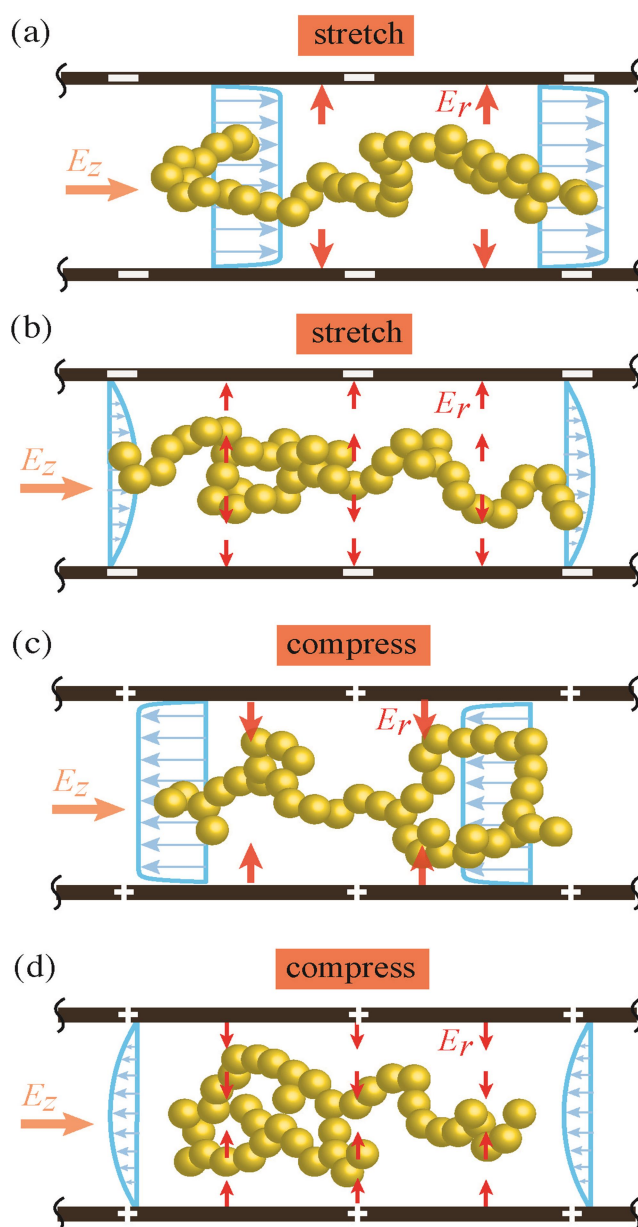


**Figure 4-11.** Schematic representations of the ssDNA transport mechanism in a nanofluidic channel resulting from the LD simulations. The DNA chain experiences a repulsive (a and b) or attractive (c and d) forces in the radial direction caused by negative or positive  $\zeta$  potentials, respectively. Depending on the ion concentration, a strong electric force acts on the molecule in the EDL. (a and b) Due to the negative  $\zeta$  potential, the channel surface repels the negatively charged DNA toward the center, the EOF field causes intramolecular interactions in the polymer chain, and the velocity gradient at lower ion concentrations results in stretching of the polymer structure as shown in (b). (c and d) The positive  $\zeta$  potential attracts the DNA to the channel surface and the EOF velocity gradient deforms the molecule in a dilute solution. As a result, the polymer structure is

## 4.5 Conclusion

Simulating the EOF velocity fields in a cylindrical nanochannel with a 15 nm radius allowed the characterization of the electrokinetic transport regimes of ssDNA via LD simulations in conjunction with a coarse-grained model. The validity of this model was verified by evaluating the diffusion coefficient, electrophoretic mobility, and radius of gyration in a free solution. The charged polymer transport properties in EOF fields were evaluated and some useful results were obtained. Focusing on the case in which  $R_g$  is similar to or greater than the radius of the channel cross-section, the relationship between the flow field and the deformation of the polymer conformation was evaluated. The electric force in the channel primarily results from the  $\zeta$  potential and this force repels (attracts) negatively charged ssDNA molecules at negative (positive) surface potentials. In the transport regime, short-chain ssDNA tend to be strongly affected by the radial electric field, the EOF, and the wall potential. Furthermore, as the ion concentration is decreased, the EOF exhibits apparent velocity gradients that lead to intramolecular interactions between the coarse-grained ssDNA molecules. Especially in dilute electrolyte solutions, setting the direction of the EOF forward or backward to the direction of the ssDNA electrophoresis leads to a deformation regime in which polymer chains are compressed or stretched, respectively. Consequently, the possibility of controlling the velocity of polymer transport by modifying the EOF profile and  $\zeta$  potential is evident.

This study is relevant to the fields of polymer physics and applied biophysics. These finding may also lead to the development of novel single-molecule manipulation techniques in liquid flows. Examples of possible applications include recently reported experiments aimed at slowing ssDNA translocation through a nanochannel by adjusting the electric potential<sup>56</sup>, and stretching ssDNA exposed to external liquid flows near substrate surfaces<sup>57,58</sup>.

## Reference

1. J. B. Heng, C. Ho, T. Kim, R. Timp, A. Aksimentiev, Y. V. Grinkova, S. Sligar, K. Schulten, and G. Timp, "Sizing DNA Using a Nanometer-Diameter Pore," *Biophys J.* **87**(4), 2905-2911 (2004).
2. C. Dekker, "Solid-state nanopores," *Nat. Nanotechnol.* **2**, 209–215 (2007).
3. M. Zwolak, and M. Di Ventra, "Colloquium: Physical approaches to DNA sequencing and detection," *Rev. Mod. Phys.* **80**, 141–165 (2008).
4. J. D. Cross, E. A. Strychalski, and H. G. Craighead, "Size-dependent DNA mobility in nanochannel," *J. Appl. Phys.* **102**(2), 024701 (2007).
5. M. Tsutsui, Y. He, M. Furuhashi, Sakon. Rahong, M. Taniguchi, and T. Kawai, "Transverse electric field dragging of DNA in a nanochannel," *Sci. Rep.* **2**, 394 (2012).
6. T. Yasui, S. Rahong, K. Motoyama, T. Yanagida, Q. Wu, N. Kaji, M. Kanai, K. Doi, K. Nagashima, M. Tokeshi, M. Taniguchi, S. Kawano, T. Kawai, and Y. Baba, "DNA Manipulation and Separation in Sublithographic-Scale Nanowire Array," *ACS Nano.* **7**(4), 3029–3035 (2013).
7. T. Ohshiro, M. Tsutsui, K. Yokota, M. Furuhashi, M. Taniguchi, and T. Kawai, "Detection of post-translational modifications in single peptides using electron tunnelling currents," *Nat. Nanotechnol.* **9**, 835–840 (2014).
8. S. Rahong, T. Yasui, T. Yanagida, K. Nagashima, M. Kanai, A. Klamchuen, G. Meng, Y. He, F. Zhuge, N. Kaji, T. Kawani, and Y. Baba, "Ultrafast and Wide Range Analysis of DNA Molecules Using Rigid Network Structure of Solid Nanowires," *Sci. Rep.* **4**, 5252 (2014).
9. Y. He, M. Tsutsui, C. Fan, M. Taniguchi, and T. Kawai, "Controlling DNA Translocation through Gate Modulation of Nanopore Wall Surface Charges," *ACS Nano* **5**(7), 5509–5518 (2011).
10. S. Ghosal, "Effect of Salt Concentration on the Electrophoretic Speed of a Polyelectrolyte through a Nanopore," *Phys. Rev. Lett.* **98**, 238104 (2007).
11. S. W. Kowalczyk, D. B. Wells, A. Aksimentiev, and C. Dekker, "Slowing down DNA translocation through a nanopore in lithium chloride," *Nano Lett.* **12**(2), 1038–1044 (2012).

12. Y. He, M. Tsutsui, R. H. Scheicher, F. Bai, M. Taniguchi, and T. Kawai, "Thermophoretic Manipulation of DNA Translocation through Nanopore," *ACS Nano* **7**(1), 538–546 (2013).
13. D. Fologea, J. Uplinger, B. Thomas, D. S. McNabb, and J. Li, "Slowing DNA Translocation in a Solid-State Nanopore," *Nano Lett.* **5**(9), 1734–1737 (2005).
14. W. X. Qian, K. Doi, S. Uehara, and S. Kawano, "Theoretical study of the transpore velocity control of single-stranded DNA," *Int. J. Mol. Sci.* **15**(8), 13817–13832 (2014).
15. E. Stellwagen, Y. Lu, and N. C. Stellwagen, "Unified Description of Electrophoresis and Diffusion for DNA and Other Polyions," *Biochemistry.* **42**(40), 11745–11750 (2003).
16. A. E. Nkodo, J. M. Garnier, B. Tinland, H. Ren, C. Desruisseaux, L. C. McCormick, G. Drouin, and G. W. Slater, "Diffusion coefficient of DNA molecules during free solution electrophoresis," *Electrophoresis.* **22**(12), 2424 (2001).
17. J. Fu, and P. Mao, "A Nanofilter Array Chip for Fast Gel-Free Biomolecule Separation," *Appl Phys Lett.* **89**(26), 263902 (2005).
18. G. B. Salieb-Beugelaar, J. Teapal, J. V. Nieuwkastele, D. Wijnperlé, J. O. Tegenfeldt, F. Lisdar, A. v. d. Berg, and J. C. T. Eijkel, "Field-Dependent DNA Mobility in 20 nm High Nanoslits," *Nano Lett.* **8**(7), 1785-1790 (2008).
19. Z. Cao, and L. Yobas, "Gel-Free Electrophoresis of DNA and Proteins on Chips Featuring a 70 nm Capillary-Well Motif," *ACS Nano.* **9**(1), 427–435 (2015).
20. K. Doi, T. Haga, H. Shintaku, and S. Kawano, "Development of coarse-graining DNA models for single-nucleotide resolution analysis," *Trans. R. Soc. A.* **368**, 2615–2628 (2010).
21. S. Uehara, H. Shintaku, and S. Kawano, "Electrokinetic Flow Dynamics of Weakly Aggregated  $\lambda$ DNA Confined in Nanochannels," *Trans. ASME, J. Fluids Eng.* **133**(12), 121203 (2011).
22. K. Doi, H. Takeuchi, R. Nii, S. Akamatsu, T. Kakizaki, and S. Kawano, "Self-assembly of 50 bp poly(dA)·poly(dT) DNA on highly oriented pyrolytic graphite via atomic force microscopy observation and molecular dynamics simulation," *J. Chem. Phys.* **139**, 085102 (2013).

23. S. Tanaka, Tsutsui, M, H. Theodore, H. Yuhui, A. Arima, T. Tsuji, K. Doi, S. Kawano, M. Taniguchi, and T. Kawai, "Tailoring Particle Translocation via Dielectrophoresis in Pore Channels," *Sci. Rep.* **6**, 31670 (2016).
24. J. W. Yeh, and K. Szeto, "Stretching of Tethered DNA in Nanoslits," *ACS Macro Lett.* **5**(10), 1114-1118 (2016).
25. Y. He, M. Tsutsui, R. H. Scheicher, C. Fan, M. Taniguchi, T. Kawai, and T. Kawai, "Mechanism of How Salt-Gradient-Induced Charges Affect the Translocation of DNA Molecules through a Nanopore," *Biophys J.* **105**(3), 776-782 (2013).
26. D. Branton, D. W. Deamer, A. Marziali, H. Bayley, S. A. Benner, T. Butler, M. Di Ventra, S. Garaj, A. Hibbs, X. Huang, S. B. Jovanovich, P. S. Krstic, S. Lindsay, X. S. Ling, C. H. Mastrangelo, A. Meller, J. S. Oliver, Y. V. Pershin, J. M. Ramsey, R. Riehn, G. V. Soni, V. T. Cossa, M. Wanunu, M. Wiggin, and J. A. Schloss, "The potential and challenges of nanopore sequencing," *Nat. Nanotechnol.* **26**, 1146–1153 (2008).
27. P. G. de Gennes, "Reptation of a polymer chain in the presence of fixed obstacles," *J. Chem. Phys.* **55**, 572–579 (1971).
28. T. Odijk, "The statistics and dynamics of confined or entangled stiff polymers," *Macromolecules.* **16**, 1340-1344 (1983).
29. J. L. Viovy, "Electrophoresis of DNA and other polyelectrolytes: Physical mechanisms," *Rev. Mod. Phys.* **72**(3), 813–872 (2000).
30. Y. L. Chen, "Electro-entropic excluded volume effects on DNA looping and relaxation in nanochannels," *Biomicrofluidics.* **7**(5), 054119 (2013).
31. A. Jain, and K. D. Dorfman, "Evaluation of the Kirkwood approximation for the diffusivity of channelconfined DNA chains in the de Gennes regime," *Biomicrofluidics.* **9**(2), 024112 (2015).
32. G. B. Salieb-Beugelaar, K. D. Dorfman, A. van den Berg, and J. C. T. Eijkel, "Electrophoretic separation of DNA in gels and nanostructures," *Lab Chip.* **9**(17), 2508–2523 (2009).
33. K. D. Dorfman, "DNA electrophoresis in microfabricated devices," *Rev. Mod. Phys.* **82**, 2903–2947 (2010).
34. K. F. Luo, T. Ala-Nissila, S. C. Ying, and A. Bhattacharya, "Sequence dependence of

- DNA translocation through a nanopore,” *Phys. Rev. Lett.* **100**, 058101 (2008).
35. K. F. Luo, and R. Metzler, “Translocation dynamics of a polymer chain into a long narrow channel driven by longitudinal flow,” *J. Chem. Phys.* **134**(13), 135102 (2011).
  36. G. W. Slater, S. G. Guillouzie, M. G. Gauthier, J. F. Mercier, M. Kenward, L. C. McCormick, F. Tessier, “Theory of DNA electrophoresis ( $\sim$  1999-20021/2),” *Electrophoresis*. **23**, 3791–3816 (2002).
  37. G. W. Slater, C. Holm, M. V. Chubynsky, H. W. de Haan, A. Dubé, K. Grass, O. A. Hickey, C. Kingsburry, D. Sean, T. N. Shendruk, and L. Zhan, “Modeling the separation of macromolecules: A review of current computer simulation methods,” *Electrophoresis*. **30**(5), 792–818 (2009).
  38. S. Nagahiro, S. Kawano, and H. Kotera, “Separation of long DNA chains using a nonuniform electric field: A numerical study,” *Phys. Rev. E*. **75**, 011902 (2007).
  39. R. M. Jendrejack, E. T. Dimalanta, D. C. Schwartz, M. D. Graham, and J. J. de Pablo, “DNA Dynamics in a Microchannel,” *Phys. Rev. Lett.* **91**, 038102 (2003).
  40. R. M. Jendrejack, D. C. Schwartz, M. D. Graham, and J. J. de Pablo, “Effect of confinement on DNA dynamics in microfluidic devices,” *J. Chem. Phys.* **119**, 1165-1173 (2003).
  41. R. M. Jendrejack, D. C. Schwartz, J. J. de Pablo, and M. D. Graham, “Shear-induced migration in flowing polymer solutions: Simulation of long-chain DNA in microchannels,” *J. Chem. Phys.* **120**(13), 2513-2529 (2004).
  42. Y. Wang, P. Koblinski, and Z. Chen. “Viscosity calculation of a nanoparticle suspension confined in nanochannels,” *Phys. Rev. E*. **86**:036313 (2012).
  43. M. Abramowitz, and I. Stegun, A. Handbook of Mathematical Functions with Formulas, Graphs, and Mathematical Tables, Dover Publications, New York (1972).
  44. S. Levine, J. R. Marriott, G. Neala, and N. Epstein, “Theory of electrokinetic flow in the cylindrical capillaries at high zeta-potentials,” *J. Colloid Interface Sci.* **52**(1), 136–149 (1975).
  45. C. L. Rice, and R. Whitehead, “Electrokinetic Flow in a Narrow Cylindrical Capillary,” *J. Phys. Chem.* **69**(11), 4017–4024 (1965).
  46. R. B. Schoch, J. Han, and P. Renaud, “Transport phenomena in nanofluidics,” *Rev.*

- Mod. Phys.* **80**, 839–883 (2008).
47. J. F. Zhang, B. D. Todd, and K. P. Travis, “Viscosity of confined inhomogeneous nonequilibrium fluids,” *J. Chem. Phys.* **121**, 10778 (2004).
  48. T. Yasui, S. Rahong, K. Motoyama, T. Yanagida, Q. Wu, N. Kaji, M. Kanai, K. Doi, K. Nagashima, M. Tokeshi, M. Taniguchi, S. Kawano, T. Kawai, and Y. Baba, “DNA Manipulation and Separation in Sublithographic-Scale Nanowire Array,” *ACS Nano.* **7**(4), 3029-3025 (2013).
  49. S. Guillouzic, and G. W. Slater, “Polymer translocation in the presence of excluded volume and explicit hydrodynamic interactions,” *Phys. Lett. A.* **359**, 261–264 (2006).
  50. Y. L. Chen, H. Ma, M. D. Graham, and J. J. de Pablo, “Modeling DNA in Confinement: A Comparison between the Brownian Dynamics and Lattice Boltzmann Method,” *Macromolecules.* **40**(16), 5978-5984 (2007).
  51. K. Grass, and C. Holm, “On the importance of hydrodynamic interactions in polyelectrolyte electrophoresis,” *J. Phys: Condens. Matter.* **20**, 494217 (2008).
  52. J. P. Hernández-Qrtiz, and J. J. de Pablo, “Self-consistent description of electrokinetic phenomena in particle-based simulations,” *J. Chem, Phys.* **143**, 014108 (2015).
  53. K. Doi, T. Uemura, and S. Kawano, “Molecular dynamics study of solvation effect on diffusivity changes of DNA fragments,” *J. Mol. Model.* **17**(6), 1457–1465 (2011).
  54. S. Levine, and G. H. Neale, “The Prediction of Electrokinetic Phenomena within Multiparticle Systems. I. Electrophoresis and Electroosmosis,” *J. Colloid. Int. Sci.* **47**, 520-529 (1974).
  55. J. E. Butler, O. Berk Usta, R. Kekre, and A. J. C. Ladd, “Kinetic theory of a confined polymer driven by an external force and pressure-driven flow,” *Phys. Fluids.* **19**, 113101 (2007).
  56. Y. Liu, and L. Yobas, “Slowing DNA Translocation in a Nanofluidic Field-Effect Transistor,” *ACS Nano.* **10**(4), 3985-3994 (2016).
  57. I. Hanasaki, N. Yukimoto., S. Uehara, H. Shintaku, and S. Kawano, “Linearisation of  $\lambda$ DNA Molecules by Instantaneous Variation of the Trapping Electrode Voltage Inside a Micro-Channel,” *J. Phys. D.* **48**, 135402 (2015).
  58. I. Hanasaki, S. Uehara., S., Y. Arai, T. Nagai, and S. Kawano, “Threshold-Free

Evaluation of Near-Surface Diffusion and Adsorption-Dominated Motion from Single-Molecule Tracking Data of Single-Stranded DNA through Total Internal Reflection Fluorescence Microscopy,” *Jpn. J. Appl. Phys.* 54, 125601 (2015).

# Chapter 5

## *General Conclusions*

Recently, the breakthrough in the nanofluidics research field has led the evolution in the progress of single molecule identification and analysis, which supplies the opportunity to accomplish the ultrafast and high throughput measurement. We have investigated the DNA transport phenomena in nanofluidic structures to clarify the mechanism of DNA transport at nanoscale. The main findings of this thesis are summarized as follows.

In Chapter 2, we have investigated the electrokinetic transport of long dsDNA molecules in a nanofluidic device consisting of microchannel, nanochannel, and nanopore under nonuniform electric fields. We developed a computational model and carried out simulations in order to verify the transport dynamics of dsDNA passing through the nanogap mounted in a micro/nano-fluidic channel. Langevin dynamics simulations were applied to a bead-spring model of  $\lambda$ -DNA under nonuniform electric fields due to the stepwise flow channel. Translocation time through a nanogap was measured, clarifying the detailed mechanism of  $\lambda$ -DNA which passed through the confined narrow space. It was found that the multiple connections of different-sized channels, which induced a very strong electric field in the nanogap, were effective to uncoil and smoothly introduce DNA into the narrow gap. Furthermore, asymmetric transports of DNA in cis and trans channels were caused by deformations of the long-chained molecule in such a distinguishing shape of channel. In comparison with previous theoretical and experimental results, a better understanding could be obtained for the electrokinetic transport of dsDNA from a dynamical point of view.

In Chapter 3, the translocation mechanism of a ssDNA molecule in a nanofluidic channel was investigated using Langevin dynamics simulations. A coarse-grained bead-spring model was developed to simulate the dynamics of ssDNA chain passing through a rectangular cross-section nanopore embedded in a nanochannel, under the influence of a nonuniform electric field. Varying the cross-sectional area of the nanopore was found to allow optimization of the translocation process through modification of the electric field in the flow channel, since a drastic drop in the electric potential at the nanopore was induced by changing the cross-section. Furthermore, the configuration of the polymer chain in the nanopore was observed to determine its translocation velocity. The competition between the strength of the electric field and confinement in the small pore produces various transport mechanisms and the results of this study thus represent a means of optimizing the design of nanofluidic devices for single molecule detection.

In Chapter 4, we investigated the electrokinetic transport of single-stranded DNA in a cylindrical nanochannel, employing a coarse-grained bead-spring model that quantitatively reproduced the radius of gyration, diffusion coefficient, and electrophoretic mobility of the polymer. Using this practical scale model, transport regimes of ssDNA with respect to the wall surface potential of the channel, the ion concentration, and the polymer length were successfully characterized. It was found that the relationship between the radius of gyration of ssDNA and the channel radius was critical to the formation of deformation regimes in a narrow channel. We conclude that a combination of EOF velocity gradients and electric fields due to electrically polarized channel surfaces affects the alignment of molecular conformations, such that the ssDNA is stretched (compressed) at negative (positive) wall surface potentials in low-concentration solutions. Furthermore, this work suggests the possibility of controlling the center-of-mass position by tuning the salt concentration. These results must be applicable to the design of molecular manipulation techniques based on liquid flows in micro/nanofluidic devices.

In this thesis, we clarified the dsDNA translocation dynamics in nanopore (Chapter 2), ssDNA translocation mechanism through nanopore (Chapter 3) and nanochannel (Chapter 4). The computational approaches we developed and the results presented above are useful for the further development of the advanced manipulation / analysis platforms for DNA in the future.

# List of Publications

## Journal Articles

- [1] Weixin Qian, Kentaro Doi, Satoshi Uehara, Kaito Morita, and Satoyuki Kawano, “Theoretical study of the transpore velocity control of single-stranded DNA”, *International Journal of Molecular Sciences*, 15(8), 13817-13832, 2014.
- [2] Weixin Qian, Kentaro Doi, and Satoyuki Kawano, “Effects of Polymer Length and Salt Concentration on the Transport of ssDNA in Nanofluidic Channels”, *Biophysical Journal*, <http://dx.doi.org/10.1016/j.bpj.2017.01.027>, 2017.
- [3] Kentaro Doi, Weixin Qian, Satoshi Uehara, Makusu Tsutsui, Masateru Taniguchi, Tomoji Kawai, and Satoyuki Kawano, “Langevin Dynamics Study on Electrokinetic Transport of long-Chained DNA through Nanogap Embedded in Nanochannel,” *International Journal of Emerging Multidisciplinary Fluid Sciences*, 2017, in press.

## International Conference Proceedings

- [1] Weixin Qian, Kentaro Doi and Satoyuki Kawano, “Langevin Dynamics Simulation of Single-Stranded DNA Translocation through Nanopore in External Non-Uniform Electric Field”, The 15<sup>th</sup> International Conference on Biomedical Engineering (ICBME 2013), Singapore, December 4<sup>th</sup> to 7<sup>th</sup>, 2013. (Oral presentation in English)

## Domestic Conference Proceedings

- [1] Weixin Qian, Kaito Morita, Kentaro Doi, and Satoyuki Kawano, “Coarse-grained Molecular Dynamics Study on Electrophoresis of DNA in Nanochannel”, The 2013 Conference of Japan Society of Mechanical Engineers, September 8<sup>th</sup> to 11<sup>th</sup>, 2013. (Oral presentation in English)

## Acknowledgment

This research would not have been accomplished without the collaborations and support of the gentle people around me. I would like to thank the all laboratory members for their participation to help me getting results of better quality.

First and foremost, my deepest gratitude goes to my supervisor Professor Satoyuki Kawano, for his kindness to provide me the opportunity to conduct my research in his lab and undergo so many memorable experiences in Japan. I also appreciate his priceless support on my job hunting activities from last March. I am thankful for his keenness to guide and advise me not only in research related matters, but also in the life in general. I will always bear his words in mind and spare no effort to bridge the friendship between China and Japan.

Second, I would like to express my heartfelt gratitude to my Assoc. Prof. Kentaro Doi for his insightful academic advices and priceless patience on my research. He has walked me through all the stages of these five years during my Master and Doctor courses. Without his consistent and illuminating instruction, this thesis could not have reached its present form. I am also truly thankful for his speechless education of teaching me what a true researcher is and what the attitude towards work is. He is really a living example of the ideal man, which will keep influence and encourage me to be a better man in my rest life. It is my honor to carry out the research under such outstanding mentor.

I would also like to thank the rest of my thesis committee, Professor Shigenobu Ogata and Professor Kazuyasu Sugiyama, for their valuable comments and encouragement to enrich my research from various perspectives. I would like to take this change to personally thank Prof. Kazuyasu Sugiyama for his advice and counsel of my job hunting.

I am also greatly indebted to the Assoc. Prof. Itsuo Hanasaki, Assist. Prof. Hirofumi Shintaku, and Assist. Prof. Tetsuro Tsuji, for their help, support, guidance for my research.

My special thanks to my best Japanese friends in Osaka University, Mr. Ryosuke Nii and Mr. Yoji Kataoka. We have so much impressive experience and wonderful memories in my life in Japan. The time we spent together, the jokes we shared, the games we played, these memories are my precious treasure in the heart and made the study period very enjoyable.

I would like to thank all my fellow lab members for the unforgettable lab trips and lab events, for the countless nights we fight for the deadline and endless academic reports. I am grateful to Dr. Szarek Paweł, Dr. Osman Omran Osman Mosa, Dr. Satoshi Uehara, Dr. Sawanya Suwannawong, Mr. Chenfei Ye, Mr. Shoji Tanaka, Mr. Yoichi Maeda, Mr. Mustafa Ibrahim Hussein, Ms. Ayako Yano, Mr. Ryo Nagura, Mr. Kosuke Kozai, Mr. Sho Saita, Mr. Kanji Kawashima, Mr. Syuto Onitsuka, Ms. Aishah Mahmoud, Ms. Asuka Nakayama, Ms. Fumika Nito, Mr. Yuta Sasai, and Mr. Takeo Yoshida for their precious friendship.

My additional thanks to my wife, for her kind company during these years. It is her encourage and support that makes what the man I am now. I cannot expect any better life companion better than her and it is my best lucky to have her during my rest life.

Last but not least, I wish to express my highest gratefulness to my beloved family for their loving considerations and great confidence in me all through these years in Japan. It is their love that supported me spiritually throughout completing this study and my life in general.